Spectral Aerosol Optical Depths and Radiative Forcing : Seasonal and Spatial Variations

A THESIS

submitted for the Award of Ph. D. degree of

MOHANLAL SUKHADIA UNIVERSITY

in the

Faculty of Science

by

Rohit Srivastava

Under the Supervision of

Dr. S. Ramachandran
Associate Professor

Space and Atmospheric Sciences Division
Physical Research Laboratory, Ahmedabad, INDIA

DEPARTMENT OF PHYSICS

FACULTY OF SCIENCE

MOHANLAL SUKHADIA UNIVERSITY

UDAIPUR

2011

CERTIFICATE

I feel great pleasure in certifying the thesis entitled "**Spectral aerosol optical depths and radiative forcing : Seasonal and spatial variations**" by Rohit Srivastava under my guidance. He has completed the following requirements as per Ph.D. regulations of the University:

(a) Course work as per the university rules.

(b) Residential requirements of the university.

(c) Regularly submitted six monthly progress reports.

(c) Presented his work in the departmental committee.

(d) Published/accepted minimum of one research paper in a referred research journal.

I am satisfied with the analysis of data, interpretation of results and conclusions drawn.

I recommend the submission of thesis.

Date: 2011

Dr. S. Ramachandran
(Supervisor)
Physical Research Laboratory
Ahmedabad, India.

Countersigned by
Head of the Department

DECLARATION

*I, Rohit Srivastava, S/o Mr. Suraj Prasad Srivastava, resident of B 005, PRL residences, Navrangpura, Ahmedabad - 380009, hereby declare that the research work incorporated in the present thesis entitled "***Spectral aerosol optical depths and radiative forcing : Seasonal and spatial variations***" is my own work and is original. This work (in part or in full) has not been submitted to any University for the award of a Degree or a Diploma. I have properly acknowledged the material collected from secondary sources wherever required. I solely own the responsibility for the originality of the entire content.*

Date:

Rohit Srivastava

(Author)

रोचसे दिवि रोचसे अन्तरिक्षे
पतंग! पृथ्व्यां रोचसे रोचसे अप्स्वन्तः
उभा समुद्रौ रुच्या व्यापथ

अथर्ववेदः १३.२.३०

You shine in the heaven. You shine in the space,
O Sun ! You shine on the Earth and you shine inside the waters.
You have pervaded both the oceans with your shining.
Atharvaveda 13.2.30

To my

Family

Acknowledgments

Noble efforts have been taken to frame the thesis in its present form. It is my great delight to thank all who gave their support with dedicated spirit and have been part of my life as teachers, friends, colleagues and family members.

I feel honored in expressing my deepest sense of gratitude to Dr. S. Ramachandran under whose able guidance I could shape out my thesis. I am grateful to him for his constant support, inspiration, encouragement and motivation during this entire work period. I have greatly benefitted from his vast scientific knowledge and positive attitude. His supervision helped me throughout my research and writing of this thesis.

I am very much indebted to Dr. Varun Sheel for his suggestions and thorough review of the thesis work. I place on record my thanks to Mr. T. A. Rajesh for his help and suggestions, and for his help in maintaining all the instruments.

I would like to thank Prof. J. N. Goswami, Director, Physical Research Laboratory (PRL), and Prof. A. S. Joshipura, Dean, PRL for providing me all the necessary facilities to accomplish the thesis work.

I thank Prof. B.L. Ahuja, Head, Physics Department, Prof. Rajesh Pandey (Physics Department), and Prof. K.Venugopalan, Dean, Post Graduate Studies, Mohanlal Sukhadia University for their kind cooperation throughout the thesis work.

I am grateful to Profs. A. Jayaraman, Shyam Lal, R. Sekar, R. Ramesh, M. M. Sarin, U. Sarkar, S.D. Rindani, S. Mohanty, V.K.B. Kota, J. Banerji, P K. Panigrahi and Drs. B. Bapat, K.P. Subramanian, D. Pallamraju, Sunil Singh, J. S. Ray, K. K. Marhas, R. Rangarajan, Jitesh Bhatt, Namit Mahajan and H. Mishra for encouragement at various stages of my thesis.

I thank Drs. Y. B. Acharya, Dibyendu Chakrabarty, R. Rengarajan, Ravi Bhushan, M. G. Yadava, Som Kumar Sharma and Navin Juyal for their support on various occasions.

Thanks are due to Venkataramani sir, Sunil Bhai, Narayanan ji, Bhavsar Bhai, Neeraj Bhai, Ubale ji, Pranav Bhai, Manan Bhai, Johnson Bhai, A. D. Shukla ji , R. P. Singh ji for their help and support. I am thankful to the staff of Infrared Observatory, Mount Abu for providing nice hospitality and support during the observation periods at Gurushikhar.

My sincere thanks to Dr. Prabhakar Sharma for his help and care during course work at PRL, and Dr. Bhushit for advice and help during reviews at PRL and Ph.D. registration at Udaipur.

I would like to thank Dr. R. P. Singh for his concern towards the progress of my work.

I am thankful to Dr. Angom Dilip Kumar Singh, for his training on various numerical

and computational methods and I thank Prof. R. Ramesh for improving my knowledge on statistical methods.

I wish to thank Drs. K Krishna Moorthy and Suresh Babu (Space Physics Laboratory, VSSC, Trivandrum) and C. B. S. Dutt (NRSC, Hyderabad) for their help and support. I thank ISRO-GBP, ISRO Headquarters, Bengaluru, for funding support. I acknowledge National Oceanic and Atmospheric Administration (NOAA) Air Resources Laboratory, USA for the HYSPLIT model and NOAA- Cooperative Institute for Research in Environmental Science (CIRES) Climate Diagnostic Center, USA for providing National Centers for Environmental Prediction (NCEP) reanalysis data of wind, relative humidity and columnar water vapor. Columnar ozone from Ozone Monitoring Instrument (OMI), Goddard Chemistry Aerosol Radiation and Transport (GOCART) model derived aerosol optical depths (AODs) and MODerate Resolution Imaging Spectroradiometer (MODIS) AODs are downloaded from Goddard Earth Sciences Data and Information Services Center (GES-DISC), National Aeronautics and Space Administration (NASA) USA.

I am grateful to Drs. B.N. Holben (NASA GSFC, Mongu, Abu Dhabi, Karachi, and Gandhi College), A.L. Contreras (Mexico City), E.C.-Agullo (Tamanrasset), P. Goloub (Djougou), Ramesh P. Singh and S. N. Tripathi (Kanpur), S.-C. Liew and S.V. Salinos Cortijo (Singapore), Y.J. Kim (Gwangju), and I. Sano (Osaka), the principal investigators of the respective AErosol RObotic NETwork (AERONET) sites, for their efforts in establishing and maintaining the AERONET, the data of which are used in the study.

PRL high performance computing cluster (PRL-HPC) is used for the coated sphere Mie calculation and radiative forcing computation. I thank Jigar Bhai and Anish Parwage for their help and support.

I thankfully acknowledge the help from all the members of computer center Dholakia ji, Jigar Bhai, Tejas Bhai, Mishra ji, Alok and Mrugesh regarding computational/technical support. I thank Nishtha madam, Pragya, Alam and other library staff members for their cooperation and facilitating me with the required books and journals. Thanks are due to Parul madam, Pauline madam, Priti madam, Nandini madam, Jayashree madam, Ranganathan sir, Gupta ji, Ghanshyam Bhai, Pradeep Kumar Sharma, Senthil Babu, Pillai sir, Yadav ji and Sivadasan ji for their help in various stages.

I am thankful to Drs. Sumita Kedia and Ramya S. Raman for their help and support during the period of my thesis work.

I thank all my seniors, Drs. D. Ganguly, H. Gadhavi, L. K. Sahu, N. Rastogi, P. Pathak, Santosh K. Rai, Rudraswami, Y. C. Nagar, Madhav Krishna Murari, Bhavesh G. Patel,

J. P. Das, Subimal, Shreyas, Rajesh Kushawaha, Ritesh, Salman, Akhilesh, Santosh K. Singh, Ashutosh K. Singh, Shilpy, Shuchita, Sumanta, Kirpa Ram, Waliur Rahaman, Gyan, Naveen, Sanjiv, Ram Ajor Maurya, Ashwini Kumar, Lokesh Dewangan, Latha, Mala, Sunita, Zeen, Rubi and Amitava, for their concern and help. I also thank Mr. Alok Saini, B. K. Mani, Bhavik, Vishal, Harinder and Manan Vyas for their help and support.

I am thankful to my cheerful batchmates Ashok, Vivek, Sreekanth, Vimal, Vineet, Amzad, Anand, Rabiul, Naveen, Arvind, Soumya, Sandeep, Pankaj, Jayati, Nageshwar, Bhaswar, Suman, Priyam and Suratna for providing a happy environment during my stay in PRL. I would like to thank my friends Ribu (IIT, Bombay), Padma (NARL, Gadanki), P. R. Sinha (TIFR, Hyderabad), Sumit (IITM, Pune), Shilpa (Goa University), Binita Pathak (Dibrugarh University), Shailesh (Dalhousie University, Halifax, Canada) and Nishi (IISc, Bangalore) for their help.

I wish to thank Prashant, Arvind Saxena, Srinivas, Chinmay, Neeraj Awasthi, Patra, Satinder, Vaity, Shashi, Arun, Sharad, Reddy, Moumita, Kabitri, Fazlul, Naveen Negi, Amrendra, Koushik and many others have helped me in several ways in the course of my Ph.D.

I am grateful to Drs. Sanjay Pandey and Ajai Kumar (L.B.S. P. G. College, Gonda, U.P.), and Profs. J. P. Srivastava, S. K. Singh and Mr. S. K. Gupta (Aligarh Muslim University, Aligarh) who always provided helpful suggestions to me.

I am always owed, from my inner core to friends for their suggestions, invaluable cooperation and constant encouragement.

I am very thankful to Dr. Rohit Srivastava (P.D.P.U., Gandhinagar) for his care, affection and support at various stages.

Finally, I thank all the members of my family, to whom this thesis is dedicated. It is my pleasant duty to recall with gratitude the ever lasting affection, encouragement and all support I have been receiving from my parents. I cannot forget the innocent love of my younger sisters Shailley and Shachi which has always been a source of inspiration to me.

Lastly, I thank all the persons who have, directly or indirectly, helped me during my Ph.D. Thesis.

Rohit Srivastava

Abstract

Atmospheric aerosols modulate the Earth - atmosphere radiation balance by scattering and absorbing the incoming solar and outgoing terrestrial radiation, and the strength of this perturbation is quantified as the "*aerosol radiative forcing*". The thesis work concerns with the regional and seasonal variations of aerosol optical and radiative properties, and the uncertainties in aerosol radiative forcing associated with mixing state of aerosols. The mixing state of aerosol can also have regional and temporal variations depending upon the availability of different aerosol species and favorable meteorological conditions. The objective of the work is to study the spatio-temporal variabilities in aerosol optical properties and their effect on aerosol radiative forcing over, urban, polluted and other different environments spread across the globe. The probable mixing state of aerosol is determined using measured and modeled spectral aerosol optical properties, and the seasonal variations of aerosol mixing state over environmentally distinct locations (such as urban, polluted, dust dominant, and biomass burning influenced regions) over the globe including the Indo-Gangetic plain (IGP), and the implications of aerosol mixing state on aerosol radiative forcing are studied.

Aerosol radiative forcing at the Earth's surface is estimated by collocated measurements of broad-band global fluxes and aerosol optical depths (AODs) over an urban location, Ahmedabad in western India, during 2008. AOD at 0.5 μm shows large seasonal variability with higher values (0.52) during monsoon. The enhancement in AOD during monsoon is mainly due to increase in relative humidity which overwhelms the effects of wet removal of aerosols and addition of sea salt. The influence of different single scattering albedo (SSA) values on aerosol radiative forcing is determined using the SSA obtained from ground-based measurements and columnar SSA derived from remote sensing instrument and model. Forcing efficiency for monsoon season is lower when compared to other seasons due to higher SSA in monsoon. Model estimated surface forcing using surface based SSA is about two times higher than observed forcing for different seasons except for monsoon. However, model estimated forcing using columnar SSA agrees well with observations except in monsoon.

The influence of aerosol mixing state on aerosol optical properties and radiative forcing is investigated over Ahmedabad. Aerosol forcing at the surface calculated

from measurements matches well with forcing estimated for probable mixing states determined for SSA derived from Ozone Monitoring Instrument (OMI) except in monsoon. Probable mixing states of aerosols and variable mass fractions of aerosol species (black carbon (BC), dust, sea salt, water soluble (WS) and insoluble) involved in core-shell mixing vary as a function of season and with SSA. Atmospheric forcing for probable mixing states derived for in situ SSA is $\sim$ 3 to 7 times higher when compared to those obtained for OMI SSA. The study reveals that aerosol mixing state is important in assessing the impact of aerosols on regional and global climate.

Seasonal variations in mixing states of aerosols over an urban and a rural location in the Indo-Gangetic plain (IGP) are determined. More than one probable mixing state is identified during a season over the urban (Kanpur) and rural (Gandhi College) locations of IGP. The degree of mixing i.e. percentage mass fraction of aerosols involved in core-shell mixing is found to exhibit seasonal variations. Different fractions of BC and WS aerosols in core-shell mixing emerges as probable mixing state during winter, monsoon and post-monsoon over Kanpur. Differences exist between measured and model derived asymmetry parameter (g) owing to non-sphericity of aerosols. However, aerosol radiative forcing is found to be weakly sensitive to the variation in g.

Aerosol mixing states are determined over environmentally distinct locations *viz.*, Maryland, Mexico City, Tamanrasset, Djougou, Mongu, Abu Dhabi, Karachi, Singapore, Gwangju and Osaka spread across the globe and their influence on aerosol radiative forcing is examined. Over locations influenced by biomass burning aerosols BC (core)-water soluble (WS, shell) is a preferred mixing state, while dust gets coated with anthropogenic aerosols (BC, WS) over urban regions influenced by dust. In Abu Dhabi, the change in aerosol forcing is maximum during pre-monsoon and monsoon owing to significant differences in SSA between external mixture (low SSA) and core-shell (high SSA). Karachi, a dust dominated urban location, exhibits similar features as that of Abu Dhabi. The spatiotemporal variations in mixing state of aerosols and their radiative radiative impact will be useful in regional and global climate assessment.

Key words: *Atmospheric aerosols, Aerosol optical depth, Single scattering albedo, Radiative forcing, Observations, Model estimates, Mixing state, Urban, polluted and rural locations, Environmentally distinct regions, Regional-Global scale influence.*

Contents

Chapter 1

Introduction

Earth's atmosphere is a thin layer of gases that surrounds the Earth and composed of about 78% nitrogen, 21% oxygen by volume, and trace constituents *viz.,* argon, carbon dioxide, ozone, methane and water vapor etc. are also present. In addition, particulate matter (*aerosols*) are present which are widely variable in space and time. The aim of the thesis is to study the seasonal and regional variations in optical and radiative properties of atmospheric aerosols. In this chapter the different sources, size distribution and sinks of particulate matter are described. The role of aerosols in the atmosphere is also highlighted. Finally, motivation and the objectives of thesis are described in this chapter.

1.1 Atmospheric aerosols : Source, distribution and sinks

Aerosols are a mixture of tiny solid or liquid particles suspended in air. The sources of aerosols vary widely and differ on a regional and seasonal basis leading to spatio-temporal variations in optical, physical and radiative properties of aerosols. Aerosols originate in the atmosphere by natural processes and manmade (anthropogenic) activities. They are directly emitted from different sources and/or can be formed by chemical reactions and physical processes in the atmosphere. The natural sources of aerosols include sea spray, wind blown mineral dust, volcanic aerosols (directly emitted and formed due to gas to particle conversion), biogenic aerosol production, smoke from biota burning on land, and natural gas to particle conversion products *e.g.,* sulfate aerosols formed by dimethyl sulfide emitted from ocean surface.

Humankind has important influence on terrestrial atmosphere. The concen-

tration of particulate matter (aerosols) has increased considerably due to industrial activities and transportation (*IPCC*, 2007). Anthropogenic aerosols are produced by human activities from industrial wastes, exhausts from vehicle, fire and explosions, biomass burning, soil erosion in agriculture and open mining. At present the contribution of the anthropogenic aerosol to the total aerosol mass is significant (*IPCC*, 2007).

The size span of aerosol ranges from 0.001 μm to 100 μm. According to their sizes they are divided as: (i) nucleation mode (0.001 to 0.1 μm), (ii) accumulation mode (0.1-1.0 μm), and (iii) coarse mode aerosols (>1.0 μm). The nucleation mode aerosols are newly emitted from processes involving condensation of hot vapors, or freshly formed particles through gas to particle conversion. Nucleation mode aerosols have higher number concentration, but due to their smaller size they account for lower mass fraction of airborne particulate matter. Due to their high number concentration they are exposed to rapid coagulation and/or condensation of vapors and they get converted into the accumulation mode. The accumulation mode aerosols generally account for most of aerosol surface area and contribute substantially to aerosol mass. The coarse mode aerosols are mainly formed by mechanical attrition processes and hence soil dust, mineral dust, sea spray and industrial dust fall within this mode.

The presence of different types of aerosols over a location due to local sources and long-range transport can result in different mixing states because of aging and interaction among different aerosols. In the atmosphere aerosols can exist in different mixing states. For example, in external mixing there exists no physical and chemical interaction among the different aerosol species. In core-shell mixing, one type of aerosol (*e.g.,* black carbon) gets coated by other type of aerosol (*e.g.,* sulfate). In homogeneous internal mixing all types of aerosols can be mixed together which results in an aerosol entity with the same chemical composition. The diversity of aerosols present over a location due to regional sources and long-range transport results in a complex mixture of different aerosol species in the atmosphere (e.g., *Ramanathan et al.*, 2001a). The mixing state of aerosols also exhibit spatial and temporal variations (e.g., *Ramanathan et al.*, 2001b; *Hasegawa and Ohta*, 2002; *Zhang et al.*, 2003; *Clarke et al.*, 2004; *Mallet et al.*, 2004; *Arimoto et al.*, 2006).

Aerosols are removed from the atmosphere by different removal processes. Dry deposition (sedimentation) is a more efficient removal process for larger aerosols, wherein the aerosols get settled down due to gravity. Aerosol mobility in the lower atmosphere is less when compared to higher altitudes, as the atmosphere is denser at lower altitudes. As the settling velocity is directly related to mobility, aerosols at lower altitude have less settling velocity. Wet deposition process can be divided into three categories *viz.,* rainout, washout and sweepout and is the most efficient sink process for particles smaller than 1 μm. In the rainout process aerosols act as cloud condensation nuclei and subsequently fall to the surface as rain drops. If aerosol already exists in cloud drop, and it grows to larger size to fall as rain, then the aerosols get washed out. The raindrop can impact the aerosols present below the base of a raining cloud and can lead to the incorporation of the aerosols into the raindrop, and then are swept out from the atmosphere (*Seinfeld and Pandis*, 1998).

After the production of aerosols in the atmosphere they can travel a long distance prior to their removal from the atmosphere. Aerosols can undergo coagulation and/or condensation and the size of aerosol can increase. The residence time of aerosols in the atmosphere is mainly influenced by the processes of formation, coagulation, removal and transformation (*Jaenicke*, 1993). At steady state, the residence time of aerosol is defined as the ratio of aerosol concentration present at that time to the production/loss rate. Residence time is determined by the combined effects of the possible production and removal processes. The residence time of aerosols in the atmosphere mainly depends on the size of aerosols and the altitude where they are present. The residence time of nucleation mode aerosols is about a day in the atmosphere. Accumulation mode aerosols have a longer residence time when compared to nucleation and coarse mode aerosols. Accumulation mode particles have a typical atmospheric lifetime of around 1-2 weeks, as removal by scavenging or dry deposition is not very efficient. Therefore, accumulation mode aerosols are involved in long-range transport. Coarse mode aerosols are more efficiently removed through sedimentation. The residence time of aerosols in the size range of 0.01 to 10 μm is about a week in the lower troposphere and it increases with altitude. In the stratosphere the residence time of aerosols ranges from a few months to years.

1.2 Role of aerosols in the atmosphere

Solar energy is the major driving force behind the Earth's atmosphere. The incoming flux (solar energy per unit area per unit time) should be equal to the outgoing terrestrial radiation at the top of the atmosphere on an annual mean basis. Atmospheric aerosols can modulate the radiative balance between the incoming solar and outgoing terrestrial radiation and thereby affect the Earth-atmosphere radiation budget. The corresponding imbalance in the net irradiance at any level in the atmosphere due to any species in the atmosphere (*e.g.,* greenhouse gases, solar irradiance, ozone and aerosols) quantified in units of watts per square meter, is known as '*radiative forcing*'. The negative forcing due to a species in the atmosphere indicates a loss of energy and results in a cooling effect, while positive forcing due to a species represents a gain of energy and indicates warming effect.

The greenhouse gases in the atmosphere exhibit positive radiative forcing as they absorb the infrared radiation and warm the atmosphere. These gases have longer residence times and are globally well mixed, and the radiative effects of greenhouse gases are homogeneous throughout the globe. Conversely, aerosols are one of the important species which can absorb as well as scatter the radiation and have significant impact on the Earth - atmosphere radiation balance either directly and/or indirectly. In direct effect, aerosols alter the balance of Earth-atmosphere system by scattering and absorbing the solar and terrestrial radiation. The scattering and absorption properties of aerosol depend on its chemical composition, refractive index and the size distribution. Different types of scattering and/or absorbing aerosols can reduce the radiation reaching the Earth's surface which leads to a cooling of the surface, while their effect in atmosphere varies with altitude (*Haywood and Boucher*, 2000; *IPCC*, 2007). In the indirect effect aerosols affect the life time and microphysical properties of cloud. Atmospheric aerosols can act as cloud condensation nuclei, from which the cloud drops are produced. Clouds formed in polluted environment can result in the formation of larger number of smaller droplets which causes an increase in cloud albedo and leads to a cooling effect (*Twomey*, 1977). The direct and indirect effects are strong function of aerosol abundance, composition, size distribution and their mixing

states. The present study mainly focuses on the direct effect of aerosols and their regional and temporal variations.

Black carbon (BC) aerosols have emerged as significant component of aerosols due to their role in affecting air quality and their influence on regional and global climate. Black carbon aerosols are mainly generated as primary particles from incomplete combustion of fossil fuel and biomass burning. Thus, most of the BC in the atmosphere mainly originates from manmade activities. Biofuel combustion produces large amount of BC in South Asia (*Venkataraman et al.*, 2005). BC is recognized as the second strongest contributor to global warming after carbon dioxide due to absorption of sunlight and their warming effect (*Ramanathan and Carmichael*, 2008).

Global climate model studies suggest that greenhouse gases and solar radiation contribute about 20% to total positive radiative forcing, while 10 and 20% of total radiative forcing goes in heating the Earth, almost all into the oceans and balanced by cooling by volcanic aerosols respectively since 1950 (*Murphy et al.*, 2009). The rest 50% of the positive forcing is accounted for by anthropogenic aerosols (*Murphy et al.*, 2009). The diurnal mean shortwave aerosol radiative forcing (ARF) at the top of the atmosphere (TOA) over the global oceans using satellite data during 2000-2001 was estimated to be -0.5 $\pm$ 1.7 Wm^{-2} (*Christopher and Zhang*, 2004). The ARF over northern hemisphere was found to be about 1.5 times higher than the forcing value over southern hemisphere (*Christopher and Zhang*, 2004). However, clear sky shortwave aerosol radiative forcing over global land areas during 2000-2001 using the same methodology was found to vary between -3.5 Wm^{-2} and -7.8 Wm^{-2} with a global mean of -5.1 $\pm$ 1.1 Wm^{-2} (*Patadia et al.*, 2008). ARF over the land area of the northern hemisphere was about 10% higher than that of the southern hemisphere (*Patadia et al.*, 2008).

Global annual mean BC forcing at the top of the atmosphere is 0.9 Wm^{-2} (varies between 0.4 to 1.2 Wm^{-2}) and is equivalent to $\sim$ 55% of the forcing due to CO_2 (*Ramanathan and Carmichael*, 2008). However, the other aerosols such as sulfates, nitrates and organics scatter the radiation and give rise to a negative forcing at top of the atmosphere. The aerosol radiative forcing values obtained by many general circulation climate models (GCMs) are mostly in the lower range of 0.2 Wm^{-2} to 0.4 Wm^{-2} (*Jacobson*, 2001), one of the possible causes could be the lack of information of the in-

ternal mixing state of BC with other aerosols (*IPCC*, 2007). Observations showed that BC is internally mixed with sulfates, organics and other aerosols (e.g., *Guazzotti et al.*, 2001) and such mixing enhances the BC forcing by a factor of two (*Jacobson*, 2001).

GCM results indicated that anomalous heating of the atmosphere by absorbing aerosols can give rise to an advancement and strengthening of Indian monsoon and can lead to an enhancement in rainfall anomaly over Indo-Gangetic Plain (IGP) in India and Bay of Bengal (*Lau et al.*, 2006). Natural and anthropogenic aerosols over the IGP get accumulated in the base of Himalayas during pre-monsoon (March - May) and act as an elevated heat source. These aerosols absorb the solar radiation and heats the air above the slope of Himalayas. The warm air rises over the southern downhill of the Tibetan Plateau, and afterward more warm and moist low level air are drawn from the Indian Ocean at the onset of monsoon season (*Lau et al.*, 2006).

Global climate model study of *Menon et al.* (2002) explored the role of aerosols in changing precipitation trend in recent decades over China and India. It was found that increasing BC concentration trend from different industrial and vehicular emissions and fossil fuel combustion could increase rainfall in the south and drought in north China (*Menon et al.*, 2002). BC being an absorber reduces the amount of solar radiation reaching the Earth's surface and this mechanism enhances the atmospheric instability and can significantly contribute to the increased rainfall over south China (*Menon et al.*, 2002). Nevertheless, this process can increase dust storms and drought in north China, in addition can be responsible for climate change in India (*Menon et al.*, 2002). Due to the complexity of aerosol generation processes and relative shorter life times the physical, optical and radiative properties of aerosols are rather variable. A detailed information of aerosol characteristics is necessary for a complete understanding of variabilities in aerosol properties over different environments, and their influence on the regional as well as global climate. Therefore, consistent, high quality real time data on aerosol characteristics are necessary on a regional basis. These aerosol characteristics can be used in modeling for an accurate assessment of climate impact of aerosols.

1.3 Motivation

The role of aerosols in the Earth's radiation budget is one of the largest sources of uncertainty in validating the model prediction of climate change (*IPCC*, 2007). The three major sources that contribute to the uncertainty on aerosols and their radiative forcing are, inaccuracy in atmospheric burden and the anthropogenic contribution, uncertainties in the optical parameters, and uncertainties/assumptions involved while implementing the optical properties to obtain quantitative estimates of radiative forcing (*IPCC*, 2001). The inaccuracies in aerosol optical parameters arise from uncertainties in size distribution, chemical composition and paucity of observations and knowledge on the state of mixing. The uncertainties in aerosol radiative forcing from the given atmospheric burdens and optical parameters arise from uncertainties in parameterization of relative humidity effects (e.g., *IPCC*, 2001).

South Asia is densely populated and therefore is a potential source region of aerosols which produces various anthropogenic aerosols such as sulfate, nitrate and black carbon etc. (*Menon et al.* 2002; *Ramanathan et al.* 2005). The influence of radiative effects of aerosols on Earth's radiation budget over this region on regional scale and its global impact are important as it is a hot spot. Aerosol optical depth (AODs) are found to increase across India in the last decade and AOD trends exhibit spatial, seasonal and annual mean variations over the Indian subcontinent (*Ramachandran et al.*, 2011). An increase in AODs was seen over the places dominated by manmade and natural sources of aerosols. The increase in the amount of fine mode aerosols results in an enhancement in AODs over manmade aerosols dominated region, while an increasing trend in AODs over the region influenced by natural aerosols indicates an increase in aerosols from natural sources (*Ramachandran et al.*, 2011).

In majority of investigations, aerosol optical properties are measured and used in the radiative transfer models to estimate aerosol radiative forcing. Assumptions associated with aerosol optical properties can cause uncertainties in aerosol radiative forcing estimates made using radiative transfer models (*IPCC*, 2007). However, aerosol radiative forcing estimated from direct flux measurements which are highly sensitive and accurate can have less uncertainty than that estimated using models.

So far over India, the aerosol radiative forcing was estimated using measured aerosol optical properties as inputs in a radiative transfer model. For the first time, in this study, aerosol radiative forcing on a seasonal mean basis is obtained using the measured fluxes and aerosol optical properties over western India, and compared and contrasted with the model results, and inferences are drawn. Aerosol forcing from observations are rare and available only for a particular season (*e.g.,* winter and dry seasons) over India (e.g., *Pandithurai et al.*, 2004). The seasonal variation of surface aerosol forcing estimated from the observed flux over India is so far not available during all the seasons, to the best of our knowledge.

In most models aerosols are assumed to be externally mixed which is the simplest form from a computational perspective (e.g., *Lohmann et al.*, 1999). However, different types of aerosol mixing states are observed in several field studies and it strongly varies with location and season (e.g., *Ramanathan et al.*, 2005; *Hasegawa and Ohta*, 2002; *Zhang et al.*, 2003; *Mallet et al.*, 2004). Although, the observations show that in the atmosphere aerosols are present in an internally mixed state, it is difficult to incorporate in climate models. The assumption of various mixing states of aerosols increases the number of degrees of freedom enormously which are associated with the system of composite particles. In addition, mixing changes the aerosol size and chemical composition which are dependent on relative humidity (e.g., *Lesins et al.*, 2002; *Pilinis et al.*, 1995).

In the present study, seasonal variations of aerosol optical properties and aerosol radiative forcing deduced from flux measurements and estimated from radiative transfer model over an urban location, Ahmedabad, are presented. The thesis also documents the probable mixing state of aerosols and its seasonal variation over environmentally different locations over India and around the world, and discusses the radiative implications. The knowledge on the probable mixing state over environmentally distinct regions over the globe and its impact on aerosol radiative forcing will be useful in assessing the role of aerosols on regional and global climate.

1.4 Objectives

The objectives of the research work are to measure and estimate aerosol radiative forcing by utilizing spectral aerosol optical properties, determine the mixing state of aerosols, and study their seasonal variations for different environments in India and globe.
The specific objectives of the thesis work are as follows:

1. *To study the seasonal variations in aerosol radiative forcing from the measured spectral aerosol optical properties and ground reaching global, direct and diffuse fluxes over an urban location.*

2. *To investigate the cause of differences between the aerosol radiative forcing deduced from observation and estimated by a radiative transfer model using measured spectral aerosol optical properties and fluxes.*

3. *To determine the mixing state of aerosols using measured and modeled spectral aerosol optical properties, and study seasonal variations of aerosol mixing state over environmentally distinct locations (such as urban, polluted, dust dominant and biomass burning affected regions) over the globe including the Indo-Gangetic plain, and to study the implications of aerosol mixing state on aerosol radiative forcing.*

Chapter 2 provides a brief description of the various instruments used in the study alongwith their measurement techniques. Methodology to estimate optical properties for different types of core-shell mixing of aerosols for a range of relative humidities is also described in *Chapter 2*. Spectral variations of aerosol optical properties and radiative forcing for different continental aerosol models are also described in *Chapter 2*. The results on the differences between aerosol radiative forcing at the Earth's surface estimated by simultaneous measurements of broadband global fluxes and spectral aerosol optical depths (AODs), and calculated using radiative transfer model over an urban location in western India, namely, Ahmedabad are discussed in *Chapter 3*. In order to understand these differences in radiative forcing, the influence

of aerosol mixing state on aerosol optical properties and radiative forcing are also investigated and discussed in *Chapter 3*.

The seasonal variations in probable mixing states over an urban and a rural location in the Indo-Gangetic plain (IGP) India, and their impact on radiative forcing are discussed in *Chapter 4*. *Chapter 5* documents the seasonal and spatial variations of probable mixing state of aerosols and their radiative implications over different environments around the world. The study locations are chosen to investigate the variations in mixing state of aerosols over different regions where sources of aerosols and source regions that contribute to the aerosol distribution are different. These results are important and provide a continental - global scale of understanding on aerosols and their radiative effects. The conclusions from the results obtained and the scope for future research are projected in *Chapter 6*.

Chapter 2

Measurements, Data Analysis and Methodology

The main goal of the thesis is to study the spectral aerosol optical properties and aerosol radiative forcing, and its seasonal and regional variations. The instruments used in the study and brief description of their measurement techniques are discussed in this chapter. A methodology is proposed to calculate aerosol optical properties for different external and core-shell mixing scenarios and influence of relative humidity on optical properties is discussed. In addition, the approach to estimate aerosol radiative forcing using a radiative transfer model is described. The spectral dependence of aerosol optical properties and radiative forcing for continental aerosol models are discussed.

2.1 Aerosol optical depth : Microtops - II sunphotometer

Aerosol optical depth (AOD) is a measure of the attenuation of the solar radiation due to aerosols present in the atmospheric column. In the present study spectral AODs obtained from Microtops - II sunphotometers and AErosol RObotic NETwork (AERONET) are utilized.

Microtops - II sunphotometer

Aerosol optical depth measurements at five wavelengths (0.38, 0.44, 0.50, 0.675 and 0.87 μm) using Microtops II (*Solar Light Co. U.S.A.*) sunphotometer were conducted at 1-hr resolution between 0900 to 1700 IST (Indian Standard Time, GMT + 5.5 hrs) over Ahmedabad in 2008. Microtops sunphotometer has a field of view 2.5^o

and bandwidth of each wavelength channel is 0.01 μm (*Morys et al.*, 2001). Microtops has five accurately aligned optical collimators which are capable of a full field view of 2.5^o. The internal reflection is eliminated by the internal baffles which are integrated into the device. A narrow-band interference filter and a photodiode for the particular wavelength range is fitted with each channel. When the image of the sun is centered in the sun target point of Microtops, all the optical channels are oriented directly at the solar disk. As radiation reaches the collimator, bandpass filters transfer this radiation onto the photodiodes, producing an electrical current that is proportional to the radiant power.

Theoretical background

Aerosol optical depth at each wavelength is derived from the measurements of direct solar irradiances using the *Beer-Lambert-Bouguer* law. Following Beer-Lambert-Bouguer's law, the total column integrated optical depth (τ) in the atmosphere at a wavelength λ is given as :

$$\tau(\lambda) = \frac{-1}{m}\left[ln\left(\frac{I(\lambda)}{I_0(\lambda)}\right) - 2ln\left(\frac{r_o}{r}\right)\right] \tag{2.1}$$

where $I(\lambda)$ is the instantaneous solar irradiance at a particular wavelength λ, $I_o(\lambda)$ is the solar irradiance at the top of the atmosphere, m is the relative air mass which is the ratio of slant path length traveled by light beam in the atmosphere to vertical path, and r/r_o is ratio of instantaneous Sun-Earth distance to the Sun-Earth distance when $I_o(\lambda)$ is evaluated. The air mass m is calculated from the solar zenith angle (χ) using an empirical relation given by:

$$m = sec\chi - 0.0018167(sec\chi - 1) - 0.002875(sec\chi - 1)^2 - 0.0008083(sec\chi - 1)^3 \tag{2.2}$$

Equation 2.2 accounts for Earth's curvature effect and atmospheric refraction, and provides better accuracy up to zenith angles of 85^o. However, equation 2.2 is approximated to secχ for homogeneous plane parallel atmosphere and for smaller zenith angles (<60^o). The solar zenith angle is estimated from the coordinate of the measurement location and the universal time (UT). The algorithm to calculate χ was

tested and the maximum error was found to be $\pm 0.03^o$ for the entire range of latitudes and longitudes (*Morys et al.*, 2001).

Sunphotometer was periodically calibrated at a high altitude remote site Gurushikhar (24.65^{o}N, 72.78^{o}E, 1.7 km AMSL). Top of the atmosphere irradiance $I_o(\lambda)$ is calculated using Langley plot technique for all the five wavelengths listed above. The natural logarithm of the measured solar irradiance at the Earth's surface is linearly fitted with the airmass, and the intercept of best fitted line with the air mass axis provides $I_o(\lambda)$. Total columnar optical depths ($\tau(\lambda)$) are calculated for each wavelength (equation 2.1). Aerosol optical depth (τ_a) calculated by subtracting the contribution of Rayleigh scattering by air molecules and molecular absorption of different gases, and is expressed as,

$$\tau_a = \tau - \tau_r - \tau_m \tag{2.3}$$

where τ_r is the optical depth due to Rayleigh scattering by air molecules, τ_m is the optical depth due to molecular absorption by ozone, water vapor and nitrogen dioxide. The wavelength dependence of Rayleigh scattering optical depth is derived from the Rayleigh scattering coefficients of *Penndorf* (1957) :

$$\tau_r = (16.407 - 8.5284 \times 10^{-5}\lambda + 1.1522 \times 10^{-10}\lambda^2)\frac{P}{P_o} \tag{2.4}$$

where λ is wavelength in μm and P is the pressure of the atmosphere in millibar (mb) and P_o is the standard pressure (1013.25 mb). Three major sources of error in the AOD derivation arise from instrumental error due to bias and precision, ignoring the forward scattering contribution to the measured irradiance, and errors in estimation of optical depth due to Rayleigh scattering and molecular absorption. The overall uncertainty in the AOD is estimated to be 2-5% at all the wavelengths (*Kedia and Ramachandran*, 2011).

2.2 Global and diffuse fluxes : Pyranometers

Ground reaching broad-band global and diffuse fluxes in the wavelength range of 0.31 to 2.8 μm were measured using a set of pyranometers (*Kipp and Zonen Model CM21*)

over Ahmedabad. Kipp and Zonen pyranometers were calibrated at the Kipp and Zonen calibration facility. The calibration factor for pyranometer was obtained from the side-by-side comparison with a similar type reference radiometer under stable laboratory calibration lamp. The sources of uncertainty in the flux measurements and their values are given in Table 2.1. The maximum error in pyranometer measured fluxes taking into account all the sources is about 2%. Downwelling fluxes measured at each second during cloudy and clear sky days of year 2008 and averaged for five minutes are used in the study.

Table 2.1: *Sources of uncertainty in the flux measurement using CM21 Pyranometer*

Source	Uncertainty
Sensitivity	between 7 and 17 μV/Wm^{-2}
Response time	5 s
Nonlinearity	$< \pm 0.2\%$
Nonstability	$< \pm 0.5\%$ sensitivity change per year
Spectral selectivity	$\pm 2\%$
Temperature dependence of sensitivity	$<\pm$ 1% (-20^o to +50^{o}C)
Directional error	$< \pm 2\%$
Cosine response	$\pm$ 2% deviation from ideal at 60^o SZA $\pm$ 8% deviation from ideal at 80^o SZA
Tilt error	$<\pm$ 0.2% (beam 1000 W/m-2)
Total uncertainty	2%

The flux data over were available for a total of 274 days including cloudy and clear sky days of 2008. Simultaneous measurements of clear sky flux and AOD were necessary for the present study, which brought down the number of days to 91 spread over different seasons during the year.

2.3 Aerosol absorption and scattering coefficients

Single scattering albedo (SSA) is defined as the ratio of scattering to light extinction by aerosol and is the second most important parameter after AOD necessary to determine aerosol radiative forcing. Aerosol absorption and scattering coefficients were measured using a multiwavelength Aethalometer (*AE-47, Magee Scientific, USA*) and 3-wavelength Integrating Nephelometer (*model 3563, TSI Inc., USA*) respectively over

Ahmedabad. The absorption and scattering coefficients data for year 2008 are utilized.

2.3.1 Multiwavelength Aethalometer

Aerosol absorption coefficients were measured using a seven wavelength aethalometer (*AE-47, Magee Scientific, USA*). This instrument measures the attenuation of light beam at wavelengths 0.37, 0.47, 0.52, 0.59, 0.66, 0.88 and 0.95 μm transmitted through the sample collected on a quartz fiber filter (Figure 2.1) (*Hansen et al.*, 1984). The attenuation is directly proportional to the amount of black carbon (BC) loading in the filter deposit. The light transmission is detected using a set of two photo diodes, one through the sample spot and the other through a blank or an unsampled portion of the filter which is called the reference spot (Figure 2.1).

Absorption coefficients of aerosols as a function of wavelength are calculated following *Bodhaine* (1995) and *Weingartner et al.* (2003) as,

$$\beta_{abs}(\lambda) = \frac{-1}{C\,R}\frac{A\,ln(i_2/i_1)}{Q\,\Delta t} \tag{2.5}$$

where i_1 and i_2 are intensities of the sample and the reference beams respectively after a sampling time interval Δt, Q is the volume of air sampled during the time interval Δt, and A is the area of the exposed spot on the filter where aerosols are collected. C is the correction factor applied to account for any change in the absorption occurring due to multiple light scattering effects on the filter. R is an empirical correction factor and describes the change in the aethalometer response with increased particle loading on the filter. From the absorption coefficients black carbon mass concentrations are determined following *Bodhaine* (1995) and *Weingartner et al.* (2003) the details of which are given in *Ramachandran and Kedia* (2010). Aethalometer was operated at a flow rate of 3 l min^{-1} for 24 h/d at a time resolution of 5 min.

The most notable uncertainties in absorption coefficient and BC mass concentration estimates using aethalometer measurements arise due to the changes in filter scattering due to aerosol loading, underestimation of the measured aethalometer signals (or BC mass concentrations) with increasing filter loads, and empirical conversion from optical absorption to BC mass (*Bodhaine*, 1995; *Weingartner et al.*, 2003;

Bond and Bergstrom, 2006).

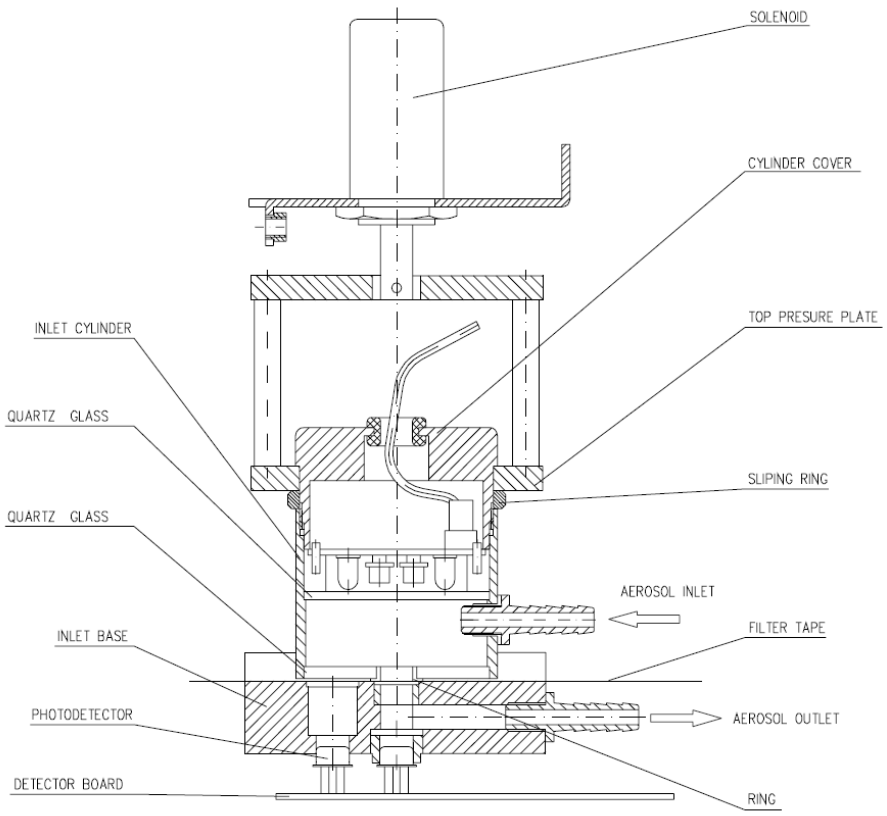

Figure 2.1: *Optical arrangement of the seven wavelength aethalometer (AE-47, Magee Scientific, USA) used for the measurement of aerosol absorption coefficient. (Source: Aethalometer, Magee Scientific Company, Berkeley, CA).*

In the present study, wavelength dependent values for C following *Bodhaine* (1995) and *Bond and Bergstrom* (2006) are used. The underestimation of BC mass concentrations with increasing filter loads, denoted by R, was found to be very prominent for pure soot particles in case of very low SSA while it was almost negligible for aged atmospheric aerosols (*Weingartner et al.*, 2003). As the annual average SSA over Ahmedabad is found to be 0.80 $\pm$ 0.10, R is assumed to be unity, and therefore the uncertainties in BC mass concentrations with increasing filter loads can be negligible (*Ramachandran and Kedia*, 2010). The value of C is found to vary depending upon the measurement location. *Collaud Coen et al.* (2010) obtained a range of C values at 0.66

μm varying from a minimum of 2.88 over a free tropospheric location (Jungfraujoch), to a maximum of 4.26 over a polluted city (Thessaloniki). The range of R (at 0.66 μm) was found to vary between 0.87 and 1.02 with a mean of 1.01 over Jungfraujoch. However, R was found to vary between 1.00 and 1.27 with a mean of 1.09 over Thessaloniki. The absorption coefficient, estimated using the range of new Collaud Coen correction factors covering the maximum and minimum values of C and R, is found to differ from the absorption coefficient used in the study by 8 to 21%. The instrumental artifacts, *viz.,* flow rate, filter spot area, and detector response are estimated to contribute an error of $\sim$3%. The overall uncertainty in the absorption coefficients and BC mass concentrations is found to lie in the range of 10 - 20% including all instrument artifacts and uncertainty in correction factors (*Srivastava et al.*, 2011).

2.3.2 Integrating Nephelometer

A three-wavelength integrating nephelometer (*model 3563, TSI Inc., USA*) which measures total aerosol scattering (β_{sca}) coefficients at 0.45, 0.55 and 0.70 μm was used in the study. The ambient air sample is drawn by the instrument through a large diameter inlet port into the measurement volume. A flash lamp is used to illuminate the measurement volume and the scattered light intensity is measured by photomultiplier tubes kept perpendicular to air flow at 0.45, 0.55 and 0.70 μm respectively. The main body of the Nephelometer consists of a thin walled aluminum tubing (Figure 2.2). The receiving optics is located at one end of the main tube and a light trap is located at the other end to provide a dark reference to view the light scattered by particles and gas as shown in Figure 2.2. The Nephelometer uses a reference chopper to calibrate scattered signals. The chopper consists of three separate areas known as signal, dark and calibrate. The signal section allows all light to pass through unaltered. The dark section is a very black background that blocks all light providing a measurement of the photomultiplier tube background noise. The calibrate section is directly illuminated by the light source to provide a measure of lamp stability over time.

The instrument is regularly calibrated by passing particle free air in the Nephelometer so that it is adjusted to read zero and span calibration is done by passing the gases of high scattering coefficient such as CO_2. The measurement is done in con-

tinuous mode with data averaging time of 5 minutes. The scattering coefficient measured by the nephelometer is highly sensitive to the relative humidity (RH). As SSA is calculated using the Aethalometer and Nephelometer measurements, the scattering coefficients are corrected for the truncation error but not for RH.

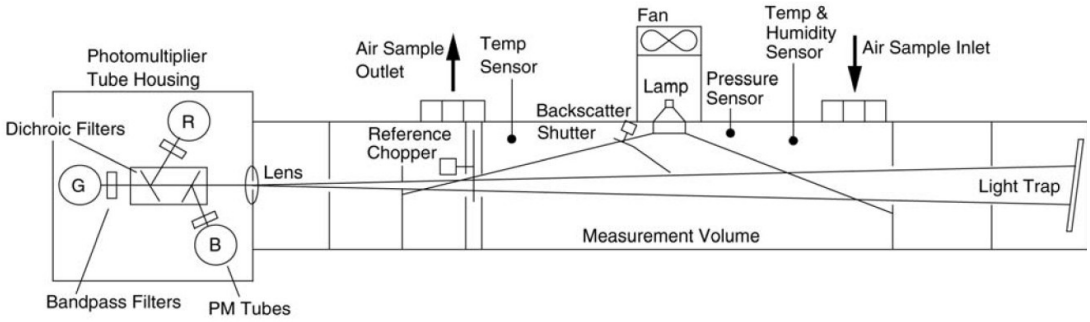

Figure 2.2: *Block diagram of the Integrating Nephelometer (model 3563, TSI Inc., USA) used for the measurement of aerosol scattering coefficient. (Source: The Integrating Nephelometer, Operation manual, TSI).*

The uncertainties in nephelometer measurements arise due to noise in the filtered air scattering coefficient, calibration drift, calibration of the instrument for Rayleigh scattering of dry air and CO_2, and truncation of near scattered forward light (*Anderson et al.*, 1996; *Anderson and Ogren*, 1998). The overall uncertainty in β_{sca} at the three wavelengths taking into account the above sources is estimated to be about 15% (*Srivastava et al.*, 2011).

Single scattering albedo can be calculated using the aerosol scattering coefficient (β_{sca}, km^{-1}) and the absorption coefficient (β_{abs}, km^{-1}) as,

$$SSA = \frac{\beta_{sca}}{\beta_{sca} + \beta_{abs}}. \tag{2.6}$$

Absorption coefficient (β_{abs}) at 0.55 μm over Ahmedabad is calculated using the mean of β_{abs} measured at 0.52 and 0.59 μm. Absorption coefficient depends on wavelength as $\beta_{abs} = K\lambda^{-\alpha}$, where K and α are the absorption Ångström coefficients, and α is a measure of spectral dependence of aerosol absorption. β_{abs} at 0.55 μm estimated using the above relation is found to differ only by 0.6% when compared to the mean

of β_{abs} measured at 0.52 and 0.59 μm; this is because the mean of 0.52 and 0.59 μm yields a wavelength of 0.555 μm which is negligibly different than 0.55 μm at which the absorption coefficients are derived using the above relation. The SSA at 0.55 μm is then calculated using β_{sca} and β_{abs} following equation (2.6). The overall uncertainty in scattering coefficient and uncertainty in absorption coefficient which includes all the sources of instrumental error in addition to the error associated with the correction factors (C and R) in absorption coefficient estimation are used in error propagation method to calculate the uncertainty in SSA. The maximum relative standard error in SSA using the error in Aethalometer derived absorption coefficients and Nephelometer derived scattering coefficients is found to be $< 10\%$ (*Srivastava et al.*, 2011).

2.4 Aerosol optical properties

2.4.1 AErosol RObotic NETwork (AERONET)

Aerosol Robotic Network (AERONET) (*Holben et al.*, 2001) measured spectral aerosol optical depths (AODs), single scattering albedo (SSA) and asymmetry parameter (*g*) over AERONET locations in India (Kanpur and Gandhi College), and around the world *viz.,* Maryland (United States of America), Mexico City (Mexico), Tamanrasset (Algeria), Djougou (Benin), Mongu (Zambia), Abu Dhabi (United Arab Emirates), Karachi (Pakistan), Singapore (Singapore), Gwangju (South Korea), Osaka (Japan) are utilized. The type of locations, their latitude and longitude and elevation, and the data period are given in Table 2.2. Seasonal mean aerosol optical properties are estimated from the monthly level 2.0 quality assured and cloud screened AERONET data. In the current study required seasonal mean aerosol optical properties could not be calculated for the same year for all the study locations due to the unavailability of data during the same year for all the seasons (Table 2.2). Therefore, seasonal means constructed from either one year or more (Table 2.2), as the case may be, are used in the current study; this approach is adopted as, in general, aerosol properties exhibit more dominant seasonal variations (*Dubovik et al.*, 2000), than interannual variations on a time scale of few years.

The interseasonal (season to season) variation in AOD is found to be higher

($\geq$30%) when compared to interannual variation ($\sim$20%) over Kanpur and Gandhi College in the 0.34 - 1.02 μm wavelength range. These features are consistent with earlier results over Kanpur using AERONET data; *Singh et al.* (2004) reported a strong seasonal variability in AODs.

Table 2.2: *Name, latitude, longitude, altitude (mean sea level, MSL) and environment type of study locations. The period (years and seasons - Win (winter), Pre-M (pre-monsoon), Mon (monsoon) and Post-M (post-monsoon)) for which AERONET data are available over each location and used in the study is also given.*

Location	Latitude (^{o}N)	Longitude (^{o}E)	Elevation (MSL) (m)	Type of location	Data Period (Seasons)
USA					
NASA GSFC, Maryland	38.9	-76.8	87	Urban	2009-2010 (Pre-M, Mon, Post-M)
MEXICO					
Mexico city	19.3	99.2	2268	High altitude, Urban	2008-2009 (Win, Pre-M, Mon, Post-M)
AFRICA					
Tamanrasset	22.8	5.5	1377	Oasis city	2007-2009 (Win, Pre-M, Mon, Post-M)
Djougou	9.8	1.6	400	Urban	2006-2007 (Win, Pre-M, Mon, Post-M)
Mongu	-15.3	23.2	1107	Biomass burning	2007-2009 (Win, Pre-M, Mon, Post-M)
MIDDLE EAST					
Abu Dhabi	24.5	54.4	15	Coastal, Dust	2006-2007 (Win, Pre-M, Mon, Post-M)
ASIA					
Karachi	24.9	67.0	49	Coastal, Urban	2009-2010 (Win, Pre-M, Mon, Post-M)
Kanpur	26.5	80.2	123	Urban	2007-2009 (Win, Pre-M, Mon, Post-M)
Gandhi College	25.9	84.1	60	Rural	2007-2009 (Win, Pre-M, Mon, Post-M)
Singapore	1.3	103.8	1	Coastal, Urban	2008-2009 (Win, Pre-M, Mon, Post-M)
Gwangju	35.2	126.8	52	Urban, Dust	2007-2010 (Win, Pre-M, Mon, Post-M)
Osaka	34.6	135.6	50	Urban	2007-2008 (Win, Pre-M, Mon, Post-M)

The interannual variations in SSA and g are $\sim$2% and 6% of the corresponding average values respectively over both the locations in the wavelength range of 0.44 to 1.02 μm. The interseasonal variation in SSA is similar to interannual variation in SSA while interseasonal variation in g is higher than interannual variation and ranges between 1-17% of corresponding seasonal mean value of g in 0.44 - 1.02 μm wavelength

range over Kanpur and Gandhi College. The emphasis of the study is on the seasonal and spatial variations in the mixing state of aerosols, and therefore interannual variations, if any, are not considered owing to the above reasons. The data period and the seasons for which data are used is given in Table 2.2.

2.4.1.1 Aerosol optical depths

AERONET Sun/sky scanning radiometer measured aerosol optical depths at seven different wavelengths of 0.34, 0.38, 0.44, 0.5, 0.675, 0.87 and 1.02 μm (*Dubovik and King*, 2000) are used. Sun/sky radiometer measures direct and diffuse solar irradiances in the wavelength range of 0.34-1.02 μm with a field of view of 1.2^o. The absolute uncertainty in AOD under clear sky conditions is $< \pm 0.01$ when λ is > 0.44 μm and $< \pm 0.02$ for shorter wavelengths when 0.44 μm AOD $\leq$0.2 (*Smirnov et al.*, 2000). The relative standard error in AODs estimated based on *Smirnov et al.* (2000) is found to be $< 10\%$ for all the wavelengths for the range of AODs obtained over the above locations during the study period.

2.4.1.2 Single scattering albedo and asymmetry parameter

Single scattering albedo (SSA) and asymmetry parameter (g) obtained from AERONET Sun/sky measurements in the wavelength range of 0.4-1.02 μm (at 0.44, 0.675, 0.87 and 1.02 μm) are utilized. SSA and g are retrieved using an inversion algorithm which searches for the best fit of all data accounted by a theoretical model considering the different magnitudes of the accuracy in the fitted data (*Dubovik and King*, 2000). The uncertainty in the single scattering albedo retrieved by AERONET is within 0.03 for high aerosol loading corresponding to an AOD (at 0.44 μm) > 0.5, while error in SSA increases to 0.05 - 0.07 for lower AOD (*Dubovik and King*, 2000). Asymmetry parameter which describes the angular distribution of scattered light is an integral measure of aerosols and the uncertainty in the retrieval of g from AERONET lies in the range of 3 - 5% (*Andrews et al.*, 2006).

2.5 Methodology

One of the prime objectives of the thesis is to investigate the optical and radiative properties of aerosols for different mixing scenarios over environmentally distinct locations around the globe. In order to study the aerosol optical properties in different mixing scenarios a methodology is proposed and described in this section. The effect of relative humidity on optical properties of mixed aerosols is also discussed. In addition, this approach is extended to continental aerosol models and aerosol optical properties are derived, and inferences are drawn. Finally, the usage of this methodology in deriving probable mixing state of aerosols using measured and modeled aerosol optical properties is discussed.

2.5.1 Aerosol optical properties in different mixing scenarios

Aerosols are produced from different sources and have different chemical composition. In the calculations, six aerosol species *viz.*, water insoluble (soil dust and water insoluble organics), water soluble (sulfate, nitrate and other soluble organics), black carbon (BC), mineral dust (coarse, accumulation and nucleation), sea salt (coarse and accumulation), and sulfate are considered to estimate the optical properties (aerosol optical depth, single scattering albedo and asymmetry parameter) of aerosols. These six aerosol species (*Hess et al.*, 1998) broadly represent the different types of aerosols present in the atmosphere (*IPCC*, 2001; *IPCC*, 2007). The optical properties of coated aerosols is estimated following the Mie theory of coated spheres, and extinction, scattering and absorption efficiencies are calculated using the *Bohren and Huffman* (1983) algorithm. Coated sphere Mie calculation requires refractive index of core and shell species, and radius of core and shell particles. Refractive index of core and shell species are taken from the Optical Properties of Aerosols and Clouds (OPAC) database (*Hess et al.*, 1998). Core to shell radius ratio (CSR) is calculated from the geometry of core-shell particles which depends upon the mass (M) and density (ρ) of the core (c) and shell (s) as,

$$CSR = \left[1 + \frac{M_s\ \rho_c}{M_c\ \rho_s}\right]^{(-1/3)} \tag{2.7}$$

where subscripts c and s correspond to core and shell respectively. All the aerosol species are assumed to follow lognormal size distribution. The size distribution parameters of core-shell mixed particles *viz.*, mode radius (r_m) and width (σ) of lognormal curve are assumed to be the same as that of the shell species distribution. This assumption is supported by scanning electron microscopy analysis of Asian dust coated by BC which showed that the mode radii of BC aggregated with dust are closer to the shell BC radii (*Arimoto et al.*, 2006).

Optical properties are calculated for different mixing states including various core-shell and external mixing scenarios. The size distribution parameters of different aerosols are taken from the OPAC database (*Hess et al.*, 1998). The mode radius (r_m, μm) and width (σ) for hydrophilic aerosols in dry state and hygroscopic aerosols at 0%, 50% and 90% relative humidities are given in Tables 2.3 and 2.4 respectively.

Table 2.3: *Physical (mode radius, μm), width of the log normal size distribution (σ) and density (ρ, g cm^{-3})) and optical (real and imaginary parts of refractive index) properties of hydrophobic aerosol species (insoluble and black carbon) corresponding to the wavelengths of 0.5, 1.0 and 3.0 μm as given in Hess et al. (1998) and used in the current study. Single scattering albedo (SSA) and asymmetry parameter (g) at 0.55 μm are given.*

Aerosol species	Mode radius	σ	ρ	Refractive index			SSA	g
				λ=0.5 μm	1.0 μm	3.0 μm		
Insoluble	0.471	2.51	2.00	1.53 -*i*8.00E-03	1.52 -*i*8.00E-03	1.16 -*i*1.20E-02	0.73	0.83
Black carbon	0.012	2.00	1.00	1.75 -*i*4.50E-01	1.76 -*i*4.40E-01	1.85 -*i*5.40E-01	0.21	0.34

Core-shell Mie calculation is done to get extinction, absorption and scattering efficiencies of single particle, then these efficiencies are integrated for the lognormal size distribution (Tables 2.3 and 2.4) to get the extinction, absorption and scattering coefficients. These core-shell composite particles are assumed to be externally mixed with other aerosols. In case of external mixing as there is no physical and chemical interaction among the aerosol species, total extinction, scattering and absorption coefficients are calculated by summing the respective coefficients of the individual species. As relative humidity (RH) plays an important role when hygroscopic aerosols are present in core or shell (*Lesins et al.*, 2002), optical properties of core-shell mixed aerosols at different RH values are estimated.

Table 2.4: *Physical (mode radius, μm), width (σ) and density (ρ, g cm^{-3})) and optical (real and imaginary parts of refractive index) characteristics of hygroscopic aerosol species (sulfate, water soluble (WS) , sea salt (SS) in accumulation, and coarse modes) corresponding to 0%, 50% and 90% relative humidity (RH) at the wavelengths of 0.5, 1.0 and 3.0 μm as given in Hess et al. (1998) and used in the current study. Single scattering albedo (SSA) and asymmetry parameter (g) at 0.55 μm are given.*

RH (%)	Aerosol species	Mode radius	σ	ρ	Refractive index λ=0.5 μm	1.0 μm	3.0 μm	SSA	g
0	Sulfate	0.069	2.03	1.70	1.43 -*i*1.00E-08	1.42 -*i*1.53E-06	1.29 -*i*9.55E-02	1.00	0.72
	WS	0.021	2.24	1.80	1.53 -*i*5.00E-03	1.52 -*i*1.55E-02	1.42 -*i*2.20E-02	0.96	0.61
	SS (acc)	0.209	2.03	2.20	1.50 -*i*1.55E-08	1.47 -*i*1.41E-04	1.61 -*i*1.00E-02	1.00	0.69
	SS (coa)	1.750	2.03	2.20	1.50 -*i*1.55E-08	1.47 -*i*1.41E-04	1.61 -*i*1.00E-02	1.00	0.79
50	Sulfate	0.098	2.03	1.25	1.37 -*i*4.21E-09	1.36 -*i*2.41E-06	1.34 -*i*2.09E-01	1.00	0.77
	WS	0.026	2.24	1.42	1.44 -*i*2.65E-03	1.43 -*i*8.21E-03	1.39 -*i*1.39E-01	0.98	0.67
	SS (acc)	0.336	2.03	1.29	1.38 -*i*4.49E-09	1.36 -*i*3.61E-05	1.43 -*i*2.09E-01	1.00	0.77
	SS (coa)	2.820	2.03	1.29	1.38 -*i*4.49E-09	1.36 -*i*3.61E-05	1.43 -*i*2.09E-01	1.00	0.85
90	Sulfate	0.135	2.03	1.10	1.35 -*i*2.23E-09	1.34 -*i*2.70E-06	1.36 -*i*2.48E-01	1.00	0.79
	WS	0.035	2.24	1.18	1.38 -*i*1.13E-03	1.37 -*i*3.51E-03	1.38 -*i*2.15E-01	0.99	0.72
	SS (acc)	0.497	2.03	1.09	1.35 -*i*2.08E-09	1.34 -*i*1.32E-05	1.39 -*i*2.52E-01	1.00	0.79
	SS (coa)	4.180	2.03	1.09	1.35 -*i*2.08E-09	1.34 -*i*1.32E-05	1.39 -*i*2.52E-01	1.00	0.86

2.5.2 Efficiency of single particle

The behavior of scattering, absorption and extinction efficiencies for a single particle of black carbon (BC) (refractive index 1.75-*i*4.40E-01), sulfate (1.43-*i*1.00E-08), BC (core)-sulfate (shell), and sulfate (core)-BC (shell) is shown in Figure 2.3 in the radius range of 0.001 to 10 μm. All these calculations are done for λ = 0.55 μm. As black carbon has an imaginary refractive index of 4.40E-01 at 0.55 μm, the extinction is only due to absorption till about 0.06 μm (Tyndall regime) and the scattering contribution is orders of magnitude less and the curve is very smooth, throughout the radius range. In stark contrast the extinction is only due to scattering for a sulfate particle throughout the radius range, while the absorption is orders of magnitude less, as the imaginary part of the refractive index is very low, and the curves of extinction and scattering, which are one and the same, tend to oscillate from about 0.2 μm when the efficiency approaches 2. The largest oscillations about this curve are those associated with scattering particles (imaginary part of refractive index $\sim$0) and the amplitude of these oscillations decreases as the imaginary part of refractive index increases, which is clearly seen in the black carbon particle as compared to the sulfate particle. On the other hand, the efficiencies of particles that are core-shell mixed show distinct behavior. The extinction efficiency resembles that of the shell (sulfate, or black carbon)

(Figure 2.3c, d).

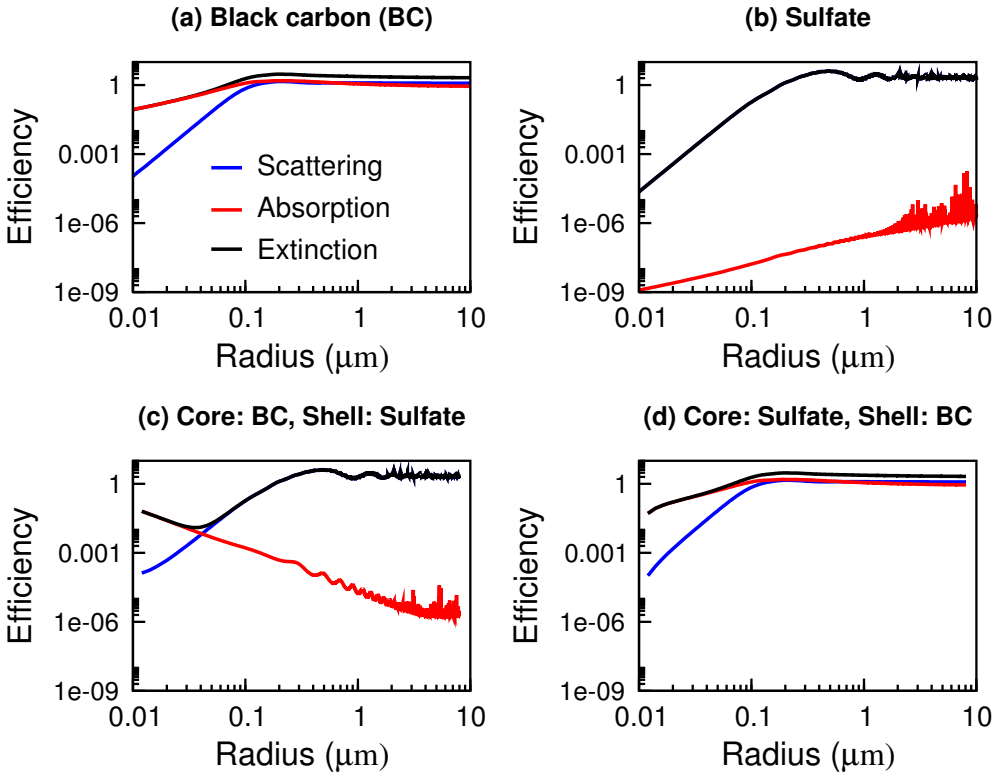

Figure 2.3: *Scattering, absorption and extinction efficiencies of single particle calculated using Mie theory at λ = 0.55 μm for (a) black carbon, (b) sulfate, (c) black carbon (core)-sulfate (shell) and (d) sulfate (core)-black carbon (shell) mixture.*

Absorption efficiency decreases almost exponentially when black carbon is in the core (Figure 2.3c), while the scattering efficiency when black carbon is in the shell (Figure 2.3d) does not vary much with respect to Figure 2.3a. This figure clearly brings out the differences in scattering, absorption and extinction efficiencies of a single particle of scattering/absorbing type and when they are core-shell mixed.

Variation in SSA for an external mixture of one particle of sulfate and black carbon, and as function of core radius for different shell thickness when BC is in core (or shell) and sulfate is in core (or shell) is plotted in Figure 2.4. SSA is close to 1 when the radius of BC is quite small for the entire radius range (Figure 2.4), while SSA is close to 0.5 when the radius of sulfate particle is quite low.

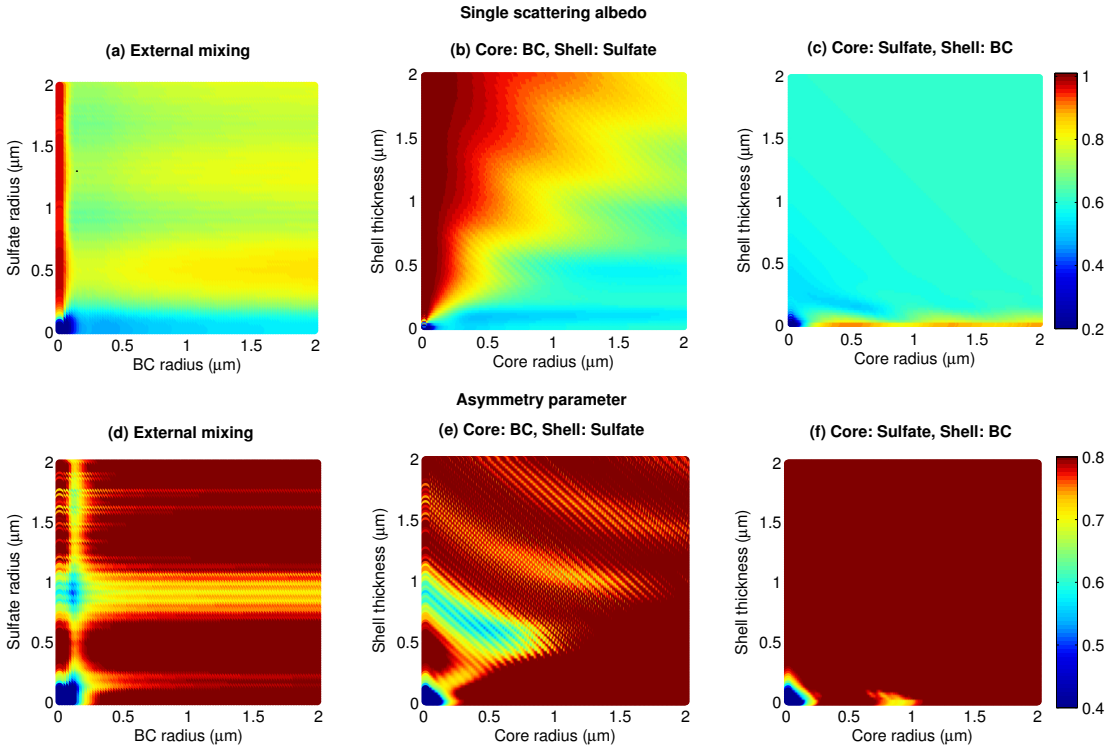

Figure 2.4: *Single scattering albedo (SSA) and asymmetry parameter for an external mixture consisting of a single particle of sulfate and black carbon each as function of radius (a and d), black carbon (core) and sulfate (shell) mixture (b and e), and sulfate (core) and black carbon (shell) mixture for different shell thickness as function of core radius (c and f) respectively. The aerosol characteristics correspond to aerosols in dry (0% relative humidity) state.*

When the radii of both sulfate and BC aerosols increase SSA is between 0.6 and 0.8 in external mixing (Figure 2.4). SSA is close to 1 for the shell thickness in the range of 0.01 to 2 μm and when the core radius is less than 0.2 μm; when core (BC) radius increases SSA decreases. SSA is even lower when the core radius (BC) is larger and shell thickness is less than 1 μm. In contrast, when sulfate is in core SSA over the entire domain is $<$0.8 and it does not significantly vary either as a function of shell thickness and/or core radius as BC (absorber as the shell) governs the SSA. SSA is close to 1 when the shell thickness is very small indicating the effect of sulfate. This suggests that when an absorbing species is in the core, and when core radius and shell thickness are higher, SSA will be higher, and when core radius is higher and shell thickness is smaller ($<$1 μm) SSA will be lower ($<$0.5). In contrast to SSA, asymmetry parameter does not

exhibit significant variation when particles are externally and core-shell mixed (Figure 2.4).

Scattering and absorption coefficients, SSA and asymmetry parameter for an aerosol size distribution containing BC (Table 2.3) and sulfate (Table 2.4) are plotted in Figure 2.5. The results are shown for external and core-shell mixing. Scattering coefficient increases as the mode radius of sulfate aerosol increases; while the absorption coefficient increases as BC mode radius increases in external mixing. SSA is close to 1 when mode radius of BC is small and decreases as mode radius of BC increases. When the mode radius of sulfate increases, as scattering dominates the extinction, SSA increases (Figure 2.5) in external mixing.

Asymmetry parameter exhibits similar variations as that of SSA in external mixing (Figure 2.5). Asymmetry parameter is higher for sulfate aerosol when compared to BC (e.g., *Hess et al.*, 1998), and increases with increase in relative humidity. Asymmetry parameter increases as the sulfate and BC mode radii increase in external mixing; as the asymmetry parameter of sulfate aerosols is higher it tends towards higher values when externally mixed, and shows a gradient as a function of the mode radii. Scattering and absorption coefficients exhibit an opposite behavior when BC is in core and sulfate is in shell. Scattering coefficient gradually increases as a function of mode radius, and is maximum when the mode radius is 2 μm and the core (BC)-shell (sulfate) ratio is quite small (Figure 2.5) as it is dominated by sulfate.

On the other hand, absorption coefficient is low up to a core-shell ratio of 0.5 and increases thereafter, peaking when the core-shell ratio is 1, because BC is in core. When BC is in core and sulfate is in shell SSA does not vary as a function of mode radius. SSA is in the 0.8-1.0 range when the core-shell radius ratio is smaller ($\leq$0.5); SSA decreases when core-shell ratio increases as BC is in core. Thus, these results reveal that SSA is less sensitive to mode radius, while it is more sensitive to core-shell radius ratio which is dependent on the mass mixing ratio.

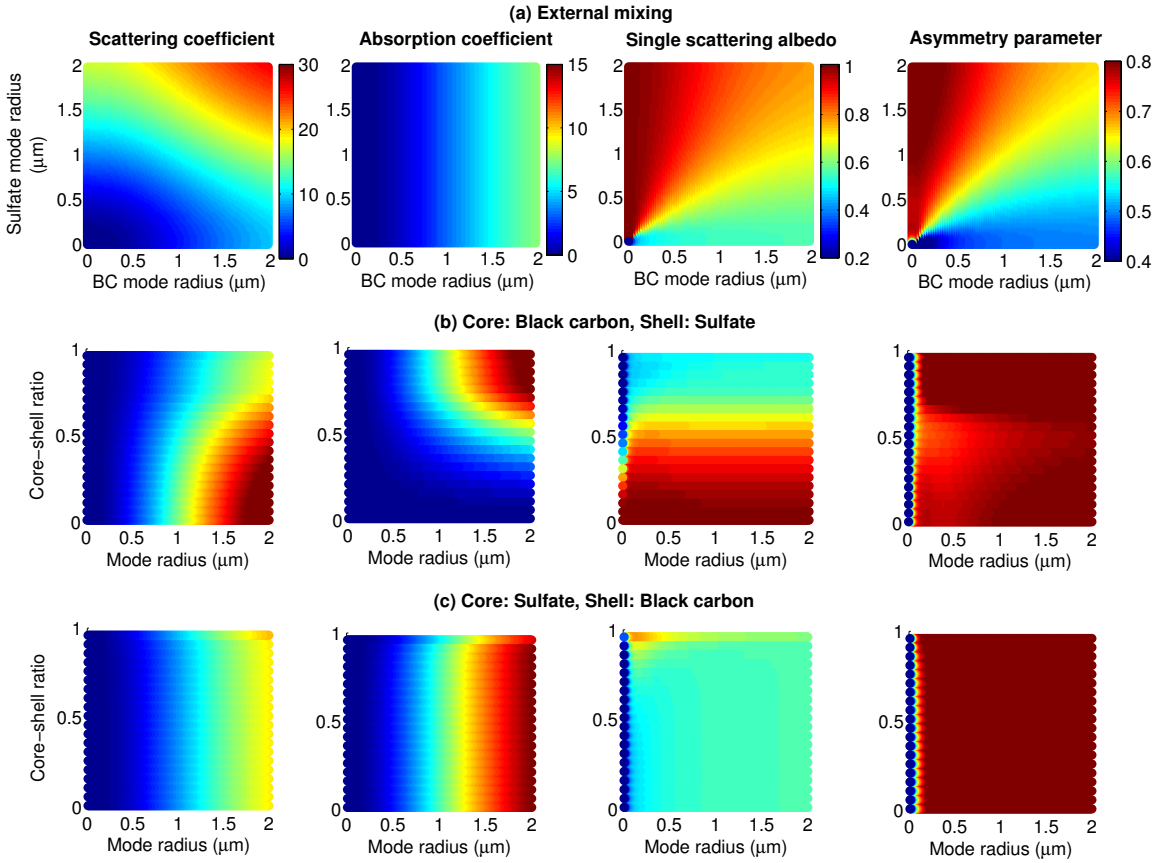

Figure 2.5: *Variation in scattering coefficient (10^{-3} km^{-1}), absorption coefficient (10^{-3} km^{-1}), SSA and asymmetry parameter for (a) external mixing of sulfate and black carbon aerosols, (b) black carbon (core)-sulfate (shell) mixture and (c) sulfate (core) and black carbon (shell) mixture. The values are given as function of mode radii for external mixture of black carbon and sulfate aerosol species, while the values are plotted as function of mode radius of core-shell mixture for different core-shell ratios. The aerosol optical properties are calculated for aerosol species in dry (0% relative humidity) state.*

In contrast, when BC (shell) coats sulfate (core) SSA is governed dominantly by BC and does not vary when mode radius increases for different core-shell radius ratios. SSA increases in sulfate (core)-BC (shell) mixing when the core-shell ratio is 1 (Figure 2.5c). It is clear that absorption gets enhanced in core-shell mixing of absorbing and scattering aerosols when compared to external mixing, thereby resulting in lower SSA (Figure 2.5). It should be noted that the single particle absorption efficiency in the Tyndall regime ($r<<\lambda$) is proportional to r/λ, where as the single particle scattering efficiency is proportional to r/λ^4 (Figure 2.3); however, the results do not follow these

proportions when an aerosol size distribution is used (Figure 2.5). Asymmetry parameter does not exhibit significant variation due to core-shell mixing and is about 0.8 for all the core-shell ratios and mode radii unlike external mixture, thus, confirming that core-shell mixing influences SSA more significantly than the asymmetry parameter.

2.5.3 Influence of relative humidity

The results discussed so far were for aerosols in dry (0% relative humidity) state. The influence of relative humidity (RH) on aerosol optical properties for different mixing scenarios are examined in this section. Extinction coefficient, SSA and asymmetry parameter at 0.55 μm as function of relative humidity along with spectral characteristics for external mixture of BC and water soluble aerosols, and their core-shell mixtures are shown in Figure 2.6. Extinction coefficient, SSA and asymmetry parameter are higher for external mixing when compared to BC (core)-water soluble (shell), and water soluble (core)-BC (shell) mixtures. The dips in SSA at around 3 μm (Figure 2.6) are attributed to an increase in the absorption characteristics of water soluble aerosols (*d'Almeida et al.*, 1991; *Lacis and Mishchenko*, 1995) (Table 2.4), while the optical characteristics of carbonaceous aerosols exhibit a gradual decrease with respect to wavelength. The real and imaginary parts of refractive index of atmospheric aerosols (Tables 2.3 and 2.4) characterize respectively their scattering and absorption capabilities. The imaginary parts of sulfate, water soluble and sea salt aerosols increase by orders of magnitude when wavelength increases from 0.5 to 3.0 μm leading to a larger absorption which results in higher extinction and lower SSA and asymmetry parameter at around 3 μm (Figure 2.6).

Extinction coefficient decreases by a factor of two when BC is in core and sulfate is in shell as compared to external mixing in the entire shortwave region for all the relative humidities. Extinction coefficient further decreases by an order of magnitude or more when water soluble aerosols are in core and BC is in shell (Figure 2.6d). SSA is higher for higher relative humidity and is lower when aerosols are in dry state. Spectral SSA exhibits the behavior of the species which acts as the shell (Figure 2.6); this is explicit when water soluble aerosol is in core and BC is in shell where the dip in SSA at 3 μm is not evident. Asymmetry parameter for external mixture of water soluble

aerosol and BC is higher than BC (core)-water soluble (shell) and increases as relative humidity increases (Figures 2.6j, k). Asymmetry parameter for water soluble (core)-BC (shell) is independent of relative humidity (Figures 2.6i, l) as BC which is in shell is hydrophobic.

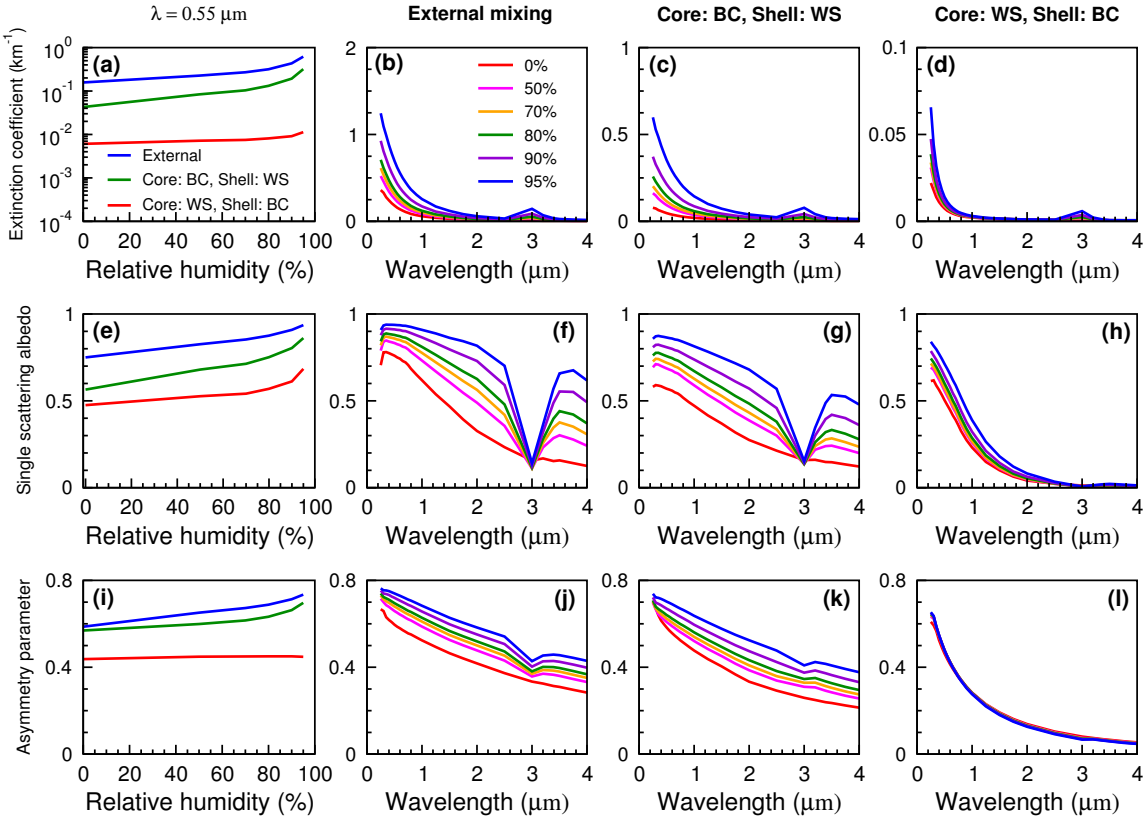

Figure 2.6: *(a) Extinction (scattering+absorption) coefficient (km^{-1}), (e) single scattering albedo and (i) asymmetry parameter at $\lambda = 0.55\,\mu m$ for a range of relative humidities for external mixture, black carbon (core)-sulfate (shell), and sulfate (core)-black carbon (shell) mixtures. Spectral behavior of aerosol extinction coefficient (km^{-1}), SSA and asymmetry parameter in the shortwave region for an external mixture of black carbon and water soluble aerosols (b, f and j), black carbon (core)-water soluble (shell) (c, g and k), and water soluble (core)-black carbon (shell) (d, h and l) respectively.*

Influence of relative humidity on AOD, SSA and asymmetry parameter for external and core-shell mixing of aerosol species corresponding to aerosol models for continent (continental clean and urban) is illustrated in Figure 2.7. Continental clean aerosol model depicts remote continental locations without or with very low anthropogenic influence. Urban model comprises water soluble, insoluble and black carbon

aerosols and represents strong pollution in urban areas (*Hess et al.*, 1998).

Table 2.5: *Mass concentrations ($\mu g\ m^{-3}$) and mass mixing ratios (%) of aerosol species water soluble (WS), insoluble (IS) and black carbon (BC) in aerosol models of continent (continental clean, average and urban) used in the study at 0, 50, 90 and 95% relative humidities.*

Aerosol model	Aerosol species	Mass concentration				Mass mixing ratio			
		0%	50%	90%	95%	0%	50%	90%	95%
Continental clean	WS	3.5	5.2	10.1	14.5	49	59	74	80
	IS	3.6	3.6	3.6	3.6	51	41	26	20
Continental average	WS	9.4	14.0	27.2	39.0	48	58	73	80
	IS	9.5	9.5	9.5	9.5	49	40	26	19
	BC	0.5	0.5	0.5	0.5	3	2	1	1
Continental polluted	WS	21.1	31.4	61.1	87.4	56	66	79	84
	IS	14.2	14.2	14.2	14.2	38	30	18	14
	BC	3.1	2.1	2.1	2.1	5	4	3	2
Urban	WS	37.6	55.9	108.9	155.8	46	56	72	78
	IS	35.6	35.6	35.6	35.6	44	36	23	18
	BC	7.8	7.8	7.8	7.8	10	8	5	4

These aerosol models are chosen (a) as they represent cleaner and polluted environments over continent, and (b) the aerosol species are common in both cleaner and polluted environments, and the polluted aerosol models have in addition black carbon aerosols. The mass mixing ratio of black carbon aerosol increases from continental average to polluted and is maximum in urban aerosol model (Table 2.5). The mass concentrations and mass mixing ratios of the aerosol components in the above models are given in Table 2.5 for 0%, 50%, 90% and 95% RH.

The mass fraction of the hygroscopic aerosol components (water soluble) in an aerosol model increases as RH increases. However, in order to maintain a constant mass mixing ratio (100%), an inherent property of the model, the mass fractions of the hydrophobic aerosols (insoluble and black carbon) decrease (Table 2.5). The core-shell radius ratio (equation 2.7) is derived on the basis of the mass mixing ratios of the aerosol species (Table 2.5), and when more than two aerosol species are present in the model, then the other species are externally mixed with the two species involved in core-shell mixing. Scattering and absorption coefficients, aerosol optical depth, single scattering albedo and asymmetry parameter calculated in this study for external mixture for all the relative humidities are exactly the same as the respective values

given in *Hess et al.* (1998) and OPAC (*Hess et al.*, 1998) suggesting that the adopted methodology is quite robust.

The vertical distribution of aerosols is given by β_{ext} (z) = β_o exp$^{-z/H}$ where β_o is the aerosol extinction coefficient at the surface, β_{ext} (z) is the aerosol extinction coefficient at an altitude z and H is the scale height which describes the slope of the aerosol profile. The scale height (H) for continental clean and urban aerosol models is 8 km (e.g., *Hess et al.*, 1998).

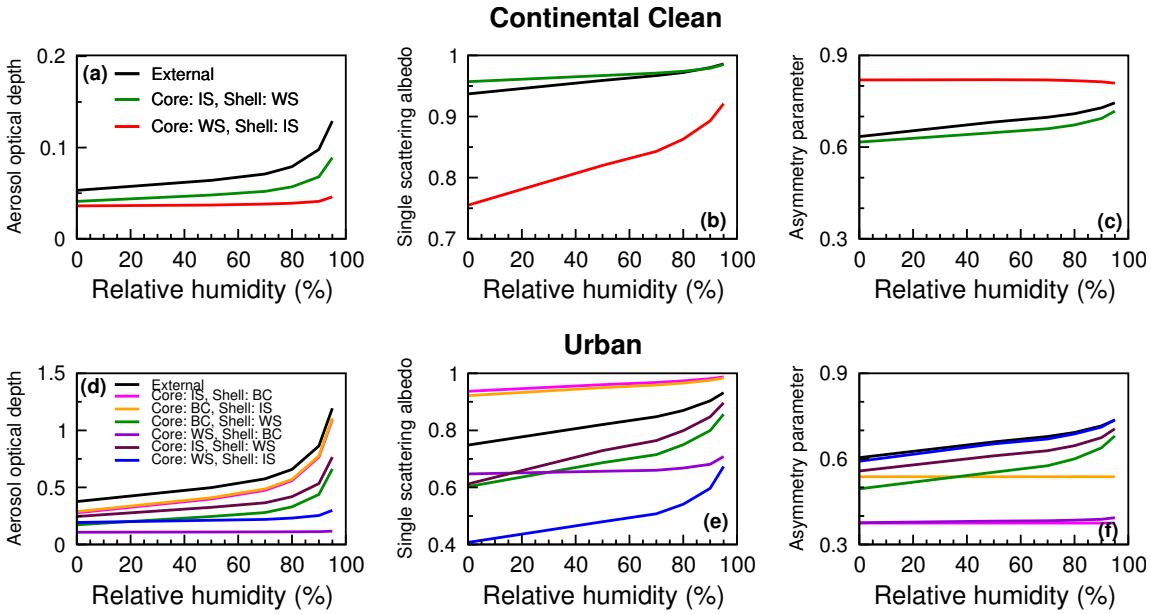

Figure 2.7: *Aerosol optical depth (a, d), single scattering albedo (b, e) and asymmetry parameter (c, f) respectively at λ = 0.55 μm as function of relative humidity for external mixtures, and core-shell mixing of aerosol species present in continental clean and urban aerosol models.*

AOD is always higher for the external mixture (Figure 2.7), and does not exhibit significant variation up to 50% RH. The rate of AOD increase is higher when RH is >70% (Figure 2.7). AOD increases by an order of magnitude between continental clean and urban aerosol models owing to an increase in the mass concentration of aerosol species (Table 2.5) and addition of black carbon aerosols.

SSA in continental clean aerosol model is lowest for water soluble (core)-insoluble (shell) mixing, and increases as RH increases. In urban aerosol model SSA for insoluble (core)-BC (shell), and BC (core)-insoluble (shell) mixing is higher than

that of external mixture. SSA is higher in the above two cases because the third species (water soluble aerosols have higher SSA) is externally mixed and dominates the mass mixing ratio (Table 2.5). SSA is quite low for water soluble (core)-insoluble (shell) mixing in continental clean and urban aerosol models. It should be noted that water soluble (core)-insoluble (shell) mixing is physically unrealistic and observations to support such mixing are unavailable so far. Asymmetry parameter is higher for water soluble (core)-insoluble (shell) in continental clean aerosol model as asymmetry parameter for insoluble aerosols is higher when compared to water soluble aerosols (Table 2.3). On the other hand asymmetry parameter decreases when BC is involved in mixing either as core/shell or external as can be seen in urban aerosol model as asymmetry parameter for BC is quite low (Figure 2.7f, Table 2.4). Thus, these results clearly illustrate that aerosol mixing at different relative humidities can modify the physical, optical and chemical nature of aerosols, and therefore are important while examining the radiative and climate impact of aerosols.

2.5.4 Sensitivity of BC mass concentration to SSA

The changes in SSA at 0.55 μm with increase in BC mass concentration due to mixing with two different types of aerosols, namely sulfate (scattering aerosols), and mineral dust (moderately absorbing aerosols) in nucleation, accumulation and coarse modes are shown in Figure 2.8. The total mass concentration of BC/sulfate and BC/dust aerosol is kept constant at 2.0 $\mu g\ m^{-3}$ and BC mass is increased from 0.01% to 99.9% of the total mass. In an urban environment BC mass concentration is $<$ 20% of total mass (*Ramachandran and Kedia*, 2010), however, as this is a sensitivity study whole range is considered. SSAs for higher total mass ($>$ 2.0 $\mu g\ m^{-3}$) are also estimated and found to be the same as reported here, as SSA is independent of the total mass. The mode radius of BC aerosol in this study is considered as 0.0118 μm following *Hess et al.* (1998). However, the mode radius of BC spherules can be in the range of 0.013 - 0.017 μm (*Jacobson et al.*, 2005). SSA is found to vary by only about 1% or less for a range of mode radii of BC (Table 2.6) when compared to 0.0118 μm, therefore, a change in the mode radii of BC aerosols is not expected to alter the results significantly. This finding is supported by *Lesins et al.* (2002). SSA for core-shell mixing of water soluble/BC are

found to exhibit similar behavior as sulfate/BC and insoluble/BC mixture has similar behavior as dust/BC (Figure 2.8). SSA decreases with increase in BC mass for external mixing, BC coated by sulfate and sulfate coated by BC. The rate of SSA decrease is found to be higher for BC shell and sulfate core. However, SSA for external mixing and core-shell mixing with BC core and sulfate shell are similar when masses of both the species are equal, and SSA for core-shell mixing cases are invariant when BC mass is further increased (Figure 2.8).

Table 2.6: *Mode radius of black carbon (BC), single scattering albedo (SSA) and percentage difference with respect to SSA obtained for BC of mode radius 0.0118 μm for the case of external mixing of BC and sulfate.*

Mode radius (r_m, μm)	SSA (0.55 μm)	% difference
0.0118	0.789	-
0.0130	0.785	0.5
0.0150	0.781	1.0
0.0170	0.779	1.2
0.0236	0.784	0.6
0.0354	0.799	1.3

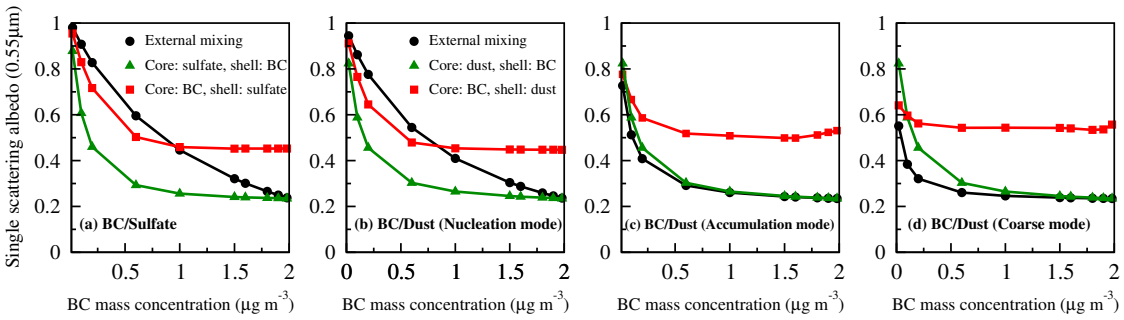

Figure 2.8: *Sensitivity of single scattering albedo (SSA) to black carbon mass concentration. (a) SSA for black carbon and sulfate mixture. SSA for black carbon and mineral dust in three modes (b, c and d).*

BC absorption is found to get enhanced when it is coated by scattering aerosols similar to the finding of *Schwarz et al.* (2008). Higher absorption corresponds to lower SSA when BC is in core and sulfate is in shell with respect to external mixing for BC mass $< 1.0\ \mu g\ m^{-3}$ (Figure 2.8). SSA is lower when BC is present in shell as compared to other mixing scenarios. SSA for BC coating of mineral dust is independent of differ-

ent modes of dust. SSA for externally mixed BC and dust in nucleation/coarse mode is higher in case of nucleation mode and lower for coarse mode when compared to BC (core) - nucleation/coarse dust (shell) mixing (Figure 2.8). SSA for BC coated by accumulation mode dust particle is almost the same as that of their external mixture (Figure 2.8). The effect of core size is not visible in SSA, as core radius is calculated using the core-shell ratio (equation 2.7). The core radius depends on the densities and the masses of core and shell species and is independent of the modal properties (mode radius and width of lognormal distribution). These results indicate that single scattering albedo of BC changes depending upon how they are mixed in the atmosphere and SSA is very sensitive to BC mass fraction.

In the case of external mixing, when BC mass concentration is less than 50% the SSA spectra is dominated by sulfate aerosols and as BC mass reaches $\geq$ 50%, spectra is mainly governed by black carbon. In core-shell mixing, spectral SSA of mixed aerosols predominantly follows the spectral characteristics of the shell species (Figure 2.9).

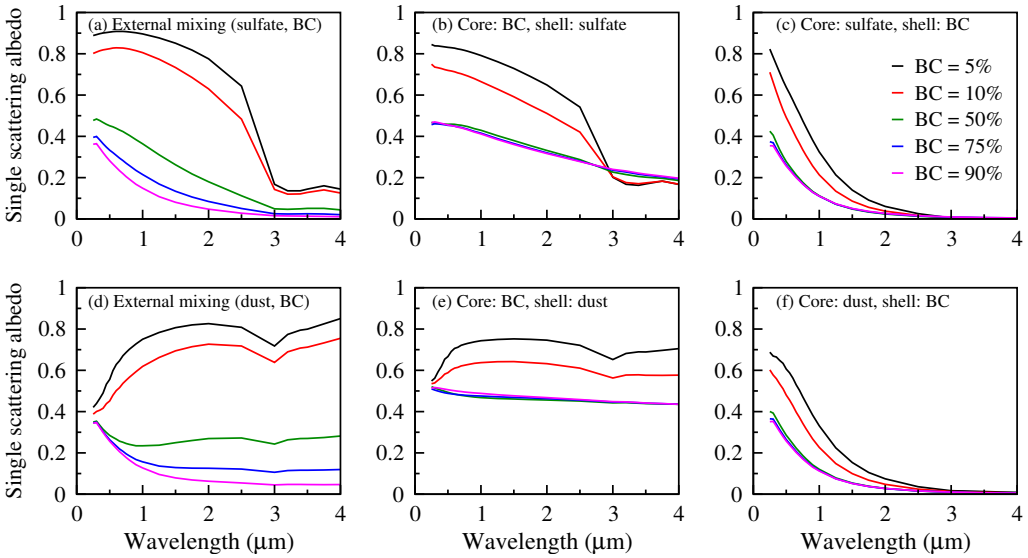

Figure 2.9: *Sensitivity of single scattering albedo spectra in shortwave region to black carbon mass concentration. SSA for black carbon and sulfate mixture in (a) external, (b) BC in core and (c) BC in shell mixing scenarios. SSA for black carbon and mineral dust in accumulation mode for (d) external, (e) BC in core and (f) BC in shell mixing scenarios.*

Core (BC) and shell (sulfate or dust) mixing shows hybrid spectral behavior of

BC and sulfate or dust, and when BC mass is $\geq$ 50% the spectra merge (Figure 2.9). However, when BC is present in shell, spectral SSA of composite aerosol is dominated only by BC spectral characteristics (Figure 2.9) and for this case when BC mass reaches higher than half of the total mass, the SSA spectra remain invariant (Figure 2.9). These results indicate that SSA spectra strongly depends on the mixing type and BC mass fraction of the composite aerosols, and the changes are quite significant for lower BC mass fraction.

2.6 Determination of probable mixing state

The procedure followed to derive probable mixing state of aerosols and to estimate the aerosol radiative forcing at the surface, in the atmosphere and at the top of the atmosphere is illustrated as flow chart in Figure 2.10. In order to derive the mass of different aerosol species taking into account the reported aerosol mass concentration over the study locations, the number concentration of each aerosol component *viz.*, water insoluble, water soluble, black carbon, mineral dust and sea salt is altered suitably (Figure 2.10) until the following conditions are met: (1) The root mean square (rms) difference between the measured aerosol optical depth (AOD) and modeled AOD spectra is < 0.03. (2) Ångström wavelength exponent α obtained from the measured AODs should be consistent with model derived α values. (3) The OPAC estimated total mass concentrations should lie within $\pm 1\sigma$ of the earlier reported mass concentrations. The third condition is applicable at the locations where the measurements of aerosol mass concentration are available.

The mass concentrations of different aerosol species obtained using the above criteria are used to estimate the AOD, SSA and *g* spectra for different mixing scenarios. All the three spectral optical properties AOD, SSA, and *g* are used for identifying the probable mixing state of aerosols (Figure 2.10). The case(s) for which rms difference(s) is/are < 0.03 in AOD and SSA spectra is/are designated as the probable mixing state(s). The rms difference of 0.03 corresponds to the lowest uncertainty in the AERONET retrievals of AOD, SSA and *g*. It should be noted that, in AERONET retrieval of SSA, aerosol particles are considered as homogeneous (uniform refractive index)

spheres and modeled sun/sky spectral radiances are fitted with the measured spectral radiances (*Dubovik and King*, 2000). This suggests that there are no assumptions on the refractive indicies of different aerosol species in AERONET retrieval which distinguishes absorbing aerosols from scattering aerosols.

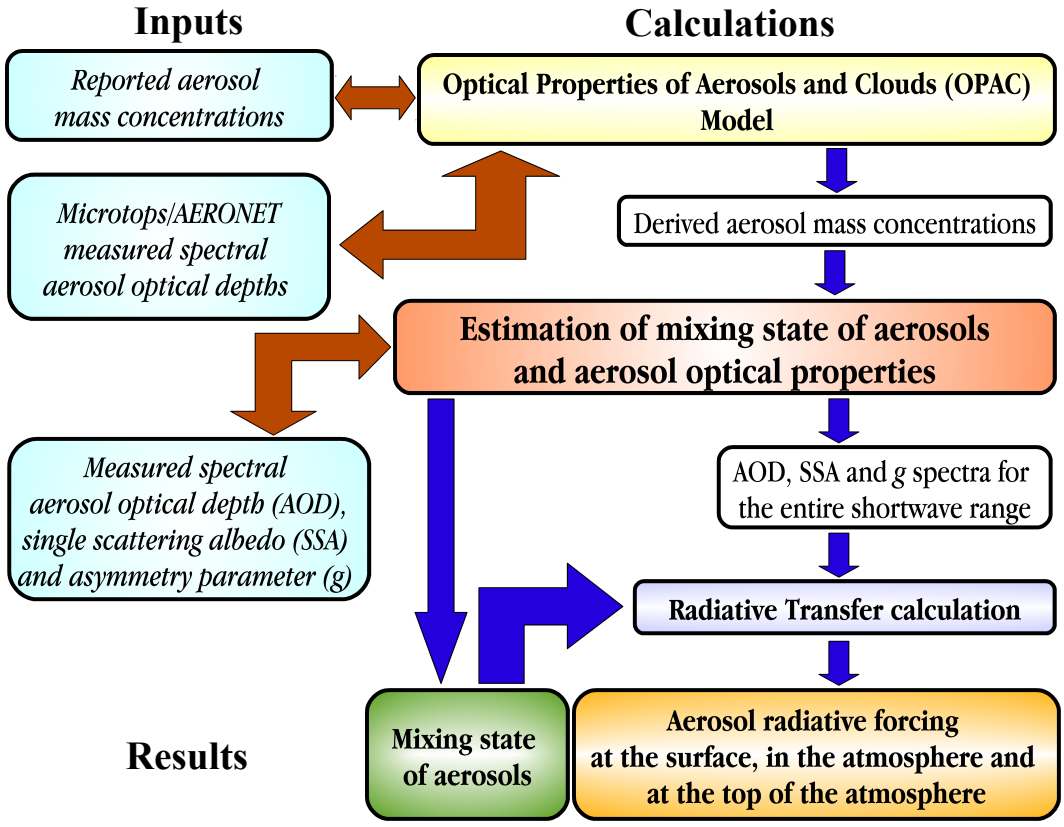

Figure 2.10: *Flow chart describing the methodology to estimate probable mixing state of aerosol and aerosol radiative forcing using reported mass concentration and measured spectral aerosol optical depth (AOD), single scattering albedo (SSA) and asymmetry parameter (g).*

Observations showed that typically 15% to 30% of dust particles' surface was covered by BC (*Arimoto et al.*, 2006). Over an urban location in Germany it was found that between 20% and 40% of the complex secondary aerosol particles contained soot inclusions (*Vester et al.*, 2007). *Hasegawa and Ohta* (2002) found that over urban and nonurban locations 19% to 72% of BC was covered with water soluble aerosol component. Following these, mass fractions of core and shell aerosol species are varied

from 10% to 100% in core-shell mixing in this study, the remaining mass fraction of aerosol species which are core-shell mixed, and other aerosol species are assumed to be externally mixed with the core-shell composite particles. Vertical profile information of aerosols is not included in this study as including the vertical distribution of aerosols did not modify the net aerosol radiative forcing (*Ramachandran and Kedia*, 2010), which is the focus of the thesis. In the present study aerosols are distributed according to the scale height (section 2.5.3). The columnar optical properties can get affected by the boundary layer height. The boundary layer height is low during winter and post-monsoon owing to less solar insolation and leads to an inversion near surface. Conversely, during pre-monsoon and monsoon the boundary layer gets broader due to increase in solar insolation (*Ramachandran and Kedia*, 2010). The boundary layer height is modified as a function of season while reconstructing the measured spectral aerosol optical properties over each location.

Over Ahmedabad SSA derived from ground-based measurements of scattering and absorption coefficients, and SSA obtained from remote sensing (OMI) in addition to Microtops spectral AOD is used for the determination of probable mixing state of aerosols. Aerosol optical properties are measured in the wavelength range of 0.4 - 1.02 μm (in case of Microtops) and 0.34 - 1.02 μm (in case of AERONET), however, spectral aerosol optical properties are required in whole shortwave range of 0.25 - 4.0 μm for the estimation of shortwave aerosol radiative forcing. Therefore, after deriving the probable mixing state of aerosols the AOD, SSA and *g* spectra for the entire shortwave range are obtained. The derived spectral aerosol optical properties are used in radiative transfer model to estimate aerosol radiative forcing at the surface, in the atmosphere, and at the top of atmosphere.

2.7 Aerosol radiative forcing

Santa Barbara DISORT Atmospheric radiative transfer (SBDART) model (*Ricchiazzi et al.*, 1998) is used for radiative transfer calculation in the shortwave range of 0.25 - 4.0 μm. SBDART solves plane parallel radiative transfer in clear sky conditions within the Earth's atmosphere. The fluxes calculated by SBDART model were found to lie within

2% of direct and diffuse irradiance measurements (*Michalsky et al.*, 2006). Aerosol radiative forcing (ARF) at the top of the atmosphere (TOA) and at the surface (SFC) are defined as the difference between the net (down minus up) radiative flux with and without aerosols as,

$$ARF_{SFC,TOA} = (F^{\downarrow} - F^{\uparrow})_{with\ aerosol} - (F^{\downarrow} - F^{\uparrow})_{without\ aerosol} \tag{2.8}$$

where $F^{\downarrow}$ and $F^{\uparrow}$ are downward and upward fluxes respectively. Aerosol radiative forcing in the atmosphere, which is the difference between the radiative forcing at the top of the atmosphere ($\sim$ 100 km) and the Earth's surface, is given as,

$$ARF_{ATM} = ARF_{TOA} - ARF_{SFC}\,. \tag{2.9}$$

The amount of energy trapped in the atmosphere due to the presence of aerosols is represented by the atmospheric forcing. Positive ARF$_{ATM}$ indicates the net gain of radiative flux due to aerosols and results in a heating, conversely, a negative ARF$_{ATM}$ shows a net loss and indicates a cooling effect.

Aerosol radiative forcing calculations are performed using 8 radiation streams at 1-hour interval for a range of solar zenith angles, and 24-hour averages are obtained, which are then used in calculating the monthly and seasonal means. Low resolution band models of LOWTRAN-7 atmospheric transmission code are used for molecular absorption. Almost all the radiatively active molecular species present in the Earth's atmosphere are taken into account. LOWTRAN-7 has wavelength resolution of 0.005 μm in visible wavelength range, while it is about 0.2 μm in thermal infrared wavelength region. The numerical integration of radiative transfer equations is performed using DISORT (Discrete Ordinate Radiative Transfer) module developed by *Stamnes et al.* (1988). The discrete ordinate method gives rise to a numerically stable algorithm for solving the plane-parallel radiative transfer equations in a vertically inhomogeneous atmosphere. Both scattered and thermally emitted radiations can be computed at different heights and in various directions. SBDART computes radiative fluxes both in shortwave (0.2-4.0 μm) and longwave (4.0-40.0 μm) range. The absolute total uncertainty in the modeled aerosol radiative forcing was found to vary in the range of 0.2

to 3.1 Wm^{-2} by considering different aerosol optical properties, and single scattering albedo was found to be the largest contributor to the above uncertainty, and the relative total uncertainties in aerosol radiative forcing were higher when fluxes were lower (*McComiskey et al.*, 2008).

For aerosol radiative transfer calculations, atmospheric profiles of temperature, pressure, ozone and water vapor are required in addition to aerosol properties. The standard tropical atmospheric profiles of temperature and pressure are used for the locations in the latitude range of 30^oS to 30^oN, and beyond this latitude range mid-latitude summer and winter atmospheric profiles for March - September period and October to February are used respectively (*McClatchey et al.*, 1972). Monthly mean columnar ozone over each study location was obtained from the daily mean data of Ozone Monitoring Instrument (OMI) on-board Aura satellite. Monthly mean water vapor was obtained from National Center for Environmental Prediction (NCEP) re-analysis over Ahmedabad, while water vapor over other locations was obtained from AERONET data. Surface reflectance measured by MODerate resolution Imaging Spectroradiometer (MODIS) onboard Terra and Aqua satellites (8Day, Level 3 Global 500m ISIN Grid product, MOD09A1 (Terra) and MYD09A1 (Aqua)) at seven wavelength bands centered at 0.469, 0.555, 0.645, 0.859, 1.24, 1.64 and 2.13 μm were utilized over all the study locations. Surface reflectance at seven wavelengths is used to reproduce the surface reflectance in the shortwave wavelength range (0.25 - 4.0 μm) using a combination of vegetation, sand and water albedos given in SBDART. The relative standard error in aerosol radiative forcing is found to be $< 15\%$ by taking into account the uncertainties in aerosol input parameters, flux estimates and additional inputs (*Srivastava et al.*, 2011).

2.7.1 Aerosol radiative forcing for different mixing scenarios

Aerosol optical depths and single scattering albedo at 0.55 μm and shortwave aerosol radiative forcing at the surface, at the top of the atmosphere and in the atmosphere for different mixing cases of urban aerosols are shown in Figure 2.11. Urban model comprises three dominant aerosol species (*Hess et al.*, 1998) *viz.*, water soluble (WS), insoluble (IS) and BC. Totally, four cases *viz.*, (1) external mixing, (2) core: IS, shell: BC;

(3) core: BC, shell: IS and (4) core: BC, shell: WS are considered for the calculations. The mass concentrations of the aerosol species correspond to 50% RH as given in *Hess et al.* (1998). In cases 2 to 4 the above mentioned two species are involved in core-shell mixing, while the third species is externally mixed.

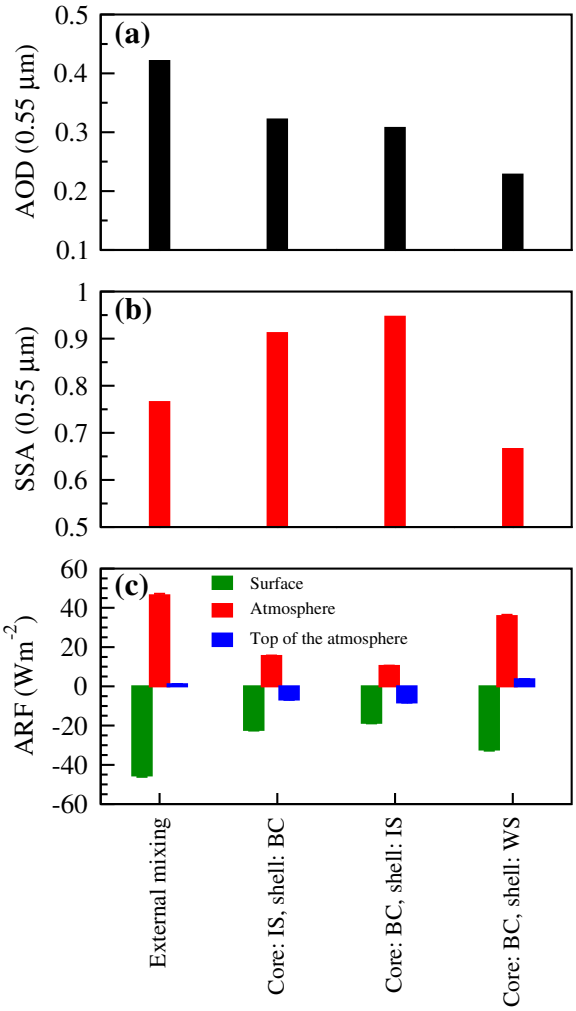

Figure 2.11: *(a) Aerosol optical depth (AOD), (b) single scattering albedo (SSA) and (c) aerosol radiative forcing (ARF) for different mixing states of urban aerosols obtained by conserving the total aerosol mass concentration.*

AOD values in other mixing scenarios e.g., core: IS, shell WS, core: WS, shell: IS; core: WS, shell: BC were too low and were excluded as such small values were considered physically unacceptable over an urban environment. AOD is higher for external mixing and lower when BC is coated by WS aerosols. SSA is higher and lower when BC

is coated by IS and WS respectively. For other mixing states SSA values are within the above two mixing states (Figure 2.11). In case of IS and BC core-shell mixing whether BC is in core or in shell, SSA is quite similar and higher (≥ 0.9) than the other two cases (Figure 2.11). Asymmetry parameter (g) is less affected by mixing states of aerosol as the radius range and size distribution parameters of core-shell mixed aerosols are same as that of the shell species. The asymmetry parameter does not have such significant impact as AOD and SSA on radiative forcing (*Mishchenko et al.*, 1997); therefore, g values for external mixing case is used for all the mixing scenarios. Surface and atmospheric aerosol radiative forcing is half when BC is coated by IS aerosol which is consistent with SSA values obtained. Top of the atmosphere (TOA) forcing is positive in case of external mixing and BC coated by WS aerosols, while TOA forcing is negative for other two cases. Thus, aerosol radiative forcing significantly depends upon the mixing states of aerosols. This issue is further examined by determining the probable mixing states of aerosols and estimating their radiative effects over Ahmedabad, an urban location in western India (*Chapter 3*), Indo-Gangetic plain (*Chapter 4*) and environmentally distinct locations over the globe (*Chapter 5*).

2.8 Spectral aerosol optical properties and radiative forcing

Aerosol optical properties *viz.,* AOD, SSA and g at 0.5 and 10.0 μm corresponding to different relative humidities (RH) for different continental (clean, average, polluted and urban) aerosol models are shown in Figure 2.12. The two wavelengths are chosen as the incoming (solar radiation) and outgoing (terrestrial) radiation peaks at 0.5 and 10.0 μm respectively. AOD at 0.5 μm is an order of magnitude higher when compared to AOD at 10.0 μm. AOD increases with relative humidity for all the models and is higher for urban model as in the urban model water soluble (hygroscopic) aerosol mass is higher.

Wavelength specific aerosol radiative forcing at 0.5 and 10.0 μm at the surface, in the atmosphere and at the top of the atmosphere (TOA) corresponding to different relative humidities (RH) for different continental aerosol models are shown in Figure 2.13. In the aerosol radiative forcing calculation presented in this section standard

tropical columnar ozone (253 Dobson Unit, DU) and water vapor (4.117 g cm^{-2}) values (*Ricchiazzi et al.*, 1998), and MODIS broadband (0.3 - 5.0 μm) surface reflectance value of 0.2 are used. Aerosol forcing at 0.5 μm is an order of magnitude higher than the forcing at 10.0 μm.

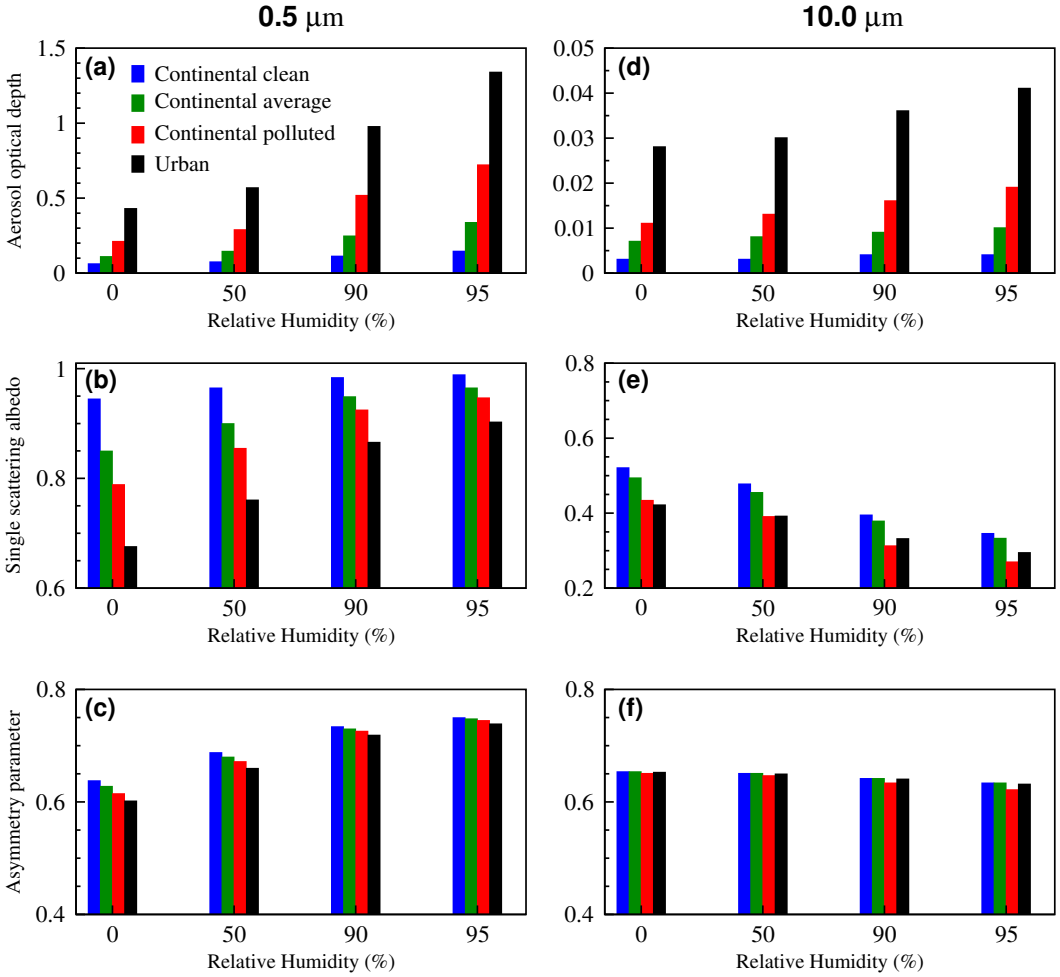

Figure 2.12: *Aerosol optical depth, single scattering albedo and asymmetry parameter at 0.5 μm and 10.0 μm as a function of relative humidity for continental aerosol models.*

Aerosol forcing is higher for urban model at the surface and in the atmosphere, which is consistent with AOD variations. In the atmosphere, forcing at 0.5 μm does not vary with relative humidity, while atmospheric forcing at 10.0 μm increases with RH. The absolute value of surface and TOA forcing increase with RH. For lower wavelength (0.5 μm) aerosol forcing is negative at the surface and positive in the atmo-

sphere, while for higher wavelength (10.0 μm) an opposite behavior is observed (Figure 2.13).

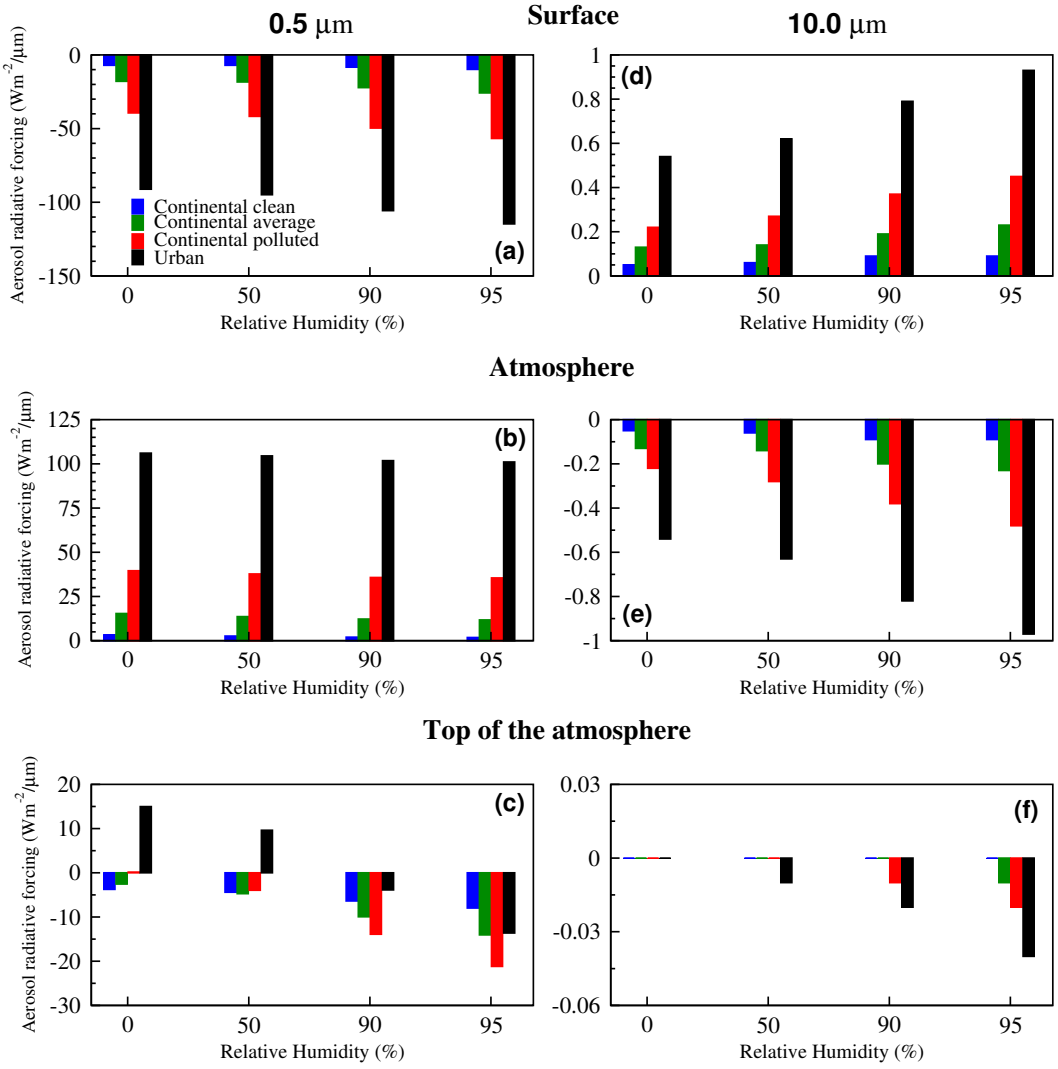

Figure 2.13: *Aerosol radiative forcing at the surface, in the atmosphere and at the top of the atmosphere as a function of relative humidity at 0.5 μm and 10.0 μm wavelength for continental aerosol models.*

In contrast to midvisible solar radiation aerosol radiative forcing which always warms the atmosphere, infrared aerosol radiative forcing can cool or warm the atmosphere. SSA at 10.0 μm is substantially low when compared to SSA at 0.5 μm (Figure 2.12), which shows higher absorption of longwave due to aerosols. This absorption of 10.0 μm radiation decreases the outgoing flux, while surface reaching flux increases

which gives rise to a cooling of the atmosphere (*Ramachandran et al.*, 2006).

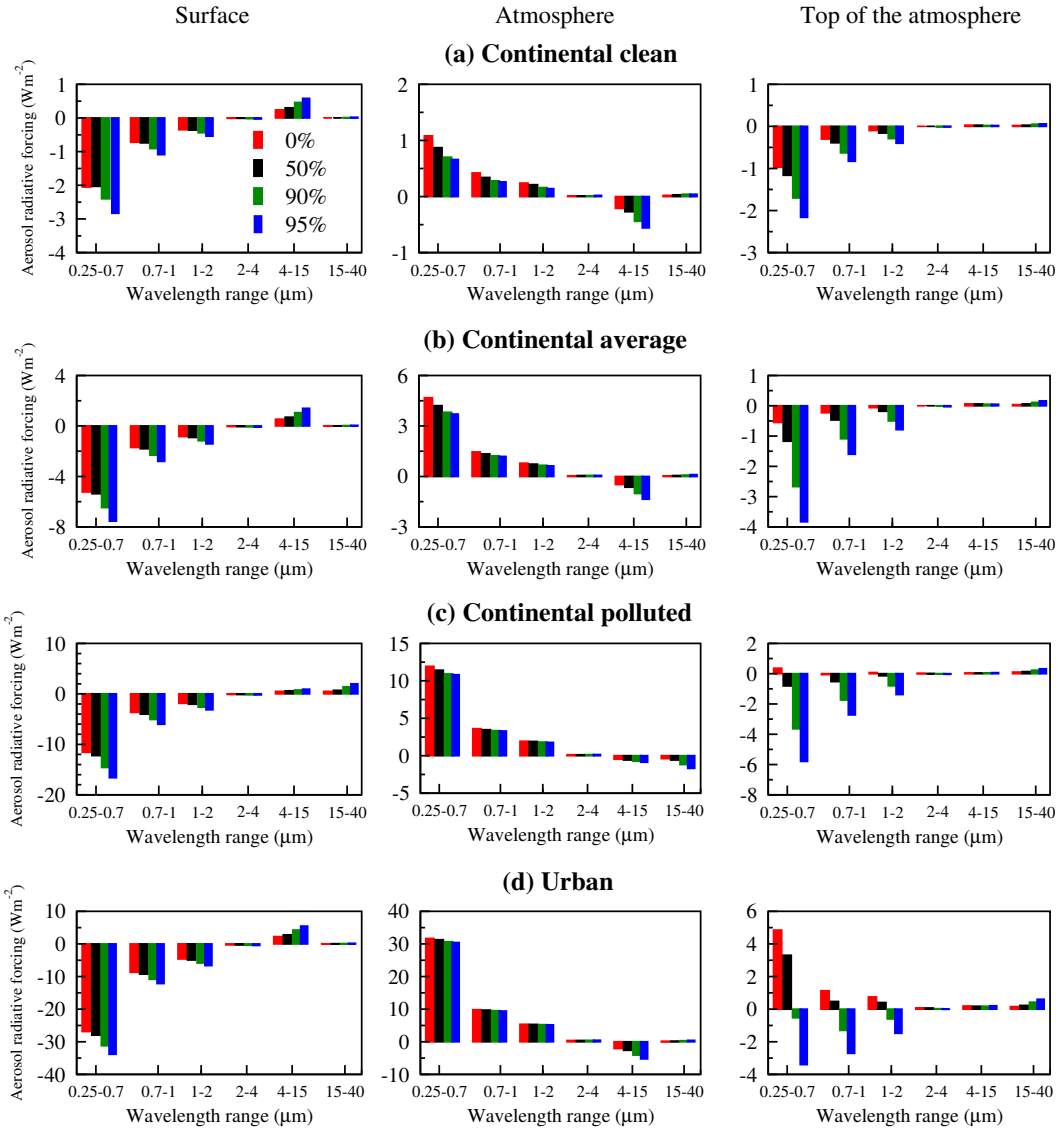

Figure 2.14: *Spectral aerosol radiative forcing at the surface, in the atmosphere and at the top of the atmosphere for different relative humidities and different continental aerosol models (continental clean, average, polluted and urban).*

Spectral aerosol radiative forcing at the surface, in the atmosphere and at the top of the atmosphere for different continental models *viz.*, continental clean, average, polluted and urban models at four relative humidities (0%, 50%, 90% and 95%) are shown in Figure 2.14. Aerosol radiative forcing increases with relative humidity for each spectral range and for each continental aerosol model. Aerosol forcing is highest

for urban aerosols followed by continental polluted and average aerosols, while it is lowest for clean aerosol model. The absolute value of aerosol radiative forcing in 2 - 4 μm wavelength range is an order of magnitude lower than the forcing in 0.25 - 0.7 μm range (Figure 2.14). Aerosol forcing in the wavelength range of 4 - 15 μm and 15 - 40 μm has opposite sign with respect to forcing in lower wavelength regime (Figure 2.14). However, the magnitude is rather high for urban and polluted aerosol models than the other aerosols.

2.8.1 Shortwave and longwave aerosol radiative forcing

Aerosol radiative forcing in shortwave (SW, 0.25 to 4.0 μm) range is negative at the surface and positive in the atmosphere. On the contrary, aerosol forcing in longwave (LW, 4.0 to 40 μm) regime is positive at the surface and negative in the atmosphere for all the aerosol models (Figure 2.15). The shortwave aerosol forcing at the top of the atmosphere can be positive or negative depending upon SSA values. For example, TOA forcing is positive for continental polluted aerosol model at 0% RH and for urban aerosol model at 0 and 50% RH as SSA is lower in polluted and urban aerosol models. SSA increases with RH due to an increase in water soluble aerosols which leads to negative TOA forcing for polluted and urban aerosol models at higher RH values. For the other continental models TOA forcing in shortwave regime is always negative (Figure 2.15).

The percentage contribution of shortwave aerosol radiative forcing defined by the relation $|ARF_{SW}|/(|ARF_{SW}| + |ARF_{LW}|)$ at the surface, in the atmosphere and at the top of the atmosphere for different aerosol models at different RH is given in Table 2.7.

Table 2.7: *Percentage contribution of shortwave aerosol radiative forcing to the total radiative forcing ($|ARF_{SW}|+|ARF_{LW}|$) for the aerosol models of continent (continental clean, average, polluted and urban) at 0, 50, 90 and 95% relative humidities.*

Aerosol	Surface				Atmosphere				Top of the Atmosphere			
model	0%	50%	90%	95%	0%	50%	90%	95%	0%	50%	90%	95%
Continental clean	93	91	89	88	90	85	74	68	97	97	97	97
Continental average	94	92	90	89	94	92	86	82	88	94	96	97
Continental polluted	95	93	91	90	96	94	90	87	74	89	96	96
Urban	95	94	92	91	96	95	93	91	95	91	79	90

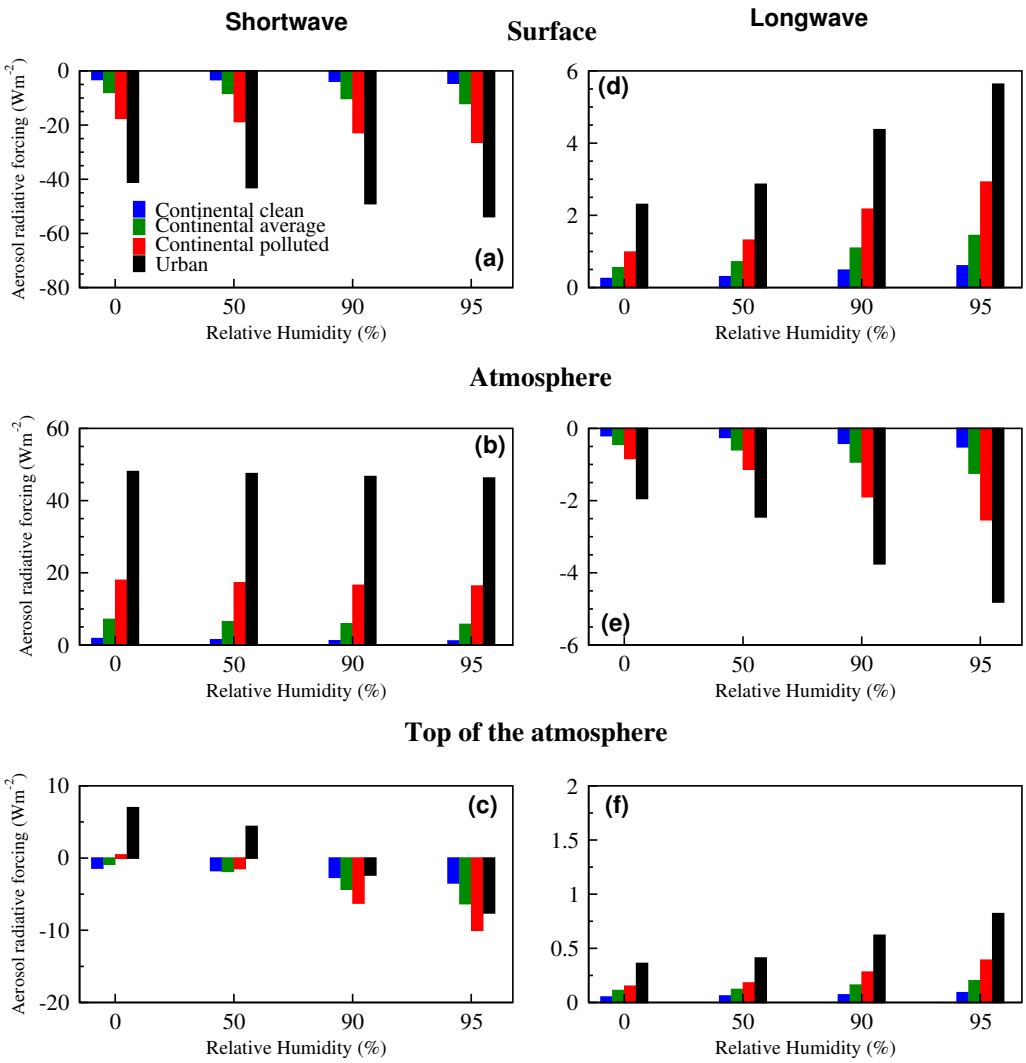

Figure 2.15: *Aerosol radiative forcing at the surface, in the atmosphere and at the top of the atmosphere for different aerosol models at different relative humidities in shortwave and longwave regimes.*

Shortwave aerosol forcing is $\geq$ 70% to the total aerosol forcing ($|ARF_{SW}| + |ARF_{LW}|$) for all continental aerosol models at all the relative humidity values. As the major impact due to aerosol is found to be in the shortwave (>70%), the present thesis focuses on aerosol radiative forcing in the shortwave range.

Chapter 3

Aerosol optical properties and radiative forcing over an urban location in western India

The role of aerosols in the Earth's radiation budget is one of the largest sources of uncertainty in validating the model prediction of climate change (*IPCC*, 2007). Surface aerosol radiative forcing was estimated based on direct measurements of surface fluxes and aerosol optical properties over tropical Indian Ocean and Kathmandu in south Asia during winter (e.g., *Conant*, 2000; *Ramanathan et al.*, 2001b; *Ramana et al.*, 2004). Flux measurements over continental India are rare except for a few e.g., *Pandithurai et al.*, (2004). Aerosol radiative forcing and its seasonal variations over western India were estimated using the measured aerosol optical properties and a radiative transfer model (e.g., *Ganguly and Jayaraman*, 2006; *Ramachandran and Kedia*, 2010). Aerosol radiative forcing on a seasonal mean basis is obtained using the measured fluxes and aerosol optical properties over Ahmedabad, an urban location, in western India, and compared and contrasted with the model results, and inferences are drawn. In this study the seasonal variation of surface aerosol forcing are derived from the observed flux which is rare and so far not available, to the best of our knowledge over India. Different methodologies are applied to estimate aerosol radiative forcing from the measured flux. Single scattering albedo (SSA) derived from ground-based measurements of aerosol absorption and scattering coefficients, Goddard Chemistry Aerosol Radiation and Transport (GOCART) model and satellite borne-sensor Ozone Monitoring Instrument (OMI) are used in the radiative transfer (SBDART) model to

simulate aerosol radiative forcing, and the influence of different SSA values on aerosol forcing is determined.

3.1 Measurement location

Ahmedabad (23.03^{o}N, 72.55^{o}E, 55 m AMSL) is an urban, industrial and densely populated city, and has a variety of large and small scale industries, and large number of vehicles (Figure 3.1).

Figure 3.1: *Measurement location Ahmedabad (Google Earth image). The metro cities (Delhi, Kolkata, Mumbai and Chennai) and Gurushikhar in Mount Abu, where the Microtops instrument is periodically calibrated are also shown.*

Thar desert and the Arabian Sea are situated in the northwest and southwest of Ahmedabad respectively (Figure 3.1), which serve as the major sources of mineral

dust and sea salt during pre-monsoon (March-May) and monsoon (June - September) respectively. The meteorological conditions over Ahmedabad exhibit large seasonal variations. The low level winds are calm and north westerly or north easterly during winter (December - February) which transport aerosols of continental origin and land derived dust particles. During pre-monsoon season (March - May), winds are north westerly or south westerly which transport mineral dust from Thar desert and the surrounding arid regions. During monsoon season of June - September the winds are south westerly, stronger and carry moist air from the Arabian sea to the study location (*Ramachandran and Kedia*, 2010). During post-monsoon season (October - November) the winds are calm and undergo a change in their direction from south west to north east.

3.1.1 GOCART model derived single scattering albedo

Monthly mean single scattering albedo at 0.55 μm over Ahmedabad is calculated from the monthly mean GOCART model simulated AODs of different species during 2001 - 2007 as GOCART data beyond 2007 were not available. The GOCART model simulates separately sulfate, sea salt, black carbon, dust and organic carbon (OC) AODs. GOCART computes aerosol optical depths of different species by adopting the published emission inventories and assimilated meteorological fields as inputs to chemical transport model (*Chin et al.*, 2002). AODs simulated by GOCART were prominently found to reproduce the spatial, temporal and inter-annual variations in measured AODs over various regions (*Chin et al.*, 2002).

The GOCART model produces a global gridded output at a lat-lon resolution of $2.0^o \times 2.5^o$. AODs of individual species are obtained at the above resolution centered around the study location corresponding to the lat-lon of 22^oN, 72.5^oE. In the present study, single scattering albedo is estimated by weighting the individual SSA of BC, sulfate, OC, dust and sea salt with their corresponding AODs following *Chung et al.* (2005). Sulfate, OC and sea salt aerosols (conservative scatterer) have an SSA of 1 at 0.55 μm, while SSA of BC is 0.2 (*Hess et al.*, 1998). SSA of dust was found to vary e.g., the midvisible SSA of aerosol sampled by aircraft during dust dominated events were in the range of 0.95 to 0.97 (*Anderson et al.*, 2003). *Chung et al.* (2005) parameter-

ized the dust SSA based on the Aerosol Robotic Network (AERONET) results reported in *Eck et al.* (2005) and several field studies reported in *Clarke et al.* (2004) and *Kim et al.* (2005). Following *Chung et al.* (2005), SSA of dust was allowed to vary from 0.98 to 0.90. The ratio of BC AOD to the sum of dust and BC AODs was chosen as the criteria to determine the dust SSA; when this ratio was less than 0.1, the dust SSA was 0.98 and when this ratio was greater than 0.5 then the dust was assigned an SSA value of 0.90. Dust SSA linearly increased from 0.90 to 0.98 when the value of the ratio decreased from 0.5 to 0.1. GOCART SSA was found to agree well with AERONET derived SSA in both seasonal variation and magnitude with little bias over Kanpur (26.51^{o}N, 80.23^{o}E) in India (*Chin et al.*, 2009). In GOCART, the threshold velocity of dust erosion, biomass burning emission factors, wind dependent sea salt flux function and biogenic OC emission are reported to be highly uncertain. The other parameters e.g., hygroscopic properties, refractive indices and mixing state, used in the calculation of mass extinction efficiency can also contribute to uncertainties in AODs derived from GOCART (*Chin et al.*, 2002). A comparison of GOCART derived SSA with AERONET measurements (*Chin et al.*, 2009) revealed that improvements in aerosol size distribution, refractive indices of dust and black carbon aerosols are necessary in order to better quantify the aerosol absorption in the atmosphere.

3.1.2 Satellite derived SSA

Monthly mean single scattering albedo at 0.50 μm is obtained from OMI. OMI is a high resolution spectrograph which measures the top of the atmosphere upwelling radiance in ultraviolet and visible regions (0.27-0.50 μm) of solar spectrum. OMI Level 3 data at a lat-lon resolution of $1^o \times 1^o$ centered around Ahmedabad are used in the study. OMI AOD and SSA were validated with AERONET sunphotometer over several locations in Asia, Africa and South America (*Torres et al.*, 2007). SSA obtained from AERONET and OMI for carbonaceous aerosols was found to agree well yielding a root mean square (RMS) difference of 0.03, while for desert dust aerosols the comparison yielded an RMS difference of 0.02 (*Torres et al.*, 2007). The SSA obtained at 0.388 μm is used to obtain SSA at 0.354 and 0.50 μm based on OMAERUV algorithm (*Torres et al.*, 2007). However, this can increase the dependence of the algorithm on the assumed

aerosol model which can lead to an uncertainty in the SSA at 0.50 μm. In addition, cloud contamination, for example, during monsoon in OMI pixels can also affect the estimation of AOD and SSA (*Torres et al.*, 2007).

3.2 Surface reflectance, ozone and water vapor

MODerate resolution Imaging Spectroradiometer (MODIS) derived surface reflectance at seven wavelength bands over Ahmedabad is shown in Table 3.1. The surface reflectance over Ahmedabad is higher during monsoon and pre-monsoon seasons (Table 3.1). Columnar ozone is high during summer (pre-monsoon and monsoon) when compared to winter and post-monsoon, which is consistent with the seasonal variations over the tropics (Table 3.2). Columnar water vapor and relative humidity are highest during monsoon season (June to September) due to transport of moisture from the Arabian sea (Table 3.2). Columnar ozone, water vapor and RH are low during winter when compared to other seasons.

Table 3.1: *MODIS derived seasonal mean surface reflectance over Ahmedabad during 2008.*

Wavelength (μm)	Winter	Pre-monsoon	Monsoon	Post-monsoon
0.469	0.132± 0.014	0.151± 0.005	0.241± 0.019	0.127± 0.004
0.555	0.220± 0.003	0.247± 0.016	0.346± 0.025	0.232± 0.000
0.645	0.068± 0.008	0.078± 0.003	0.206± 0.017	0.065± 0.001
0.859	0.111± 0.009	0.126± 0.005	0.236± 0.018	0.110± 0.002
1.24	0.234± 0.002	0.260± 0.011	0.332± 0.016	0.243± 0.005
1.64	0.228± 0.009	0.252± 0.006	0.304± 0.019	0.227± 0.012
2.13	0.188± 0.021	0.211± 0.004	0.219± 0.012	0.180± 0.008

Table 3.2: *Seasonal mean and standard deviation of columnar ozone (Dobson Unit, DU), water vapor (cm) and relative humidity (%) over Ahmedabad during 2008. Accumulated rainfall (mm) over Ahmedabad as a function of season is also given.*

Atmospheric parameters	Winter	Pre-monsoon	Monsoon	Post-monsoon
Columnar ozone (DU)	249±5	272±6	275±4	257±13
Columnar water vapor (cm)	1.4±0.6	2.0±0.4	4.7±0.6	2.3±0.5
Relative humidity (%)	30±6	37±12	84±8	43±6
Rainfall (mm)	6.1	7.1	601.7	0.3

3.3 Estimation of aerosol radiative forcing

Three different methods have been adopted to derive aerosol forcing efficiency from the measured fluxes and AODs over Ahmedabad. Surface aerosol radiative forcing is calculated in methods 2 and 3. All the methods are described below.

3.3.1 Method 1 (24 hour average net flux)

In this method, 24 hour average global flux for each clear sky day is calculated from the measured five minute interval global (direct and diffuse) fluxes. 24 hour average net surface fluxes (down minus up) are calculated from the above 24 hour average global fluxes using MODIS derived broad-band surface albedo. 24 hour average net fluxes for each month are plotted against the corresponding mean aerosol optical depths at 0.5 μm. The slope of the best fit line between the average net flux versus corresponding mean AOD yields surface forcing efficiency (*Ramana et al.*, 2004).

3.3.2 Method 2 (Hybrid approach)

This approach is partially dependent on model as radiative transfer model is used to estimate flux for aerosol free clear sky fluxes. Clear sky, aerosol free net surface fluxes for all months of 2008 are estimated using the measured columnar ozone and water vapor concentration in the Santa Barbara DISORT Atmospheric radiative transfer (SBDART) model (*Ricchiazzi et al.*, 1998). Surface reflectance at seven wavelengths is used to reproduce the surface reflectance in required wavelength range (0.31 - 2.8 μm) using a combination of vegetation, sand and water albedos given in SBDART. Radiative transfer calculation is performed using SBDART using 8 radiation streams and downwelling, upwelling and direct fluxes in the wavelength range of pyranometer (i.e. 0.31 - 2.8 μm) at 1-hour interval are estimated. Modeled aerosol free 24 hour average net flux is then subtracted from the observed 24 hour average net surface flux, and surface aerosol radiative forcing is calculated for each clear sky day of 2008. The advantage of this method is that it can be used to estimate aerosol radiative forcing for all aerosols including the background aerosols (*Conant*, 2000). The uncertainty in radiative forcing in hybrid approach is estimated to be $\sim$ 10% including the uncertainties

in measured and model estimated fluxes.

3.3.3 Method 3 (Differential approach)

This approach is completely based on the observations of the global surface flux and aerosol optical depth. Reference day among the clear sky days for each month of 2008 is chosen based on the lowest mean aerosol optical depth at 0.5 μm. 24 hour average net surface flux for the reference day (lowest AOD day) is then subtracted from average net fluxes for the rest of the days in a month and surface aerosol radiative forcing is estimated. The reference days, diurnal mean AOD and standard deviation corresponding to each month are shown in Table 3.3.

Table 3.3: *Aerosol optical depth (AOD) (0.5 μm) along with $\pm 1\sigma$ for clear sky day of each month/season over Ahmedabad during 2008 which is used as reference day.*

Month	Jan	Feb	Mar	Apr	May	Jun - Sep	Oct	Nov	Dec
Date of Reference Day	16	17	5	22	17	4 Jun	9	27	2
Mean AOD	0.265	0.236	0.228	0.316	0.333	0.416	0.286	0.167	0.276
$\pm 1\sigma$	0.008	0.002	0.048	0.008	0.013	0.030	0.002	0.021	0.023

During the reference day the diurnal variation in AOD was the lowest among the other days. The advantage of this approach is that it is independent of model uncertainty and since observed clear sky fluxes are subtracted in this approach, forcing is also not sensitive to calibration error (*Conant*, 2000). The aerosol forcing efficiency is calculated from the slope of the best fit line between daily mean surface aerosol radiative forcing and corresponding mean aerosol optical depth. In this approach as measured fluxes only are used, the uncertainty in radiative forcing estimates is less and is $\sim$ 7% (*Srivastava et al.*, 2011).

3.3.4 Aerosol radiative forcing from model based approach

Model estimation of flux for without aerosol case is already described in Method 2 (Hybrid approach, section 3.3.2), while flux with aerosols is estimated using measured aerosol optical properties in SBDART model. Measured aerosol optical parameters (AOD and SSA) are used to constrain the output of OPAC (Optical Properties

of Aerosols and Clouds) model (*Hess et al.*, 1998). Among the ten aerosol components in OPAC, the most suitable aerosols components based on aerosol source regions and transport over Ahmedabad are found to be water insoluble, water soluble, black carbon (BC), mineral dust and sea salt (e.g., *Ganguly and Jayaraman*, 2006; *Ramachandran and Kedia*, 2010). The number concentration of these aerosols is altered to match the monthly mean measured AOD spectra and SSA at ambient relative humidity for each month. The number concentration of each component is altered iteratively until the following conditions are satisfied (*Srivastava et al.*, 2011): (1) The root mean square difference between the measured AOD and model AOD spectra is < 0.03, thus constraining the rms differences to within 0.1 AOD. (2) Ångström wavelength exponent α obtained from the measured AODs in the 0.38-0.87 μm wavelength region are consistent with model derived α values. (3) BC mass concentration in OPAC should be the same as that of the aethalometer measured BC mass. (4) OPAC single scattering albedo should match with aethalometer and nephelometer, GOCART and OMI derived SSAs as the case may be.

3.4 Results and Discussion

3.4.1 Variations in aerosol optical depths

Daily and seasonal mean aerosol optical depths at 0.5 μm for year 2008 are shown in Figure 3.2. AOD shows an increasing trend from winter to monsoon and then decreases (Figure 3.2). The transport of dust by the strong north westerly wind can give rise to higher AOD during pre-monsoon. The boundary layer height is also higher during pre-monsoon and monsoon because of higher temperature and stronger convection, which provide longer atmospheric column to accommodate more natural and anthropogenic aerosols (*Kedia and Ramachandran*, 2011). Although Ahmedabad gets all of its annual rainfall during monsoon season (Table 3.2), no visible decrease is seen in AODs due to wet removal of aerosols because the rainfall is not uniformly distributed over the entire season, but occurs in discreet events. However, wet removal is found to be more efficient in reducing the near surface aerosols; for example, it has been observed that BC mass decreased from 3.9 $\mu g\ m^{-3}$ (pre-monsoon) to 2.1 $\mu g\ m^{-3}$

(monsoon) over Ahmedabad (*Ramachandran and Kedia*, 2010), while sea salt concentration is found to increase from pre-monsoon to monsoon as the winds are from the Arabian Sea during monsoon (e.g., *Raman and Ramachandran*, 2011 and references cited therein).

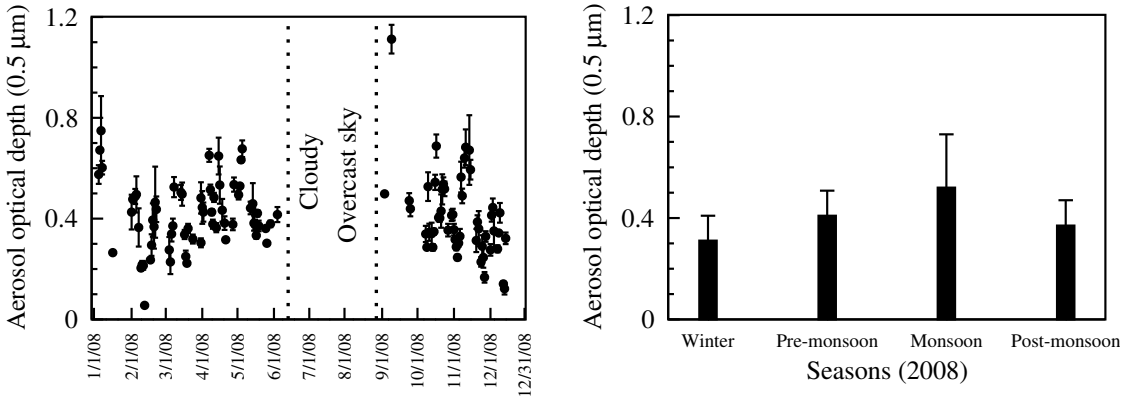

Figure 3.2: *Day to day and seasonal variation of aerosol optical depth (0.5 μm) over Ahmedabad. Vertical bars represent* $\pm$ 1 σ *deviation from the mean.*

The effects of wet removal, hygroscopic growth of aerosols and addition of sea salt on AOD is estimated using OPAC urban model. Urban aerosol model comprises three dominant aerosol species *viz.*, water soluble, insoluble and BC (*Hess et al.*, 1998). The seasonal mean relative humidity increases from 37% during pre-monsoon to 84% during monsoon over Ahmedabad (Table 3.2). AODs estimated for different scenarios taking into account the variation in the mass concentration of aerosol species and RH during pre-monsoon and monsoon are given in Table 3.4.

Table 3.4: *Mass concentrations of water insoluble (IS), water soluble (WS), black carbon (BC) and sea salt (SS) for urban environment and for different temporal conditions. Aerosol optical depth (AOD) and single scattering albedo (SSA) at 0.5 μm for different scenarios are given.*

Cases	Environment/ Condition	Mass concentration ($\mu g\, m^{-3}$)				AOD	SSA
		IS	WS	BC	SS		
1 (RH=37%)	Urban	35.6	51.2	7.8	0.0	0.51	0.74
2 (RH=37%)	Pre-monsoon	35.6	51.2	3.9	5.0	0.45	0.83
3 (RH=37%)	Pre-monsoon	35.6	51.2	3.9	10.0	0.46	0.84
4 (RH=84%)	Monsoon	35.6	94.3	2.1	10.0	0.76	0.94

Case 1 represents aerosol properties for urban aerosol model corresponding to an RH of 37%. A reduction of BC mass by half and an addition of sea salt leads to a decrease of 12% in AOD (case 2) at the same RH. This indicates that the reduction of BC mass predominantly affects the AOD, leading to a decrease as the addition of sea salt does not contribute to an increase in AOD (Table 3.4). Further, when the sea salt mass concentration is doubled with respect to its value in case 2, AOD increases only by 2% (case 3), confirming that an increase in sea salt mass concentration does not contribute significantly to midvisible AOD. In case 4, a decrease in BC and addition of sea salt accompanied with an increase in RH from 37 to 84% that lead to an increase in the water soluble aerosol mass concentration results in a 49% increase in AOD with respect to case 1 (urban environment). This feature of an increase in the water soluble aerosols and sea salt aerosol mass concentrations from pre-monsoon to monsoon is consistent with mass concentration measurements reported earlier over Ahmedabad (e.g., *Raman and Ramachandran*, 2011 and references cited therein). The simulation clearly shows that AOD increases significantly when RH increases mainly due to the hygroscopic growth of water soluble aerosols, and that this increase overwhelms the removal of BC and increase of sea salt aerosols over an urban regime (*Srivastava et al.*, 2011).

3.4.2 Single scattering albedo

Seasonal mean variation of single scattering albedo (SSA) at 0.55 μm during 2008 over Ahmedabad is shown in Figure 3.3. SSA at 0.55 μm is estimated from the absorption and scattering coefficients measured using aethalometer and nephelometer respectively. GOCART model and OMI (Aura) satellite derived SSA at 0.55 and 0.50 μm respectively are also shown in Figure 3.3. Aethalometer and nephelometer derived SSA correspond to near surface, while GOCART and OMI (Aura) SSA correspond to column. Aethalometer and nephelometer derived SSA is higher during monsoon (0.82) as compared to other seasons because black carbon mass concentration is lowest during monsoon (2.1 $\mu g\ m^{-3}$) (*Ramachandran and Kedia*, 2010). SSA during post-monsoon and winter are lower due to the dominance of absorbing aerosols. It is clear from Table 3.4 that 50% decrease in BC mass and addition of sea salt in urban environ-

ment can lead to a 12% increase in SSA with respect to case 1. The effect of doubling of sea salt can increase midvisible SSA only by 1% (cases 2 and 3), where as a decrease in BC and increase in RH from 37 to 84% results in a 27% increase in SSA (case 4), suggesting that the amount of absorbing aerosols in an urban regime primarily determines the SSA.

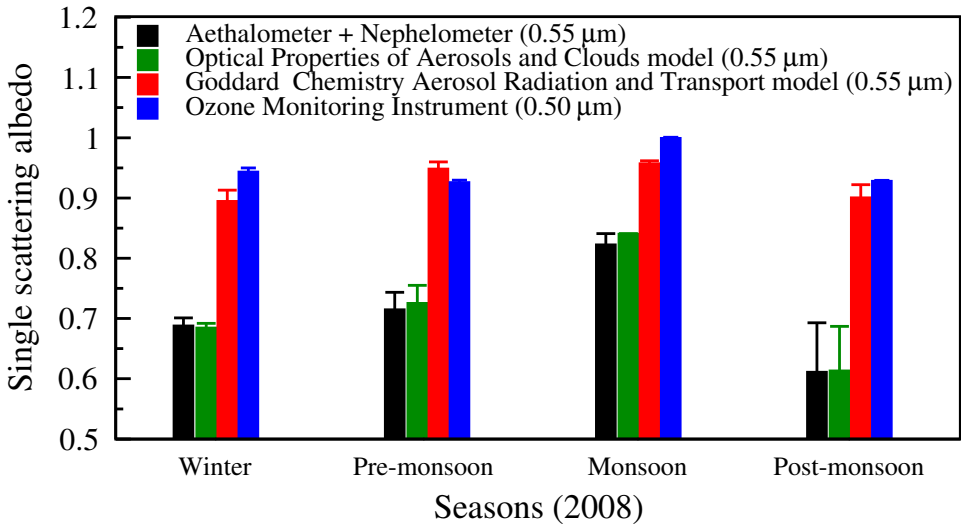

Figure 3.3: *Seasonal variation in single scattering albedo (SSA) value derived using aethalometer and nephelometer, GOCART and OMI (Aura) over Ahmedabad. SSA estimated using OPAC is also shown. Vertical bars represent* $\pm 1\sigma$ *deviation from the mean.*

SSA derived using aethalometer and nephelometer measurements are lower than GOCART and OMI derived SSA as Ahmedabad is an urban location and absorbing aerosols are more dominant near the surface. Such differences in SSA as a function of altitude have been observed earlier. SSA at the surface was found to be similar, higher and/or lower than that at other altitudes depending upon the types of aerosols and layers present at higher altitudes (e.g., *Clarke et al.*, 2004; *Magi et al.*, 2003) which could give rise to similar, higher and/or lower columnar SSA values.

3.4.3 Aerosol forcing efficiency

Diurnal mean (24 hour) global net (down minus up) fluxes are linearly fitted with aerosol optical depth at 0.5 μm in Figure 3.4. Surface aerosol radiative forcing calculated using hybrid approach (method 2) and differential approach (method 3) are

linearly correlated with corresponding mean AOD (Figure 3.4). All the three methods show the same slope within the standard error and have similar regression coefficients. Aerosol surface radiative forcing efficiency which is obtained from the slope of the least square fits is shown in Figure 3.5. Forcing efficiency could not be estimated in monsoon season for method 3 because of the reasons stated earlier.

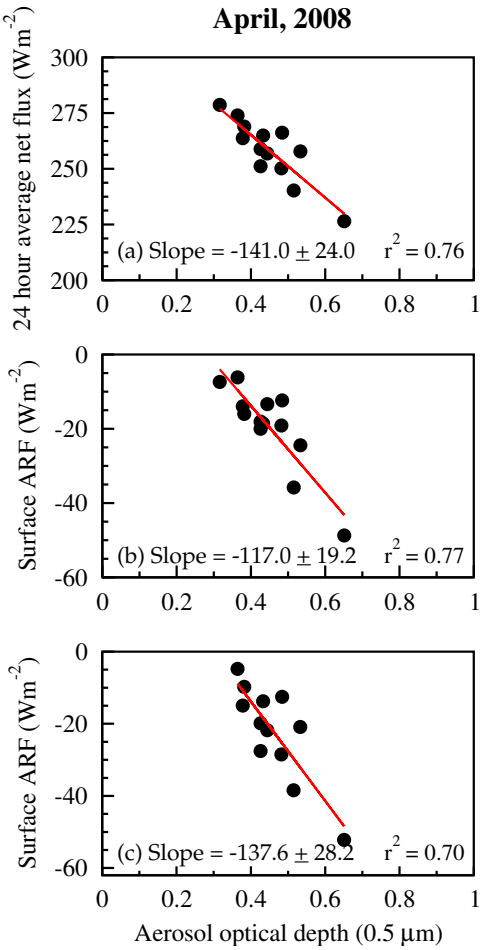

Figure 3.4: *(a) 24 hour average net surface flux, and surface aerosol radiative forcing (b) using method 2 and (c) method 3 as a function of aerosol optical depths (0.5 μm) for April 2008. The straight lines are the least square fits.*

The magnitude of forcing efficiency estimated using methods 1 and 2 is found to be the lowest in monsoon ($<$ -50 Wm^{-2}). Aerosol forcing efficiency obtained by all the methods are in the range of -67 to -89 Wm^{-2}/AOD during winter while it was found to be -73 Wm^{-2}/AOD over Kathmandu (27.67^{o}N, 85.31^{o}E) in the Himalayas.

AOD over the Himalayan region ranged from 0.2 to 0.3 and SSA varied from 0.7 to 0.9 (*Ramana et al.*, 2004), which is closer to the seasonal mean AOD (0.31) and SSA ($\sim$ 0.7) observed over Ahmedabad. During the Indian Ocean Experiment (INDOEX) from January to March 1999, forcing efficiency was found to be -75 Wm^{-2}/AOD (*Ramanathan et al.*, 2001b), which also lies in the range of forcing efficiency values observed over Ahmedabad during winter. Over another urban, tropical location, Pune, India forcing efficiency was found to be -88 Wm^{-2}/AOD during dry seasons (November - April) of 2001 and 2002 (*Pandithurai et al.*, 2004). Forcing efficiency over Ahmedabad during November to April (post-monsoon, winter and pre-monsoon) ranges from -65 to -71 Wm^{-2}/AOD. The lower forcing efficiency obtained over Ahmedabad could be due to higher values of columnar SSA as compared to Pune (0.81).

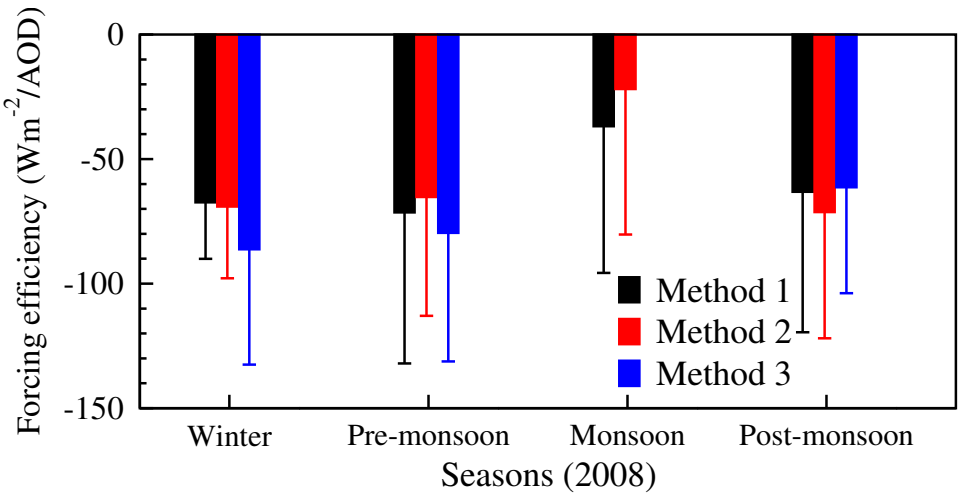

Figure 3.5: *Seasonal variation of aerosol forcing efficiency estimated by methods 1, 2 and 3. Vertical bars represent* $\pm$ 1 σ *deviation from the mean.*

3.4.4 Surface aerosol radiative forcing

Seasonal mean surface aerosol radiative forcing estimated using method 2 (hybrid approach) and method 3 (differential approach) are plotted in Figure 3.6. Seasonal mean AODs at 0.5 μm are also mentioned in the figure. It is clear from the figure that higher AOD results in higher surface forcing thereby suggesting that AOD and forcing exhibit a linear relationship. Forcing values obtained by two approaches, hybrid (semi model dependent) and differential (model independent) are consistent within $\pm 1\sigma$ for all the

seasons.

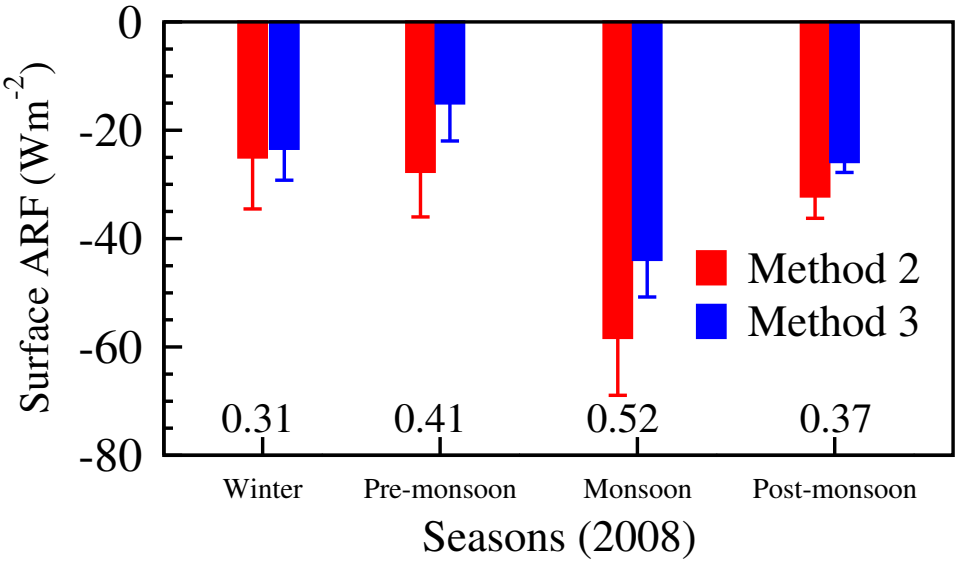

Figure 3.6: *Aerosol radiative forcing (ARF) at the surface calculated using methods 2 (hybrid approach) and 3 (differential approach). Seasonal mean aerosol optical depths are mentioned in the figure. Vertical bars represent* $\pm 1\ \sigma$ *deviation from the mean.*

The magnitude of radiative forcing estimated follows the same trend as AOD and is higher during monsoon. Forcing in both methods 2 and 3 during pre-monsoon is lower despite higher AOD (0.41). Lower radiative forcing during pre-monsoon arises due to higher SSA when compared to post-monsoon (Figure 3.3). Thus, the seasonal mean radiative forcing follows a linear behavior with corresponding AOD except for pre-monsoon over Ahmedabad.

3.4.5 Surface aerosol radiative forcing: Observation and model estimates

Surface forcing during different seasons of 2008, estimated by method 3, is compared with model estimated surface forcing over Ahmedabad for three different cases (Figure 3.7). Forcing obtained in method 3 is chosen for comparison because it is completely based on the observations. In the first case, aethalometer and nephelometer derived SSA are used, while in the second and third cases GOCART model derived and OMI derived columnar SSA respectively are used in radiative transfer model (Figure 3.7). Aerosol optical depth, columnar ozone, water vapor and surface albedo are

maintained the same for all the cases, and only the SSA spectra is changed. The measured AOD spectra and SSA for three different cases are reconstructed by altering the number concentrations of water insoluble, water soluble, black carbon, mineral dust and sea salt aerosols in OPAC model following the procedure described earlier in section 3.3.4. The observed surface forcing shows large differences when compared to the model estimated forcing when SSA is lower (case 1). However, for cases 2 and 3, model estimated forcing is in accordance with the observations during winter, pre- and post-monsoon, while it shows large deviation during monsoon season. During monsoon model estimated forcing in case 1 deviates less (15% of observed forcing) from observation while forcing in cases 2 and 3 is about a factor of two higher (less negative) when compared to the observed forcing.

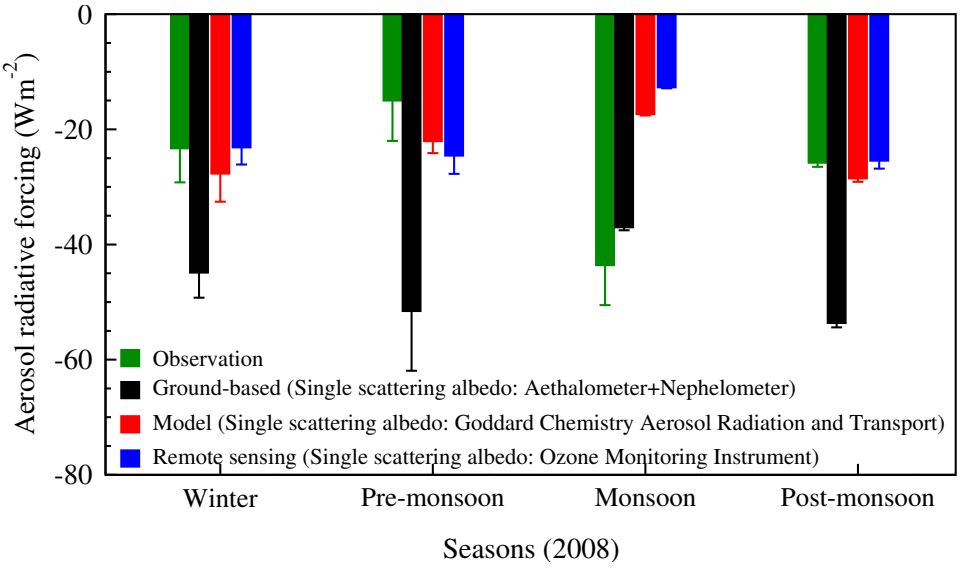

Figure 3.7: *Seasonal aerosol radiative forcing at surface from observation and model in which aethalometer and nephelometer (case 1), GOCART (case 2), and OMI (Aura) (case 3) single scattering albedo are used. Vertical bars represent* $\pm$ 1 σ *deviation from the mean.*

During monsoon forcing estimated using the near surface SSA is closer to the observed forcing, while during other seasons forcing estimated with GOCART and OMI SSA agree well (Figure 3.7). The wet removal of near surface aerosols, presence of abundant sea salt particles which is transported from the Arabian Sea, and hygroscopic growth of water soluble aerosols could have given rise to higher SSA during

monsoon over Ahmedabad (Figure 3.3, Table 3.4). The GOCART and OMI derived SSAs during monsoon are even higher than the in situ measurements. The SSA estimated using GOCART AODs during monsoon can be affected by the uncertainties related to higher relative humidity and in estimation of sea salt flux (*Chin et al.*, 2002). OMI derived SSA during monsoon is ≥ 0.99 which could occur due to the assumption that all the aerosols present in the atmosphere are scatterers. Such a high SSA obtained from GOCART and OMI can lead to lower forcing than that estimated using measured flux. Thus, it is clear that single scattering albedo is a sensitive parameter in the determination of aerosol radiative forcing and a little change in SSA can lead to a significant change in aerosol radiative forcing (*Srivastava et al.*, 2011).

3.4.6 Probable mixing states of aerosols over Ahmedabad

The probable core-shell mixing scenarios determined for different seasons for different SSAs *viz.,* in situ aethalometer and nephelometer measurements, and SSA obtained from remote sensing (OMI) are listed in Table 3.5. The mass fractions of different aerosol species involved in core-shell mixing are varied in this study, from 0 (no coating or external mixing) to 100% (completely coated), based on observations (*Arimoto et al.*, 2006) where only 15 - 30% of Asian dust particles were found covered by BC, which suggested that only a fraction of a certain species could be involved in core-shell mixing. During the determination of probable mixing state the AOD spectra in different mixing scenarios are kept the same as those measured over Ahmedabad during each season and shown in Figure 3.8. The measured and modeled AOD spectra are found to agree very well (Figure 3.8).

Single scattering albedo spectra in the wavelength range of 0.4 to 0.9 μm for different mixing scenarios for different seasons of 2008 over Ahmedabad are shown in Figure 3.9. It should be noted that in situ SSA values are lower than the remote sensing (OMI) values; because OMI SSA corresponds to the column while in situ SSA are derived from near surface measurements. Dust coated by water soluble is found to be the most probable mixing state during winter, pre- and post-monsoon for in situ SSA, while a number of mixing states are found to be probable for OMI derived SSAs (Table 3.5 and Figure 3.9).

Table 3.5: *Aerosol species viz., insoluble (IS), water soluble (WS), black carbon (BC), sea salt (SS) and mineral dust (MD) present in core and shell, and their percentage mass fractions in mixing along with model and observed single scattering albedo (SSA) during winter (Win), pre-monsoon (Pre-M), monsoon (Mon) and post-monsoon (Post-M) seasons.*

	In situ (Aethalometer and Nephelometer)						Remote sensing (Ozone Monitoring Instrument)					
	Mixing state				SSA (0.55 μm)		Mixing state				SSA (0.50 μm)	
	Core		Shell				Core		Shell			
Seasons	Species	%	Species	%	Obs.	Model	Species	%	Species	%	Obs.	Model
Win	MD	100	WS	100	0.70	0.72	IS	100	BC	100	0.95	0.96
							BC	50	WS	50	0.95	0.94
							WS	50	BC	100	0.95	0.96
							SS	20	BC	100	0.95	0.96
Pre-M	IS	100	WS	20	0.71	0.69	IS	50	BC	20	0.93	0.90
	MD	20	WS	20	0.71	0.72	SS	20	BC	20	0.93	0.90
	SS	20	IS	20	0.71	0.69						
	IS	100	SS	50	0.71	0.69						
Mon	IS	20	WS	50	0.82	0.82	MD	20	BC	20	0.99	0.98
	SS	50	WS	50	0.82	0.82						
	SS	100	IS	100	0.82	0.84						
	IS	100	SS	50	0.82	0.83						
Post-M	MD	100	WS	100	0.61	0.58	IS	50	BC	100	0.93	0.95
							BC	50	WS	50	0.93	0.92
							WS	100	BC	100	0.93	0.93
							SS	20	BC	100	0.93	0.94

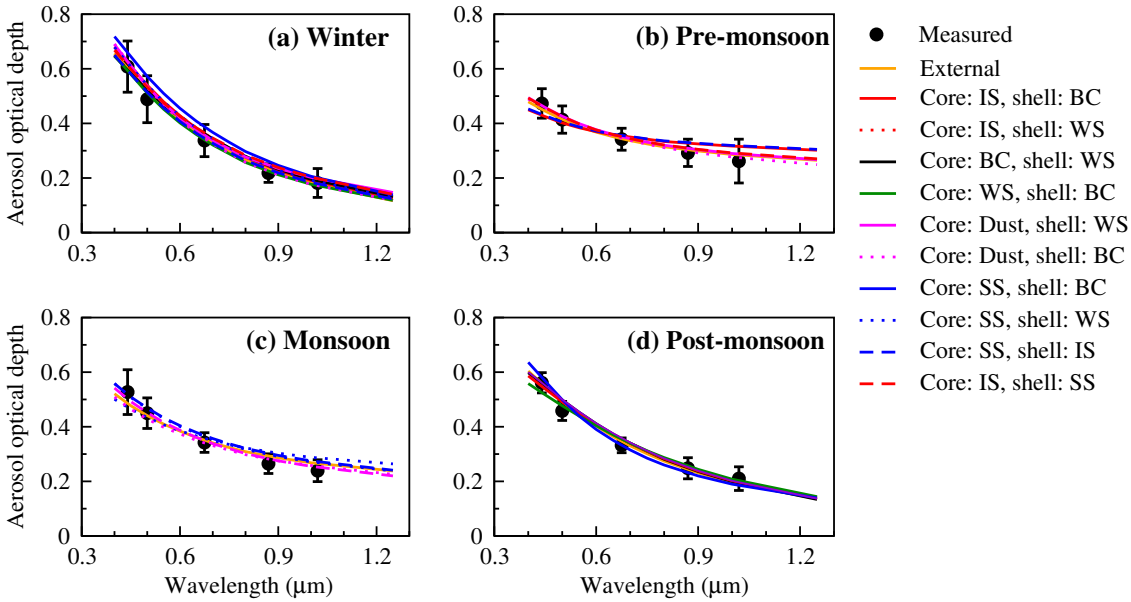

Figure 3.8: *Aerosol optical depth spectra modeled for different mixing states along with measured AODs during (a) winter, (b) pre-monsoon, (c) monsoon and (d) post-monsoon over Ahmedabad. Vertical bars in the observation represent* $\pm$ 1 σ *deviation from the mean.*

During pre-monsoon the spectral nature of SSA is different (SSA increases with wavelength) which is due to the presence of larger size dust particles (Figures 3.9b, 3.9f). Different mixing states of sea salt, insoluble and water soluble aerosols are obtained during monsoon for in situ SSA.

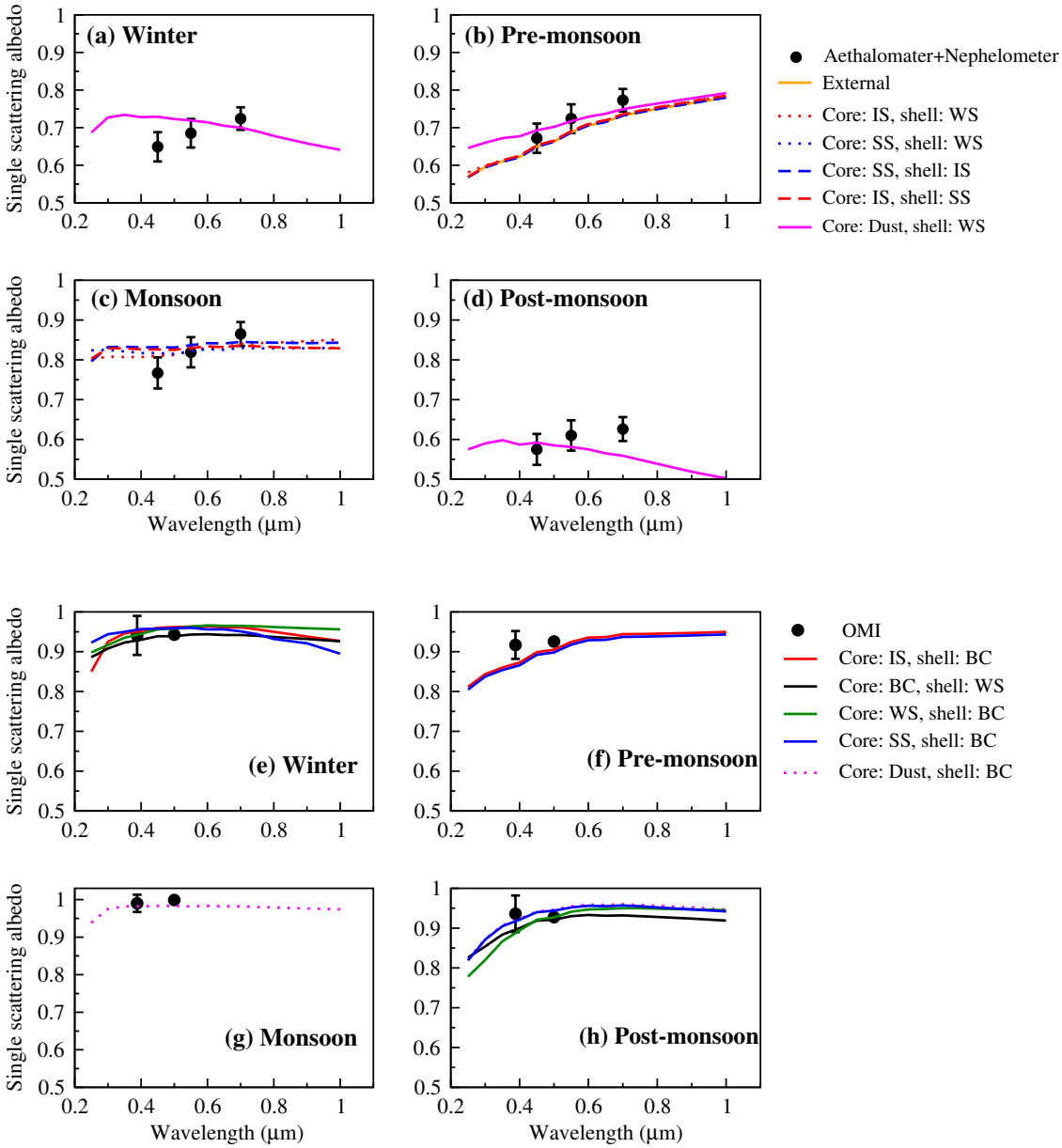

Figure 3.9: *Single scattering albedo spectra for different mixing states compared with in situ measurement (a-d) and with SSA obtained from remote sensing (OMI) during different seasons (e-h) over Ahmedabad. Vertical bars in the measurements represent* $\pm 1\,\sigma$ *deviation from the mean.*

However, only one mixing state of 20% dust in core with 20% BC in shell is found to be the most probable for OMI derived SSAs. External mixing is most probable in pre-monsoon and monsoon for in situ SSA, and in winter for OMI derived SSA. The probable mixing states obtained from in situ measurements are different than those obtained from remote sensing (OMI derived) SSAs. The results clearly bring out the fact that probable mixing states of aerosols can vary depending on the values of SSA.

3.4.7 Aerosol radiative forcing over Ahmedabad

Aerosol radiative forcing at the surface, in the atmosphere and at the top of the atmosphere over Ahmedabad are estimated for external and probable mixing states (Table 3.5) and shown in Figure 3.10. Surface aerosol forcing calculated from the pyranometer measured flux is also shown in Figure 3.10. During a particular season different mixing states produce similar AOD and SSA spectra for in situ or OMI derived SSAs. Therefore, the forcing values for different mixing states are similar in each case. Surface forcing deduced from observation matches well with the forcing estimated for the most probable mixing states determined for OMI derived SSA during winter, pre- and post-monsoon. However, forcing estimated using SSAs determined from in situ aethalometer and nephelometer measurements and in case of external mixing agree with the observed forcing within the uncertainty limits during monsoon. It should be noted that during monsoon SSA retrieval from OMI may be more uncertain (*Torres et al.*, 2007) due to cloud coverage and assumptions regarding the selection of predefined weakly absorbing aerosol model. Aerosol radiative forcing estimated using the SSA derived from in situ measurements is found to be higher than that estimated for OMI derived SSA (Figure 3.10). Aerosol forcing in the atmosphere estimated for mixing cases determined for in situ SSA is about 3 to 7 times higher than that of OMI SSA (Figure 3.10). During pre-monsoon and monsoon radiative forcing in the atmosphere is the same for external mixing and probable mixing states (listed in Table 3.5) for in situ measured SSA.

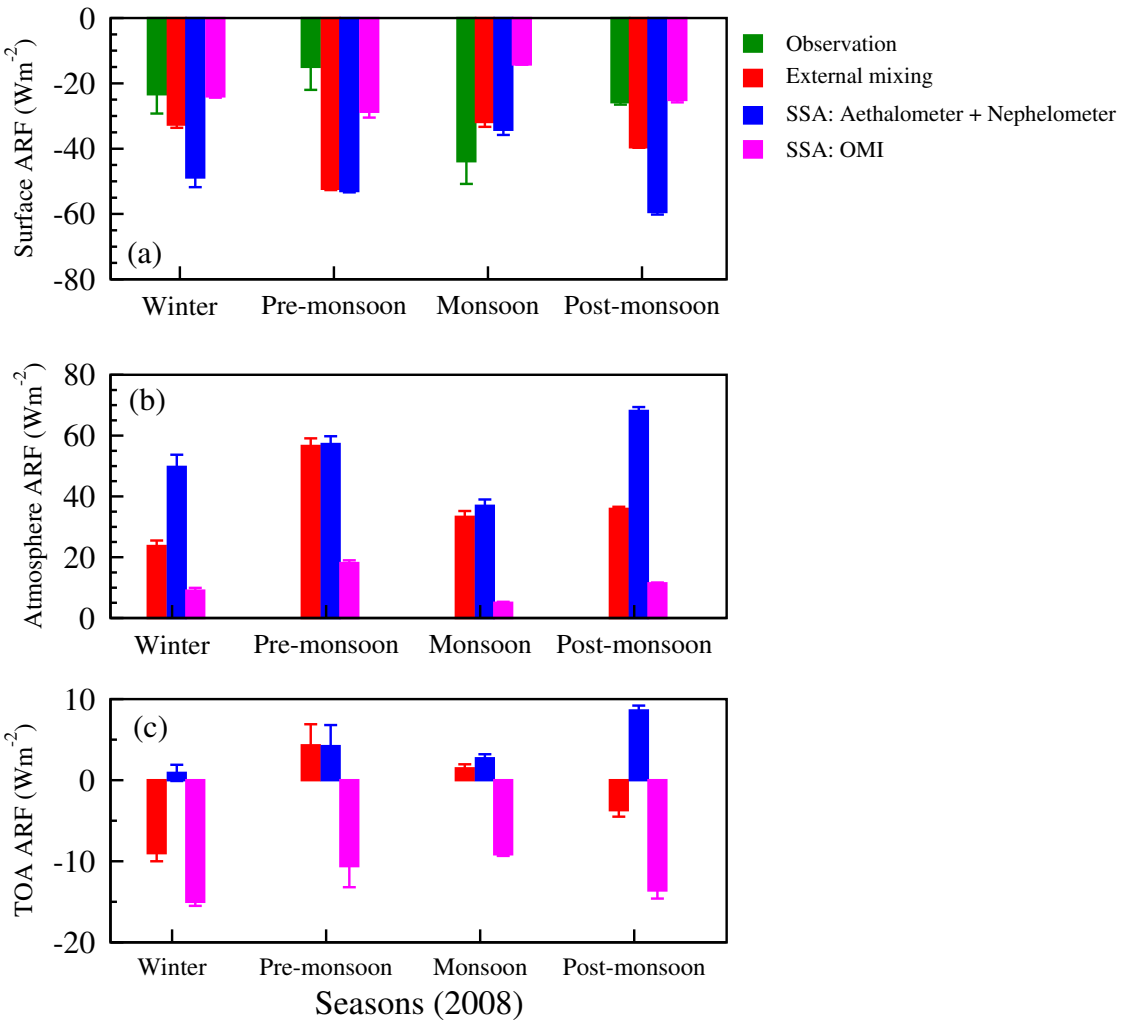

Figure 3.10: *(a) Surface aerosol radiative forcing from flux observations in comparison with model estimates for external mixing, and probable states of mixing for in situ and OMI SSA. Aerosol radiative forcing (ARF) in the (b) atmosphere and (c) at the top of the atmosphere (TOA) for external and probable mixing scenarios. Vertical bars represent* $\pm 1\,\sigma$ *deviation from the mean.*

TOA forcing is positive when SSA is < 0.85 and vice versa. TOA forcing is positive for external mixing during pre-monsoon and monsoon while it is negative during winter and post-monsoon (Figure 3.10). SSA for external mixing scenarios is < 0.85 during pre-monsoon and monsoon, while SSA is > 0.85 during winter. However, during post-monsoon SSA is < 0.85, TOA forcing is still negative, which could be due to lower surface albedo during post-monsoon when compared to that of monsoon (*Ramachandran and Kedia*, 2010). TOA forcing for probable mixing state is always posi-

tive for near surface measurements as SSA is always < 0.85; while TOA forcing is always negative for the probable mixing states derived for OMI SSA which are always > 0.85. These results show that mixing states and their effects on aerosol optical and radiative properties can be different for different SSA, and are important while estimating quantitatively the radiative impact of aerosols.

Chapter 4

Probable mixing state of aerosols over Indo-Gangetic plain and its impact on radiative forcing

Indo-Gangetic Plain (IGP) is one of the most polluted river basins in the world and is recognized as a hot spot as IGP is influenced by anthropogenic and natural aerosols which show distinct seasonal characteristics (*Dey and Tripathi*, 2008; *Tare et al.*, 2006). In this chapter the seasonal variations in probable mixing state of aerosols over the Indo-Gangetic plain (IGP) in India (Figure 4.1) are discussed. IGP is surrounded by the Himalayan mountain range in the north, Thar Desert and the Arabian Sea in the west, the Bay of Bengal in the east and Vindhyan Satputra ranges in the south (Figure 4.1). Spatial map of MODerate Resolution Imaging Spectroradiometer (MODIS) derived aerosol optical depth (AOD) at 0.55 μm are shown in Figure 4.1. MODIS level 3 collection V005 monthly Terra and Aqua mean AOD from January 2007 to December 2009 at $1^o \times 1^o$ lat-lon resolution are utilized (*Remer et al.*, 2008), and seasonal means are calculated. AOD is higher over IGP than the other Indian regions during all the seasons (Figure 4.1). The industrial growth and increasing usage of fossil fuel as well as biomass burning lead to higher aerosol loading in the region (e.g., *Singh et al.*, 2004; *Dey and Tripathi*, 2008). Not only the anthropogenic pollution but natural aerosols (mostly dust) also contribute to the regional aerosol loading in the premonsoon season (Figure 4.1). Thus, IGP is influenced by different types of aerosols and exhibit strong seasonal variations, which is expected to result in different mixing states of aerosols.

The chosen study locations (i) Kanpur and (ii) Gandhi College over IGP correspond to different environments and governed by different aerosol types (Figure 4.1). Kanpur is an urban location and influenced by local anthropogenic pollution and long-range transport, while Gandhi College is a rural location ($\sim$ 250 km from Kanpur) and situated downwind of major urban cities. Due to different environments and availability of various aerosols the most probable mixing states over these two locations is determined to highlight the seasonal variability and the differences in mixing state of aerosols over this region. The modeled optical properties in conjunction with measured optical properties (aerosol optical depth (AOD), single scattering albedo (SSA) and asymmetry parameter (g)) of aerosols are used to estimate the probable mixing states over IGP. In addition, the information of aerosol mass concentrations reported over Kanpur during winter, pre-monsoon and post-monsoon are utilized. In the only previous study *Dey et al.* (2008) derived the most probable mixing state over Kanpur during particular months of year 2005 - 2006 with an assumption that the total mass concentrations (100%) of different aerosol species were involved in core-shell mixing. In the present study the mass fractions of different aerosol species involved in core-shell mixing are allowed to vary, and the seasonal variation in aerosol mixing state are determined. This is important as observations (e.g., *Hasegawa and Ohta*, 2002; *Arimoto et al.*, 2006; *Vester et al.*, 2007) show that the total masses of two species need not be completely involved in core-shell mixing, but can have variable mass fraction of even about 10%.

4.1 Study locations and meteorology

Kanpur (26.51^{o}N, 80.23^{o}E, 123 m AMSL) and Gandhi College (25.87^{o}N, 84.13^{o}E, 60 m AMSL) are situated in Indo-Gangetic plain (Figure 4.1). Kanpur is an urban and industrial city in Uttar Pradesh state and densely populated ($>$ 4 million), while Gandhi College is a rural village located in Ballia district southeast of Kanpur. As Gandhi College is situated downwind of major urban cities (*viz.,* Delhi, Kanpur and Lucknow, Figure 4.1), the atmosphere over this location is influenced by mixture of rural (local) and urban aerosol emissions (downwind and long-range transport).

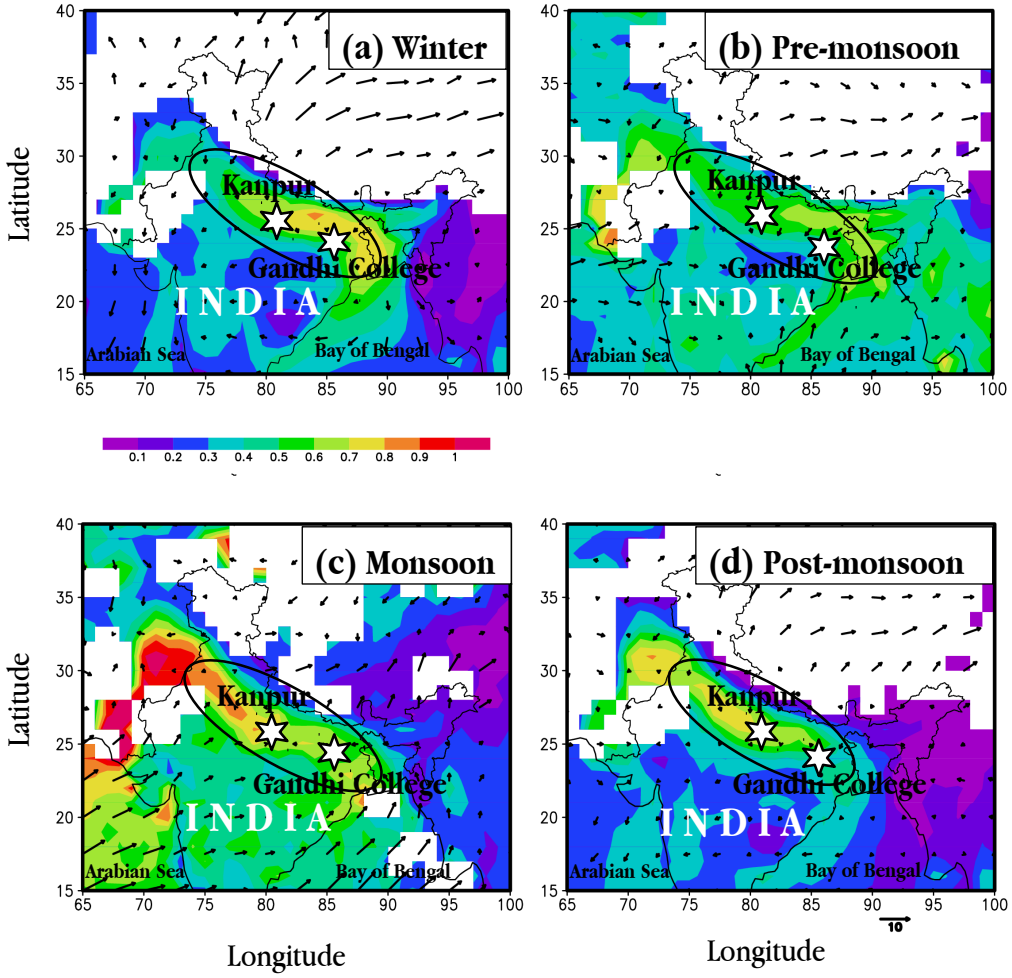

Figure 4.1: *Spatial map of aerosol optical depth (AOD) at 0.55 μm and surface winds over Indo-Gangetic plain during (a) winter, (b) pre-monsoon, (c) monsoon and (c) monsoon. The shaded contours correspond to AOD, on which, surface winds (ms^{-1}) represented by arrows are overlaid. The study locations Kanpur and Gandhi College, and the Indo-Gangetic plain are marked on map.*

The IGP experiences four distinct seasons, winter (December-February), pre-monsoon (March-May), monsoon (June-September) and post-monsoon (October-November). There is no seasonal variation in winds over Kanpur and Gandhi College due to their mixed origin during entire year. The wind speed is < 5 ms^{-1} during whole year except during monsoon (Figure 4.1). Winds are mainly northeast/or northwest during pre- and post-monsoon while during winter and monsoon the winds are seen to come from different directions (Figure 4.1). The northwesterly winds during pre-

monsoon transport dust from the Thar desert (e.g., *Chinnam et al.*, 2006). Relative humidity (RH) is higher during monsoon followed by post-monsoon and lowest during pre-monsoon season over both the locations (Table 4.1).

Table 4.1: *Seasonal mean and standard deviation of columnar ozone (Dobson Unit, DU), water vapor (cm) and relative humidity (%) over Kanpur and Gandhi College during 2007 - 2009.*

Atmospheric parameters	Winter	Pre-monsoon	Monsoon	Post-monsoon
		Kanpur		
Columnar ozone (DU)	258±15	280±11	274±8	261±9
Columnar water vapor (cm)	1.4±0.1	2.2±0.5	4.9±0.9	2.2±0.4
Relative humidity (%)	41±6	32±4	78±22	58±10
		Gandhi College		
Columnar ozone (DU)	258±15	282±12	277±9	260±9
Columnar water vapor (cm)	1.7±0.2	2.7±0.8	5.5±0.6	2.9±0.5
Relative humidity (%)	46±7	38±6	91±5	70±12

4.2 Approach

Chemical characteristics of aerosols over Kanpur during winter, pre-monsoon and post monsoon have been reported earlier (e.g., *Chinnam et al.*, 2006; *Dey et al.*, 2008; *Tare et al.*, 2006). Higher BC and dust were reported during winter and pre-monsoon respectively, and BC mass fraction at surface was lower during monsoon over Kanpur (*Chinnam et al.*, 2006; *Tare et al.*, 2006). Chemical characterization studies suggested that BC, water soluble (NH_4SO_2 and NO_3^-), salt (K^+, Na^+, Cl^-) and dust were the dominant aerosol species over IGP (*Dey and Tripathi*, 2007). The mean mass concentration of dust which consists of soil dust or fly ash from industrial emissions, and transported dust from far distance was 1 $\mu g\, m^{-3}$ in fine mode, and 5.5 $\mu g\, m^{-3}$ in coarse mode, and contributed $\sim$ 6% to total mass concentration during winter (*Dey and Tripathi*, 2007). Based on the above observation the dust mass has been divided into: (i) soil dust or fly ash in terms of insoluble aerosol, and (ii) transported mineral dust as per the specific aerosol types given in *Hess et al.* (1998). The mixing state of aerosols is determined for years 2007-2009 in which the reported mass concentration over Kanpur corresponding to year 2004 are utilized, as mass concentration measurements for year 2007-2009 are not available. This is not expected to affect the result significantly as the inter-

annual variability in aerosol properties is less when compared to seasonal variability (e.g., *Singh et al.*, 2004).

Over Gandhi College, as the mass concentration of aerosol species are not available, aerosol mass concentration obtained over Kanpur taken as a basis, and the mass concentrations of different aerosol species are modified taking into account the meteorology and long-range transport over Gandhi college. Using the measured aerosol mass concentration information the aerosol optical properties are simulated for different mixing scenarios (*Chapter 2*). In contrast to the earlier study (*Dey et al.*, 2008) where only spectral SSA was used as a constraint, here all the three measured aerosol parameters are used. However, there are cases where rms differences in the spectra of AOD and SSA are $<$0.03, but for asymmetry parameter g this condition is not satisfied (Tables 4.2, 4.3) which could be due to the asymmetry in the shape of aerosol particles. In the present study the optical properties are estimated assuming aerosols as spherical. However, in the atmosphere aerosols are present in various shapes (e.g., *Guieu et al.*, 1994). The AERONET algorithm was modified to take into account non-spherical shapes of aerosol particles such as mineral dust (*Dubovik et al.*, 2006). Therefore, the spectral g values derived in our calculation can differ from the measured g values, as in the present study all aerosols are treated as spherical. This difference in g value can give rise to change in aerosol radiative forcing (*Mishchenko et al.*, 1997). This aspect is examined later.

4.3 Results and Discussion

4.3.1 Aerosol mass fractions over Kanpur and Gandhi College

The mass fractions of different aerosol species are obtained using the criteria described in section 4.2 over Kanpur and Gandhi College are shown in Figure 4.2. BC mass over Kanpur is found to be 12 μg m^{-3} during winter. This is consistent with measurements made during winter (December 2004), which showed higher BC mass with a mean of 12 μg m^{-3} and contributed $\sim$ 10% to total mass concentration of aerosols over Kanpur (*Tare et al.*, 2006).

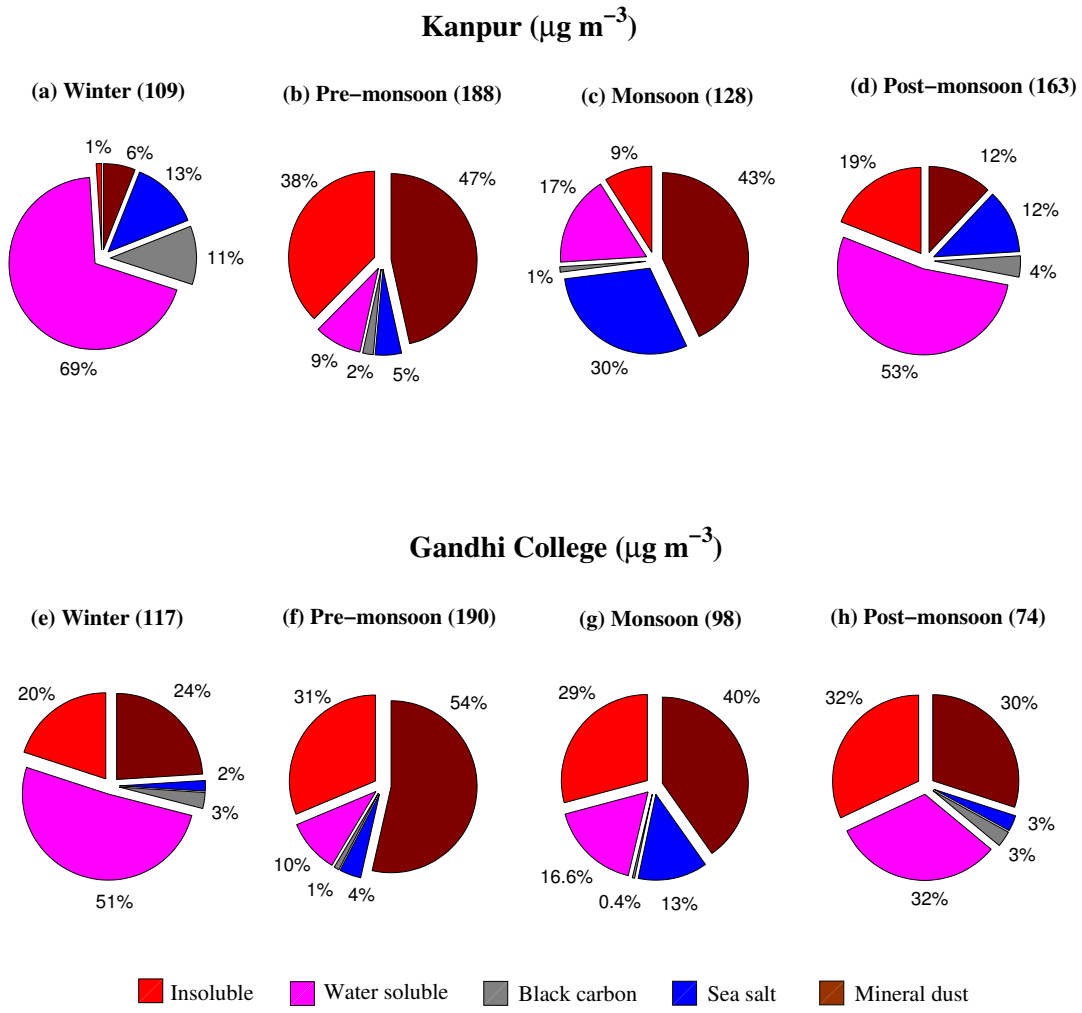

Figure 4.2: *Percentage mass contribution of different aerosol species to total mass concentration ($\mu g\ m^{-3}$) over Kanpur and Gandhi College during (a, e) winter, (b, f) pre-monsoon, (c, g) monsoon and (h, i) post-monsoon. The total mass concentrations during different seasons are also mentioned in parenthesis.*

During winter biomass burning is most prominent over IGP (*Di Girolamo et al.*, 2004; *Habib et al.*, 2006), and organic aerosols are the single largest species of biomass burning aerosols in addition to BC (*IPCC*, 2001 and references cited therein). Organic aerosol species are accounted for in OPAC in both insoluble and water soluble aerosol components (*Hess et al.*, 1998). Thus, insoluble and/or water soluble aerosols contribute the highest to the total mass over Kanpur and Gandhi College during winter

(Figure 4.2). BC aerosol reduces to 1% of total mass during monsoon due to wet removal. The decrease in BC mass fraction from winter to monsoon was also observed and reported over Kanpur (e.g., *Tare et al.*, 2006) and over other locations in India (e.g., *Ramachandran and Kedia*, 2010 and references cited therein). The mass of dust is higher and contribute $\geq$ 40% to total mass during pre-monsoon and monsoon seasons over Kanpur and Gandhi college (Figure 4.2) as northwesterly winds transport dust aerosols from Thar desert to the study locations (e.g., *Chinnam et al.*, 2006).

Mass fraction of water soluble (WS) aerosol is found to be higher ($>$ 50%) during winter, while it is lower during pre-monsoon ($\lesssim$ 10%) due to lower RH (Table 4.1). Aerosols produced locally cannot get ventilated due to lower wind speed during post-monsoon and therefore results in a higher total aerosol mass concentration (Figure 4.2) and higher AOD over Kanpur (Figures 4.1, 4.3). On the other hand AOD and total mass over Gandhi college is lower and represents the background condition in a rural environment during post-monsoon (Figures 4.1, 4.2 and 4.4). In addition, higher aerosol mass concentration is found during winter and pre-monsoon over Gandhi College (Figure 4.2), which can be attributed to the downwind transport of aerosols from major polluted urban cities (Figure 4.1). Mass fractions of aerosols obtained in the current study are found to be consistent with observations reported earlier over Kanpur (e.g., *Tare et al.*, 2006; *Chinnam et al.*, 2006).

4.3.2 Probable Mixing states in Indo-Gangetic Plain

(a) Kanpur

AERONET derived spectral aerosol optical properties and the modeled properties corresponding to probable and external mixing states of aerosols during winter, pre-monsoon, monsoon and post-monsoon are shown in Figure 4.3. The $\pm 1\sigma$ standard deviation shown as vertical bars in the AERONET data correspond to both intraseasonal and interannual variations in aerosol optical parameters. The most probable mixing states obtained and the rms differences in the measured and modeled optical properties during different seasons are given in Table 4.2. During winter coating of 20% water soluble aerosol over all the BC (100%) is found to be the only probable mixing state of aerosols. During pre-monsoon, the presence of dust aerosols which

are transported by northwesterly winds give rise to a core-shell mixing of 20% dust with 20% BC mass (Table 4.2). 20% of insoluble aerosols (mainly resuspended dust and insoluble organics) coated by 20% mass of BC is also found to be a probable mixing state. The probable occurrence of this probable mixing state is supported by the observations taken during ACE - Asia where BC coating over the dust was observed (*Clarke et al.*, 2004; *Arimoto et al.*, 2006). 20% BC and dust is found to be coated by 20% WS aerosols. However, dust coated by 20% BC also result in a probable mixing state during monsoon.

Table 4.2: *Aerosol species viz., insoluble, water soluble, black carbon and mineral dust present in core and shell, and their percentage mass fractions in mixing along with rms differences between the measured and modeled optical properties (aerosol optical depth (AOD), single scattering albedo (SSA) and asymmetry parameter (g)) in the wavelength range of 0.34 - 1.02 μm over Kanpur.*

	Mixing state				rms differences		
	Core		Shell				
Seasons	Species	%	Species	%	AOD	SSA	g
Winter	Black carbon	100	Water soluble	20	0.019	0.020	0.029
Pre-Monsoon	Insoluble	20	Black carbon	20	0.017	0.021	0.076
	Black carbon	20	Insoluble	20	0.017	0.021	0.074
	Mineral dust	20	Black carbon	20	0.018	0.028	0.087
Monsoon	Black carbon	20	Water soluble	50	0.03	0.01	0.054
	Mineral dust	100	Black carbon	100	0.03	0.026	0.09
	Mineral dust	20	Water soluble	20	0.02	0.013	0.064
Post-monsoon	Insoluble	20	Water soluble	20	0.027	0.03	0.052
	Black carbon	100	Water soluble	20	0.029	0.021	0.034

WS aerosol (*e.g.,* sulfate and nitrate) coating over dust is found to be most common due to the secondary transformation of sulfate and nitrate on dust particles during the long-range transport of dust (*Bauer and Koch*, 2005; *Wang et al.*, 2007). IS and WS in small fractions (20%), and large fraction of BC ($\geq$ 50%) with 20% WS are probable core-shell mixing states during post-monsoon. External mixing is also probable during monsoon and post-monsoon seasons, while SSAs in external mixing are lower when compared to AERONET measurements during winter and pre-monsoon.

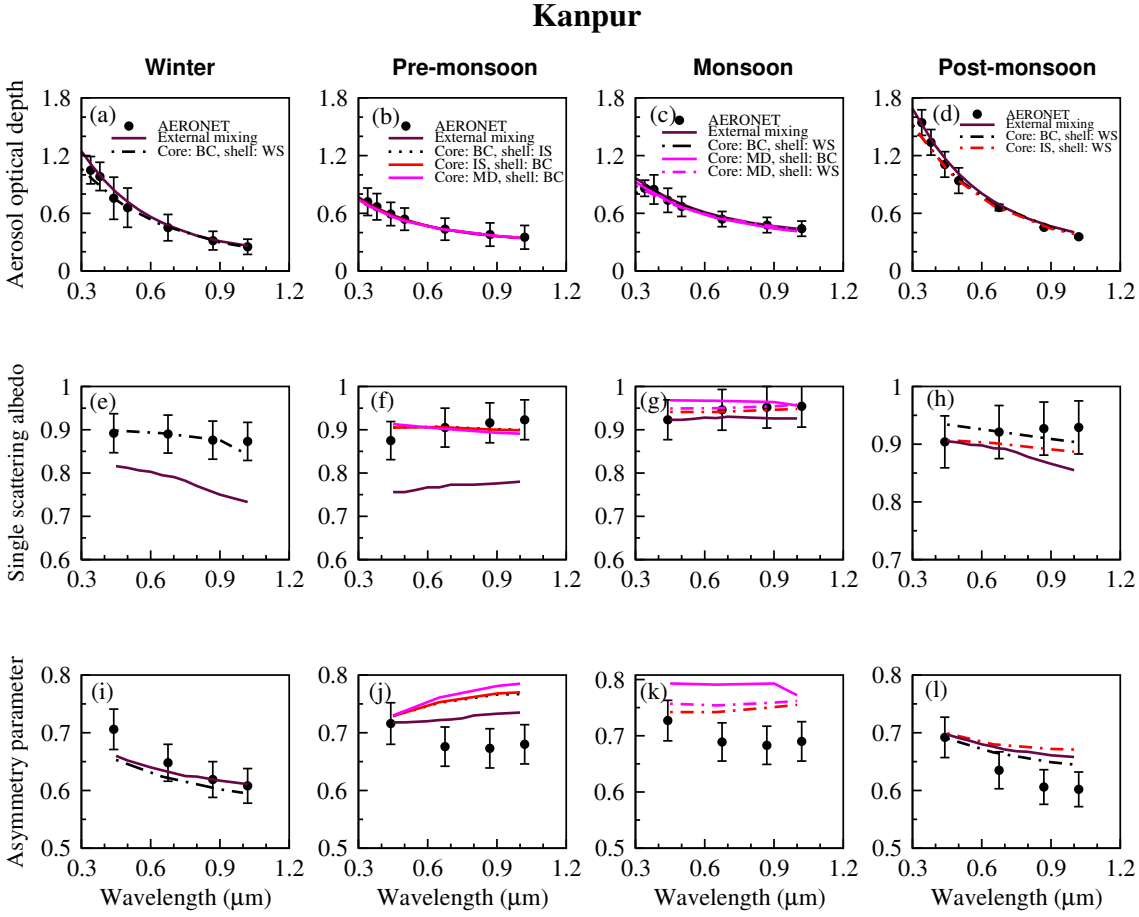

Figure 4.3: *Spectral aerosol parameters (a-d) aerosol optical depth, (e-h) single scattering albedo and (i-l) asymmetry parameter from AERONET, for external mixing and probable mixing states of different aerosol species viz., insoluble (IS), water soluble (WS), black carbon (BC), mineral dust (MD) and sea salt (SS) during winter, pre-monsoon, monsoon and post-monsoon seasons over Kanpur. Vertical bars in AERONET data represent* $\pm$ 1 σ *deviation from the mean.*

The previous finding of probable mixing states over Kanpur by *Dey et al.* (2008) is consistent for pre-monsoon and post-monsoon. However, there are differences in mixing states of aerosols between the present study and Dey et al. results which could be due to the following reasons: (1) in the present study fractions of mass of aerosols ranging from 20% to 100% are considered to be involved in core-shell mixing, while in Dey et al. study the entire mass of aerosol species which acts as core is assumed to be coated by the species acting as shell, (2) all the three optical properties *viz.*, AOD, SSA and *g*, and reported mass concentrations are used as constraints to determine

the probable mixing state of aerosols in the present study, while Dey et al. used mass concentration of species and SSA values only, and (3) the mixing states are determined when rms difference between measured and modeled AOD and SSA spectra is $<$0.03, while in Dey et al. case the rms difference in SSA spectra was much higher than the stringent condition adopted in the present study. In addition, the present study is done on a seasonal basis using the data obtained from 2007 - 2009, while Dey et al. results correspond to the months of October 2005 (post-monsoon), December 2005 (winter), and March 2006 (pre-monsoon).

(b) Gandhi College

Spectral AOD, SSA and g measured by AERONET and modeled for different probable mixing scenarios and external mixing for Gandhi College are shown in Figure 4.4. The vertical bars ($\pm 1\sigma$) in AERONET data include both the intraseasonal and interannual variations. The various core-shell mixing states and rms difference between measured and modeled properties are given in Table 4.3. A small mass fraction of IS (soil dust and organics) and SS/WS is found to be most probable in core-shell mixing during winter. This type of mixing was reported previously in which the fraction of silicate from dust was found to be internally mixed with sea salt (*Andreae et al.*, 1986). Various mechanisms such as collision of sea salt and silicate, Brownian coagulation of aerosols and electrostatic attraction between silicate and sea salt were proposed for such type of mixing (*Andreae et al.*, 1986). During pre-monsoon, dust originating from Thar desert can reach Gandhi College by passing through many urban locations (Figure 4.1). Therefore dust, which comes through the polluted regions could be mixed with the local pollutants (BC), and get coated during pre-monsoon.

The IS and BC core-shell mixing is also probable during pre-monsoon. The uptake of water soluble sulfate and nitrate on other aerosols (*e.g.,* dust) was found to be more prominent in various observations (e.g., *Bauer and Koch*, 2005; *Jordan et al.*, 2003). Analogous to the observations the core-shell mixing of WS aerosols with other aerosols (*viz.,* IS, BC, MD, and SS) is found to be probable mixing states during monsoon season which exhibits the highest (91%) RH (Figure 4.4, Tables 4.1 and 4.3). The probable mixing states during post-monsoon are IS coated by BC or BC coated by WS. During post-monsoon SS and MD coated by BC are also found to be probable mixing

states over Gandhi College.

Table 4.3: *Aerosol species viz., insoluble, water soluble, black carbon, mineral dust and sea salt present in core and shell, and their percentage mass fractions in mixing along with rms differences between the measured and modeled optical properties (aerosol optical depth (AOD), single scattering albedo (SSA) and asymmetry parameter (g)) in the wavelength range of 0.34 - 1.02 μm over Gandhi College.*

	Mixing state				rms differences		
	Core		Shell				
Seasons	Species	%	Species	%	AOD	SSA	*g*
Winter	Insoluble	20	Water soluble	20	0.03	0.01	0.04
	Sea salt	50	Insoluble	20	0.027	0.011	0.052
	Insoluble	20	Sea salt	50	0.027	0.011	0.051
Pre-Monsoon	Insoluble	20	Black carbon	20	0.029	0.021	0.086
	Black carbon	20	Insoluble	20	0.029	0.021	0.084
	Mineral dust	20	Black carbon	100	0.023	0.027	0.13
Monsoon	Insoluble	100	Water soluble	20	0.026	0.012	0.051
	Black carbon	50	Water soluble	20	0.024	0.018	0.037
	Mineral dust	50	Black carbon	50	0.029	0.016	0.092
	Mineral dust	100	Water soluble	20	0.021	0.01	0.045
	Water soluble	20	Sea salt	20	0.024	0.006	0.061
Post-monsoon	Insoluble	100	Black carbon	100	0.025	0.030	0.053
	Sea salt	100	Black carbon	100	0.023	0.026	0.047
	Black carbon	100	Sea salt	20	0.022	0.025	0.049
	Mineral dust	100	Black carbon	20	0.026	0.026	0.050

The results show that in the Indo-Gangetic plain, the mixing states of aerosols vary between urban (Kanpur) and rural (Gandhi College) locations. The probable mixing states over Gandhi College is found to be similar to that of Kanpur during pre-monsoon and monsoon. However, differences in probable mixing states of aerosols over both the locations are also observed as sea salt is not found to be involved in internal mixing over Kanpur, while over Gandhi College sea salt is found to be core-shell mixed with other aerosols during winter, monsoon and post-monsoon seasons. The probable mixing states derived from remote sensing SSA over Ahmedabad, an urban location (*Chapter 3*) is similar, but the percentage fraction of core-shell mixing is different when compared to mixing state over IGP. SS (core) - BC (shell) mixing is found to be probable over Ahmedabad during pre-monsoon and post-monsoon, while SS-BC mixing is found to be most probable during post-monsoon over Gandhi College

only, thus, indicating that the mixing state of aerosol can vary depending on the type of environments, type of aerosols and relative humidity.

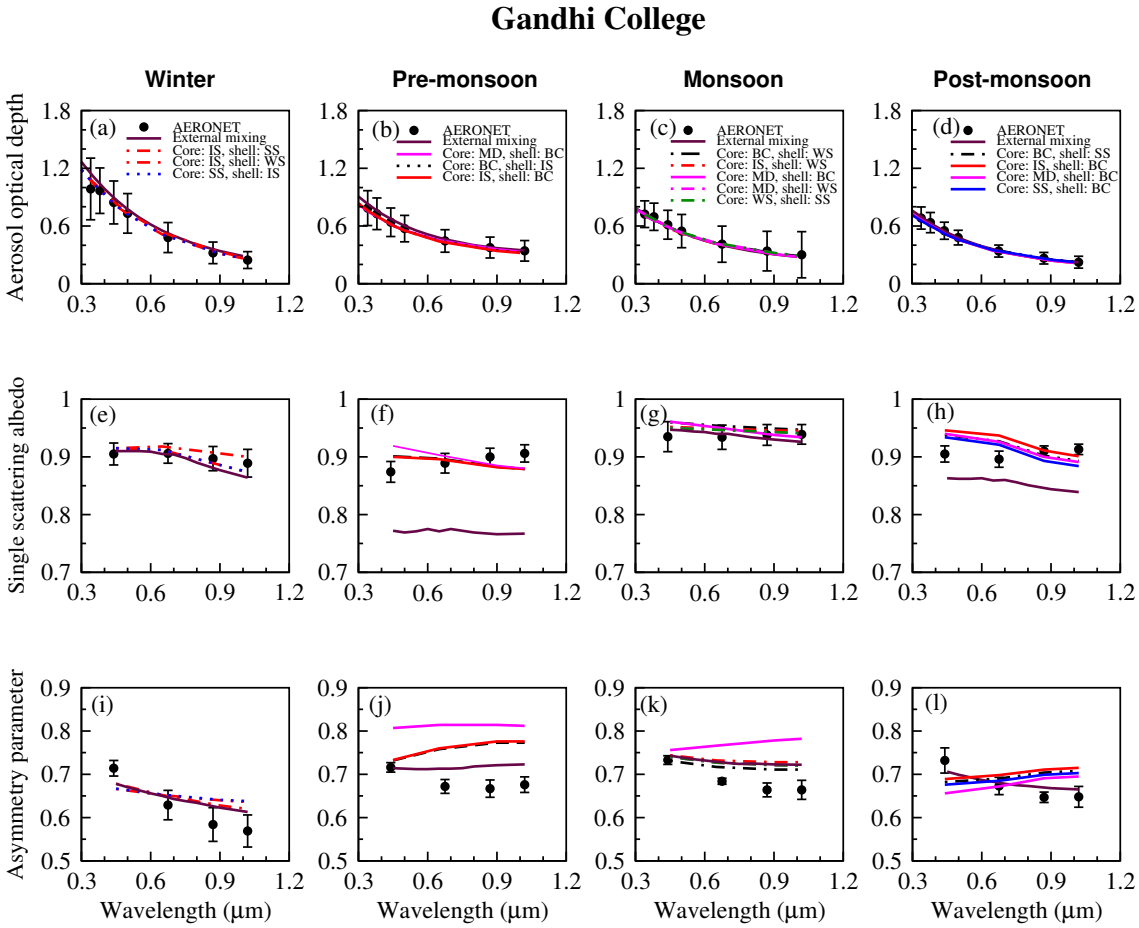

Figure 4.4: *Spectral aerosol parameters (a-d) aerosol optical depth, (e-h) single scattering albedo and (i-l) asymmetry parameter from AERONET for external mixing and probable mixing states of different aerosol species such as insoluble (IS), water soluble (WS), black carbon (BC), mineral dust (MD) and sea salt (SS) during winter, pre-monsoon, monsoon and post-monsoon seasons over Gandhi College. Vertical bars in AERONET data correspond to* $\pm$ 1 σ *deviation from the mean.*

4.3.3 Aerosol radiative forcing over Indo-Gangetic Plain

(a) Kanpur

Aerosol radiative forcing at the surface, in the atmosphere and at the top of the atmosphere (TOA) over Kanpur during different seasons estimated for the external and all the probable mixing scenarios (listed in Table 4.2) are shown in Figure 4.5.

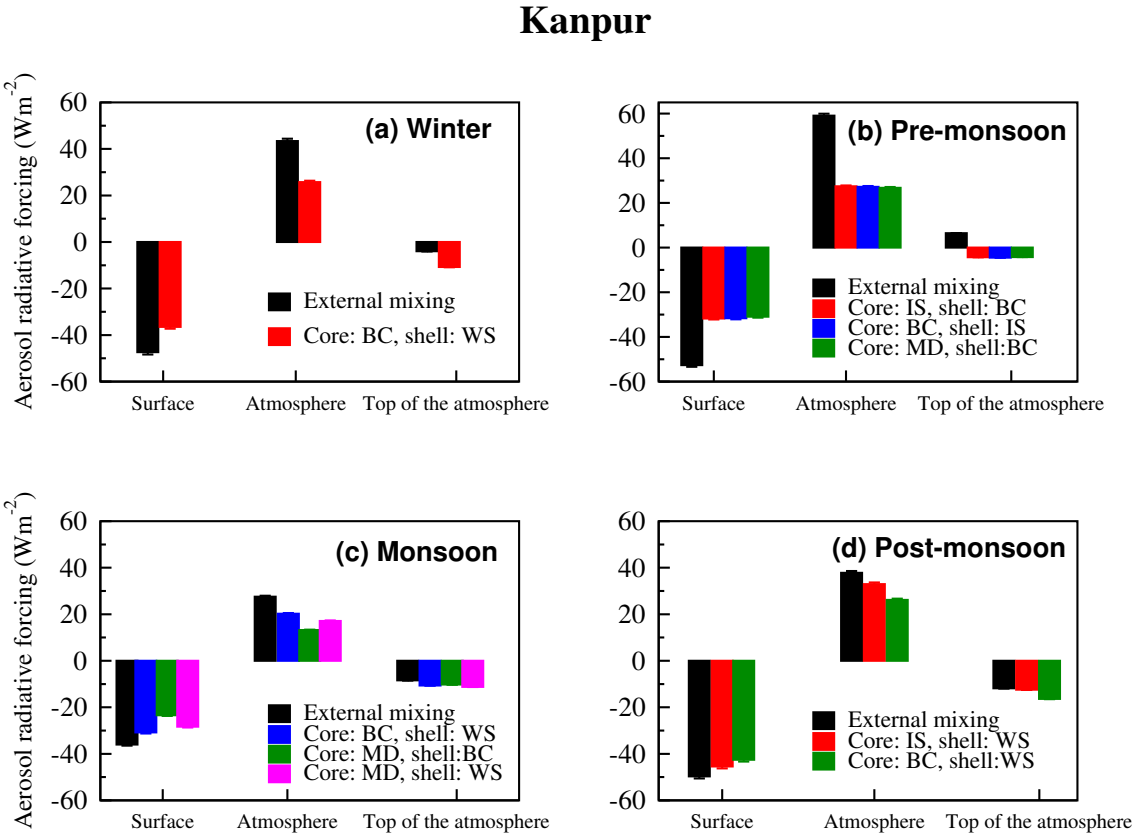

Figure 4.5: *Aerosol radiative forcing at the surface, in the atmosphere and at the top of the atmosphere for external and different probable mixing states of different aerosol species viz., insoluble (IS), water soluble (WS), black carbon (BC), mineral dust (MD) and sea salt (SS) over Kanpur during (a) winter, (b) pre-monsoon, (c) monsoon and (d) post-monsoon respectively.*

Aerosol forcing for external mixing show higher deviations from those for probable mixing cases during winter and pre-monsoon as the SSA for external mixing is lower than the measured and modeled SSA for different core-shell mixing during these seasons (Figure 4.3). Aerosol forcing for all the mixing states are higher during post-monsoon due to higher AODs. Forcing for external mixing and all the core-shell mixing scenarios agree within the uncertainty limits during monsoon and post-monsoon seasons. TOA forcing flips its sign from positive for external mixing to negative for probable mixing cases during pre-monsoon (Figure 4.5) as SSA is lower (<0.8) for external mixing case when compared to that of measured and probable mixing cases (SSA >0.8) (Figure 4.3).

(b) Gandhi College

Aerosol radiative forcing at different levels over Gandhi College during different seasons estimated for various probable mixing scenarios (listed in Table 4.3) and external mixing scenario are shown in Figure 4.6.

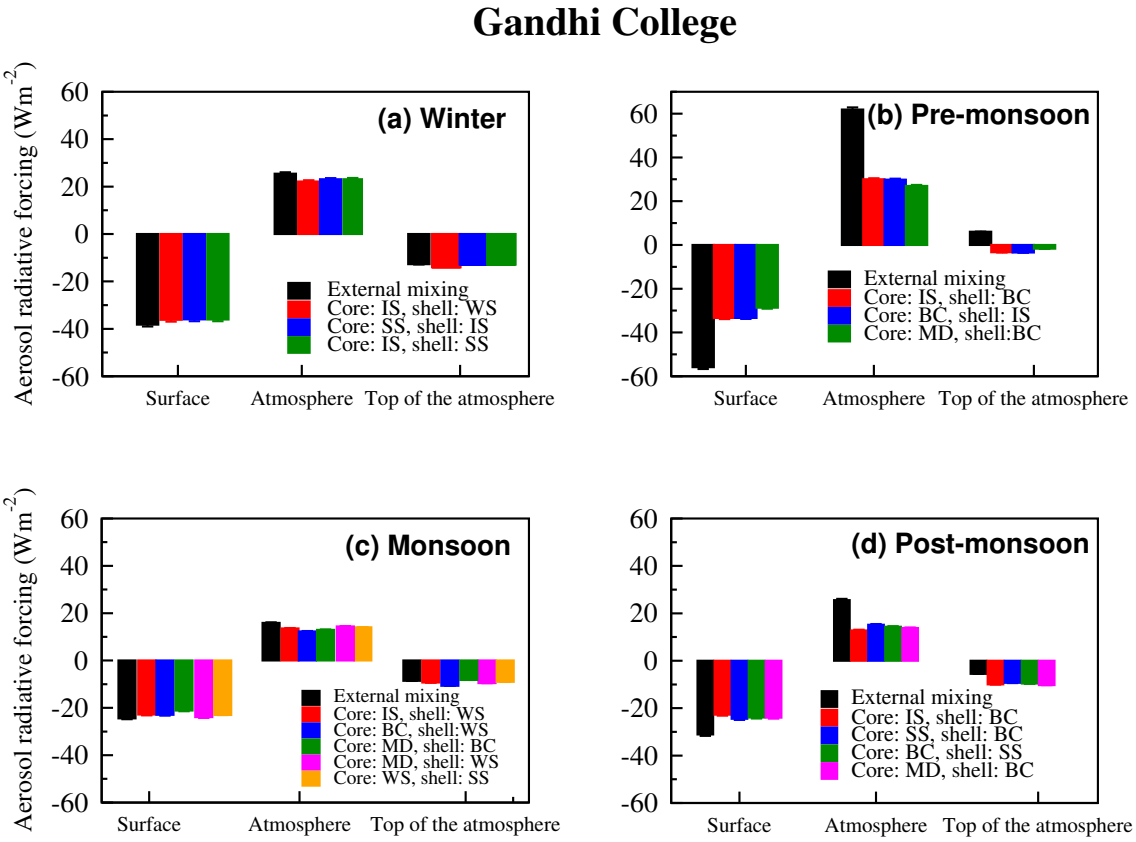

Figure 4.6: *Aerosol radiative forcing at the surface, in the atmosphere and at the top of the atmosphere for external and different probable mixing states of different aerosol species such as insoluble (IS), water soluble (WS), black carbon (BC), mineral dust (MD) and sea salt (SS) over Gandhi College during (a) winter, (b) pre-monsoon, (c) monsoon and (d) post-monsoon respectively.*

Aerosol radiative forcing at the surface and in the atmosphere is higher during pre-monsoon and significant difference in forcing is observed for probable and external mixing states of aerosols. Aerosol radiative forcing estimated for different probable mixing states is similar for a particular season. During post-monsoon aerosol forcing for external mixing is higher than those obtained for probable mixing states as SSA is lower for the external mixing (Figure 4.6). Aerosol forcing at all the levels are higher

during winter and lower during monsoon (Figure 4.6). The higher forcing during winter is attributed to higher AOD and lower SSA, while lower forcing occurs during monsoon due to higher SSA and lower AOD. TOA forcing is positive when aerosols are externally mixed, while it is negative for probable mixing state during pre-monsoon while TOA forcing is always negative for other seasons. The differences in forcing for different mixing states of aerosols are negligible during monsoon and post-monsoon.

4.3.4 Sensitivity of asymmetry parameter to aerosol radiative forcing

Asymmetry parameter (g) values can change depending on the sphericity of aerosols. Dust like aerosols are found to be non-spherical in shape (e.g., *Guieu et al.*, 1994). The aerosols are assumed to be spherical in shape in this study, therefore, the modeled g can be different when compared to measured g when dust like aerosols are mixed with other aerosols. This is corroborated by the fact that the rms differences between the measured and modeled g spectra are larger than those obtained for AOD and SSA (Tables 4.2, 4.3). The sensitivity of g on aerosol radiative forcing is estimated to examine the effect of shape of dust like aerosols on radiative forcing. Aerosol radiative forcing over Kanpur during pre-monsoon, monsoon and post-monsoon for asymmetry parameters obtained for different mixing scenarios and for the case where modeled g matches with AERONET measured g are shown in Figure 4.7.

The sensitivity calculation has not been done for winter as asymmetry parameter for different mixing cases during winter matches well (rms difference ≤ 0.03) with measured g (Table 4.2), as winter is dominated by fine mode aerosols and the contribution of dust is low (Figure 4.2). Aerosol radiative forcing at the surface and at the top of the atmosphere for modeled and measured g deviate a little but agree within the uncertainty of forcing estimation during all the seasons. Higher g value corresponds to higher forward scattering and hence results in a higher reduction of radiation at the surface and also lower TOA forcing. BC coating of dust during monsoon has the largest rms deviation (0.09) in g spectra (Table 4.2) which results in a 3 Wm^{-2} lower value in both surface and TOA forcing (Figure 4.7).

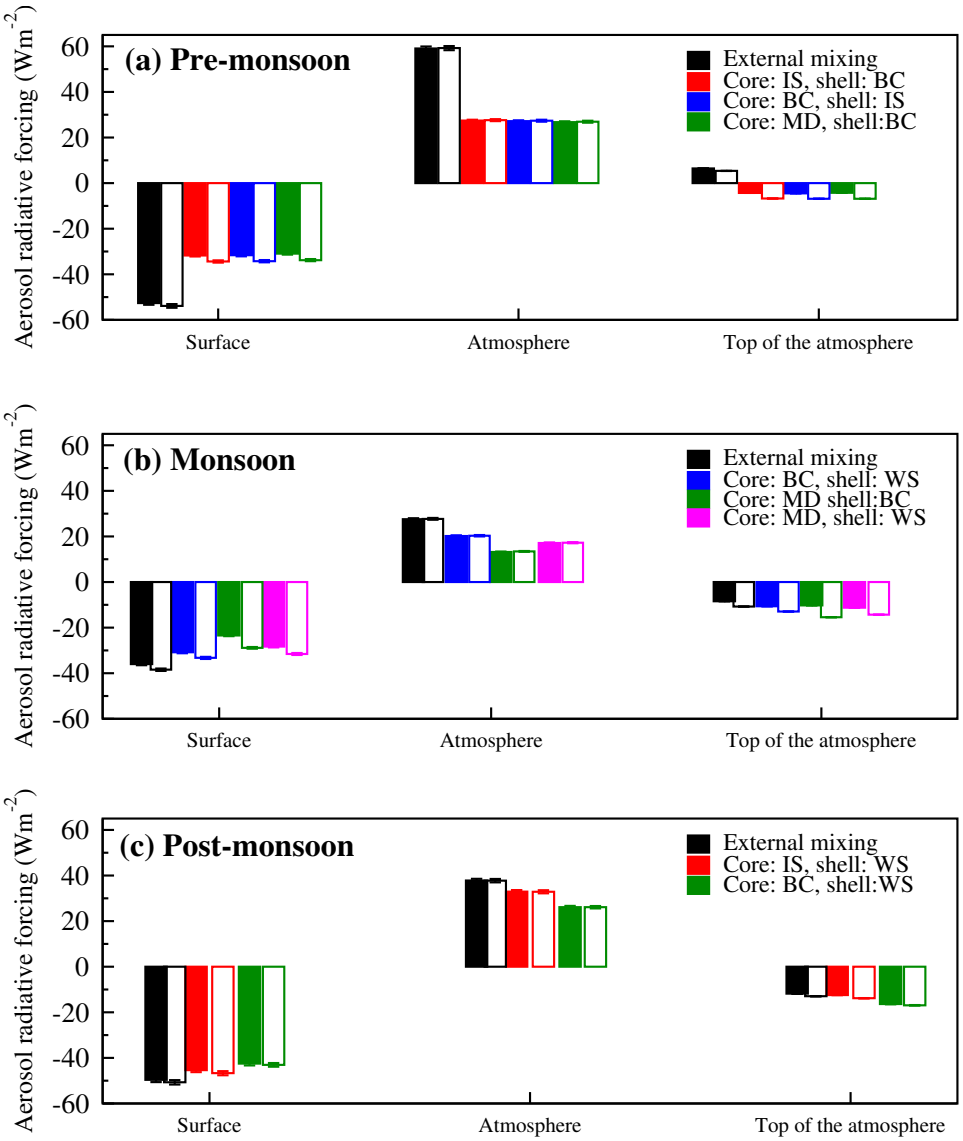

Figure 4.7: *Sensitivity of asymmetry parameter (g) to aerosol radiative forcing at the surface, in the atmosphere and at the top the atmosphere over Kanpur during (a) pre-monsoon, (b) monsoon and (c) post-monsoon. Filled bars correspond to g obtained for different mixing states of different aerosol species viz. insoluble (IS), water soluble (WS), black carbon (BC), mineral dust (MD) and unfilled bars correspond to aerosol forcing obtained using AERONET derived g, while maintaining the same spectral AOD and SSA obtained for the corresponding mixing scenarios (Table 4.2).*

The deviation in aerosol radiative forcing at the surface and at TOA cancel each other and results in the same value of atmospheric radiative forcing. The aerosol radiative forcing is weakly sensitive to g and strongly dependent on SSA over a higher

reflecting surface, which results in multiple reflections between the ground and the aerosol, conversely, the asymmetry parameter is a significant driver of surface aerosol forcing when surface albedo is lower ($\leq$ 0.1) (*McComiskey et al.*, 2008). The broadband surface albedo is higher ($\gtrsim$ 0.2) over IGP due to which aerosol forcing is less sensitive to asymmetry parameter. *Andrews et al.* (2006) found that a decrease of 10% in g resulted in a 19% reduction in TOA forcing while the surface forcing decreased by 13%. The span of g at 0.55 μm in *Andrews et al.* (2006) study was larger and g varied from 0.5 to 0.8 and the median was 0.65. The value of g at 0.55 μm ranges from 0.65 to 0.71 over Kanpur and Gandhi College, and the effect of g on forcing is similar to that obtained by *Andrews et al.* (2006). However, the difference in forcing that arises due to change in g is not higher than the uncertainty limits in aerosol radiative forcing estimation. *Mishchenko et al.* (1997) suggested that the influence of particle shape on the aerosol radiative forcing at TOA is negligibly small and forcing can be accurately estimated using Mie theory of spherical particles. Thus, this calculation reiterates that aerosol radiative forcing at TOA and surface is weakly sensitive to g and the change in aerosol forcing due to differences in g are smaller than the uncertainty limits of forcing computation.

Chapter 5

Aerosol mixing state and its effect on optical and radiative properties over different regions of the world

Aerosols are mainly regional in nature due to their short residence times and regional distribution of their sources (*Kaufman et al.*, 2002). Aerosols can be transported from their sources to longer distances depending upon the meteorological conditions and their removal mechanisms. For example, Asian dust was transported one full circuit around the globe (*Uno et al.*, 2009). Aerosol optical, physical and chemical properties are modified during the transport by atmospheric chemical reactions and removal mechanisms. Over an urban region pollutant aerosols can dominate which are produced due to manmade activities. Biomass burning affected regions are dominated by carbonaceous aerosols (organic carbon and black carbon). The diversity of aerosols present over a location/region due to local/regional sources, and long-range transport can give rise to a complex aerosol mixture. Mixing state of aerosols can change depending upon the availability of different aerosol species over a location and the meteorological conditions. Single particle aerosol analysis studies reveal that aerosols need not remain as external mixtures after long-range transport and can undergo transformation (*Guazzotti et al.*, 2001; *Hasegawa and Ohta*, 2002; *Murphy et al.*, 2006; *Spencer et al.*, 2008). The radiative forcing calculations incorporating the mixing state of aerosols on a global scale have been made using global climate models (e.g., *Chung and Seinfeld*, 2002; *Jacobson*, 2001; *Kopp and Mauzerall*, 2010); the focus of these studies has been black carbon, and how on a global scale the radiative forcing

varies when black carbon aerosols are externally, core-shell or internally mixed with other aerosol species. In contrast to the model simulations, observations have revealed that aerosol mixing can exhibit regional signatures (*Hasegawa and Ohta*, 2002; *Murphy et al.*, 2006; *Spencer et al.*, 2008), thus, indicating that the radiative effects due to aerosol mixing will also vary on a regional scale. For the first time, in this study, the seasonal and spatial variations in the mixing state of aerosols over different regions of the globe, using the measured optical and physical characteristics of aerosols have been determined. The implications of different mixing states (external and core-shell) on aerosol radiative forcing are presented, and inferences are drawn.

5.1 Study locations and aerosol optical properties data

The study locations spread across the globe (Table 2.2, Figure 5.1), are governed by different environments and seasonally varying meteorology (Figure 5.2). All the locations are in the northern hemisphere, except for Mongu; however, Mongu is within the tropical belt (20^{o}S). Therefore, the data and the results are classified as winter (December-January-February, DJF), pre-monsoon (or spring) (March-April-May, MAM), monsoon (June-July-August-September, JJAS), and post-monsoon (or fall) (October-November, ON) and discussed. Maryland (NASA GSFC) is an urban location (*Holben et al.*, 2001), while Mexico city, Mexico is a high altitude, densely populated urban location (*Vega et al.*, 2010). Tamanrasset is an oasis city and the capital of Tamanrasset province in southern Algeria. Djougou in west Africa, and Mongu in southern Africa represent mixed sites where dust and biomass burning contribute to the aerosol distribution. Abu Dhabi is a coastal site and influenced by dust storm activities (*Reid et al.*, 2008). Karachi, is a densely populated (14 million), urban, industrial, coastal city located in the southeastern part of Pakistan on the Arabian Sea (Figure 5.2) (*Dutkiewicz et al.*, 2009). Singapore, is a coastal city and influenced by local emissions from chemical industries, power plants, petroleum refineries and vehicular traffic (*Balasubramanian et al.*, 2003), and biomass burning aerosols (mainly organics and black carbon) from the biomass burning emissions of Sumatra.

Figure 5.1: *Google Earth image of the globe showing the study locations spread across different regions of the world.*

Gwangju is a major city located on the southwestern edge of Korean peninsula (*Lee et al.*, 2008), and is affected by urban emissions. Osaka is a metropolitan city. Gwangju and Osaka, in addition to being major urban centers, are also affected by dust carried by strong winds from China during pre-monsoon (*Funasaka et al.*, 2003, Figure 5.2). It is clear that the chosen study locations, in addition to being environmentally different (Table 2.2), are governed by different meteorology (Figure 5.2), and influenced by different aerosol source regions in different seasons. The important criteria for the selection of different locations around the world are the availability of (a) measured spectral aerosol optical parameters, and (b) either measured or modeled aerosol mass concentrations.

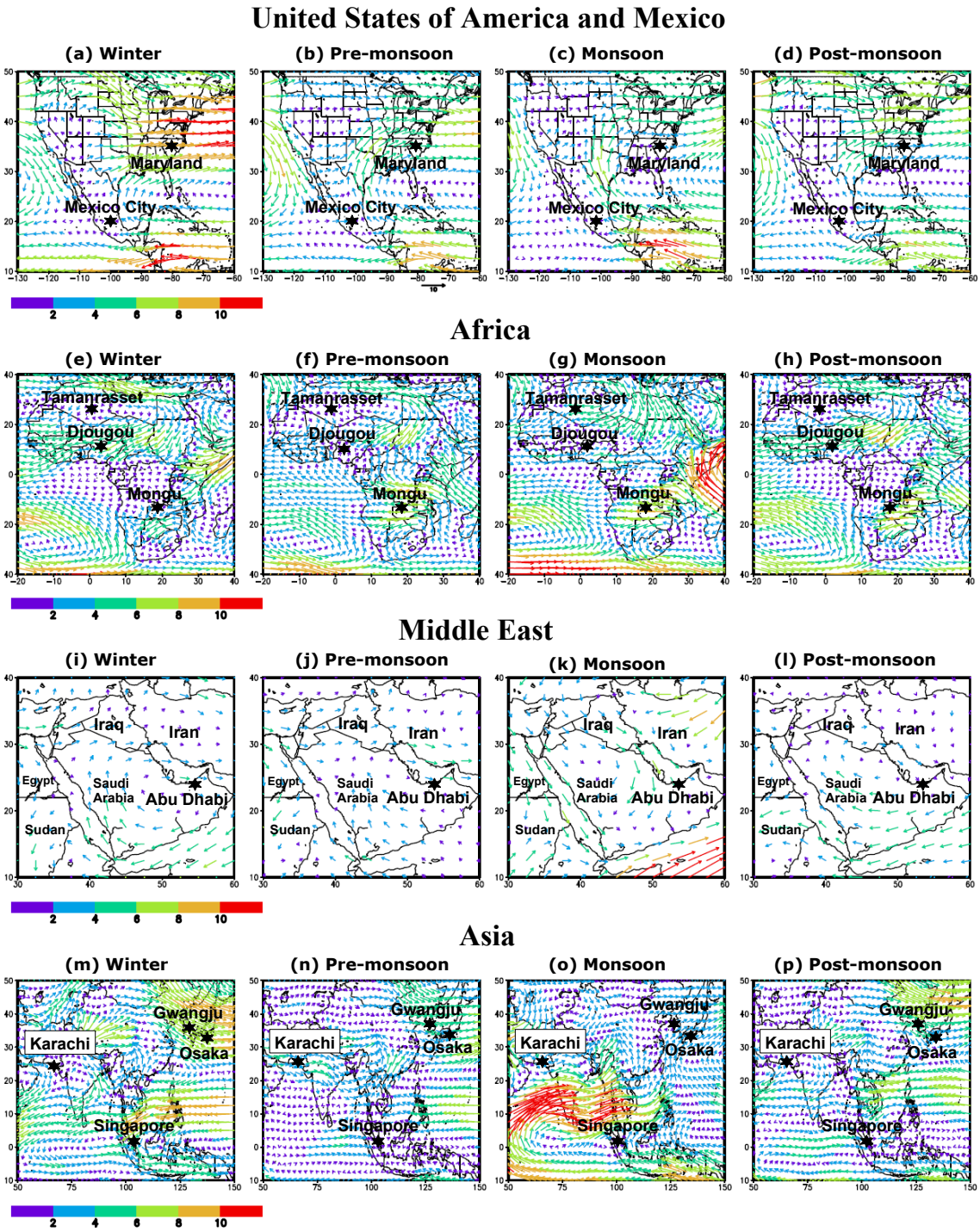

Figure 5.2: *2007-2009 mean winds (ms^{-1}, represented by arrows) at 850 hPa during winter (December-January-February, DJF), pre-monsoon (March-April-May, MAM), monsoon (June-July-August-September, JJAS) and post-monsoon (October-November, ON) seasons respectively over the study regions.*

The study locations are all AErosol RObotic NETwork (AERONET) (*Holben et al.*, 2001) locations. AERONET measured spectral aerosol optical depths (AODs), single scattering albedo (SSA) and asymmetry parameter (*g*) (section 2.4) are utilized.

5.2 Approach

Knowledge on aerosol mass concentrations, and mass concentrations of different aerosol species over a particular location is important for an accurate determination of AOD, SSA and *g*. Aerosol mass concentrations and the mass concentrations of different species or mass ratios obtained and reported over each location were used. The mass ratio of carbonaceous aerosol over Maryland was found to vary from 18% (monsoon) to ∼23% (fall) (*Takemura et al.*, 2002). Sulfate aerosols varied in the range of 37 to 57% during the year. Dust was minimum in winter (∼6%) and maximum (∼19%) in summer. $PM_{2.5}$ mass concentrations over Mexico city were found to be in the 22 to 52 μg m^{-3} range (*Vega et al.*, 2010); carbonaceous and inorganic aerosols contributed 30% each to the mass concentration while the contribution due to dust varied from 5 to 13%. The aerosol mass concentrations over southern Africa during the biomass burning period of August-September were found to be dominated by sulfate, organic and black carbon aerosols (*Magi*, 2009). Organic carbon aerosol mass concentration was in the 3-9 μg m^{-3} range when the airmass was representative of southern hemisphere African extratropics, which increased to 17-36 μg m^{-3} when the air mass came from tropics. BC, sulfate, and nitrate were also higher when the air mass was of tropical origin (*Magi*, 2009). The average aerosol mass concentrations over Abu Dhabi during August-September 2004 was 35 μg m^{-3} (*Reid et al.*, 2008). Alumino silicates, calcium carbonate, organic matter, black carbon, sea salt and sulfate were present (*Reid et al.*, 2008).

BC mass concentrations in Karachi varied from 8 μg m^{-3} in winter to 10 in post-monsoon (*Dutkiewicz et al.*, 2009). *Parekh et al.* (1987) reported the presence of dust (48%), sulfate, nitrate and sea salt during July over Karachi. Over Singapore the annual average $PM_{2.5}$ mass concentration was about 27 μg m^{-3} (*Balasubramanian et al.*, 2003). Chemical analysis revealed the presence of water soluble organics,

insoluble organics, elemental carbon, sodium, chloride, nitrates and trace metals. Annual mean $PM_{2.5}$ mass concentrations over Gwangju was ~21 μg m^{-3} (*Lee et al.*, 2008). Chemical analysis of aerosol samples over Gwangju revealed the presence of nitrate, sulfate, metals, elemental and organic carbon. The aerosol mass concentrations in Osaka during April 1999-March 2002 were found to vary by a factor from 35 μg m^{-3} (post-monsoon) to 70 μg m^{-3} (pre-monsoon) (*Funasaka et al.*, 2003); aerosol mass concentrations were ~40 μg m^{-3} during winter and monsoon. Sulfate, nitrate, potassium, trace metals, sodium and chloride were present. BC mass concentrations were in the range of 2-4 μg m^{-3} during the year (*Mukai et al.*, 2006).

The most suitable aerosol components based on the mass concentrations mentioned above over the study locations are found to be water soluble aerosols (WS) (sulfates, nitrates, organic, water-soluble substances), insoluble (IS) (mostly soil particles with certain amount of organics), black carbon (BC), sea salt (SS) in accumulation and coarse modes, mineral dust (MD) (dust produced in arid regions and transported over long distances) in nucleation, accumulation and coarse modes. It is to be noted that organic carbon species is accounted for in OPAC in both IS and WS aerosol components. WS and BC are present mostly in the submicron mode, while IS, SS and MD are present in both submicron and supermicron modes. WS and SS are hygroscopic, while IS, MD and BC are hydrophobic. Seasonally varying total (or $PM_{2.5}$) aerosol mass concentrations and mass concentrations of aerosol species were used at each study location when they were available while reconstructing the measured aerosol optical properties. In the absence of seasonal information on aerosol mass and species concentrations, aerosol mass and species concentrations obtained during a particular season were used to derive the aerosol properties in other seasons. By doing so the chemical composition information of aerosols over a particular location was maintained while their mass concentrations were modified to obtain the derived spectral aerosol optical properties. In addition, aerosol optical properties and mass concentrations over the study locations may or may not pertain to the same time period; however, this discrepancy is not expected to alter significantly the results on aerosol mixing state and radiative forcing as the chemical composition is maintained. Over NASA GSFC since measured mass concentrations were not available mass ra-

tios of different aerosol species (*Takemura et al.*, 2002) are used, while the mass concentrations obtained over southern Africa including Mongu are used as the basis for Djougou and Tamanrasset as both the study locations are in the same region (Figure 5.1). In addition, over Djougou aerosol characteristics measured during the African Monsoon Multidisciplinary Analysis for dry season (*Mallet et al.*, 2008) are utilized to constrain the measured spectral aerosol optical properties. The methodology to estimated probable mixing state of aerosols is described in *Chapter 2*.

5.3 Results and Discussion

5.3.1 Mixing state of aerosols

Seasonal mean spectral aerosol properties (AOD, SSA and *g*) over the study locations and the aerosol optical properties obtained for the most probable mixing states (Table 5.1) are plotted in Figures 5.3 to 5.12. Aerosol optical properties and the mixing states are shown for all the seasons in each study location; the complete information on the mixing state and the percentage of mixing of core-shell species at each location in each season are given in Table 5.1. AOD, SSA and *g* show large seasonal and regional variations (Figures 5.3 - 5.12). Midvisible AODs are $\leq$0.5 over Maryland, Mexico city, Tamanrasset, Mongu, Abu Dhabi, Gwangju and Osaka. AODs are about 0.8 over Djougou and Singapore. Spectral characteristics of AOD provide an indication of the fine and/or coarse mode aerosol dominance over a location. AOD spectra will fall steeply when fine mode aerosols are dominant, while the AODs will be less and the spectra will be almost linear when coarse mode aerosols dominate. Spectral AOD features indicate the dominance of fine mode aerosols over NASA GSFC, Mecico city, Djougou, and Singapore. AOD spectra is very steep in Singapore, where AOD at 0.34 μm is 0.9 and decreases to 0.2 at 1.02 μm (Figure 5.10). At Tamanrasset and Karachi, AODs are comparable in the 0.34-1.02 μm wavelength range, consistent with the dominance of coarse mode (mineral dust and/or sea salt) aerosols.

AODs decrease slightly from 0.34 to 1.02 μm wavelength at Mongu, Abu Dhabi and Osaka indicating the contribution from both fine and coarse mode aerosols over these locations.

Table 5.1: *Aerosol species (insoluble (IS), water soluble (WS), black carbon (BC), sea salt (SS) and mineral dust (MD)), and percentage mass fractions in core-shell mixing scenarios for the most probable mixing states as function of season and mean relative humidity over the study locations.*

Winter		Pre-monsoon		Monsoon		Post-monsoon	
Core (%)	Shell (%)	Core (%)	Shell (%)	Core (%)	Shell (%)	Core (%)	Shell (%)
			NASA GSFC, Maryland				
		RH=83%		*RH=74%*		*RH=85%*	
		IS (50)	BC (100)	IS (50)	BC (100)	IS (20)	BC (100)
		BC (20)	WS (50)	BC (50)	WS (20)	BC (20)	WS (100)
		MD (50)	BC (100)	MD (20)	BC (20)	MD (50)	BC (20)
				SS (50)	BC (50)	BC (100)	IS (100)
			Mexico City				
RH=54%		*RH=48%*		*RH=67%*		*RH=61%*	
BC (50)	WS (50)	BC (50)	WS (20)	BC (50)	WS (50)	BC (100)	WS (20)
		BC (100)	IS (50)			MD (100)	WS (20)
						SS (50)	WS (20)
			Tamanrasset				
RH=26%		*RH=16%*		*RH=20%*		*RH=23%*	
IS (20)	BC (20)	MD (20)	IS (20)	MD (20)	IS (20)	IS (20)	BC (20)
			Djougou				
RH=89%		*RH=89%*		*RH=93%*		*RH=94%*	
MD (50)	WS (20)	MD (20)	BC (20)	MD (20)	BC (20)	MD (20)	BC (100)
MD (20)	SS (20)	MD (50)	IS (20)	MD (20)	IS (20)	MD (20)	IS (20)
		MD (20)	SS (20)				
			Mongu				
RH=29%		*RH=15%*		*RH=17%*		*RH=26%*	
BC (50)	WS (20)	IS (100)	WS (50)	BC (100)	WS (50)	IS (100)	WS (50)
		MD (100)	WS (50)			BC (50)	WS (100)
						MD (20)	WS (50)
			Abu Dhabi				
RH=66%		*RH=50%*		*RH=51%*		*RH=63%*	
IS (20)	BC (20)	MD (20)	BC (20)	MD (10)	BC (5)	IS (20)	BC (20)
MD (20)	BC (20)					MD (20)	BC (20)
BC (20)	IS (20)					BC (20)	IS (20)
			Karachi				
RH=52%		*RH=48%*		*RH=72%*		*RH=51%*	
IS (20)	BC (50)	MD (20)	BC (20)	MD (20)	BC (20)	IS (50)	BC (50)
MD (20)	BC (50)					MD (20)	BC (50)
BC (50)	IS (20)					BC (50)	IS (50)
			Singapore				
RH=83%		*RH=83%*		*RH=82%*		*RH=85%*	
BC (20)	WS (20)	BC (50)	WS (20)	BC (20)	WS (20)	BC (20)	WS (50)
WS (20)	BC (20)	WS (20)	BC (50)	WS (50)	BC (20)	WS (20)	BC (50)
		WS (50)	BC (20)	BC (20)	IS (50)		
			Gwangju				
RH=70%		*RH=74%*		*RH=90%*		*RH=73%*	
IS (75)	BC (100)	IS (50)	BC (100)	IS (50)	WS (20)	IS (50)	BC (100)
MD (20)	BC (100)	MD (50)	BC (20)	MD (50)	BC (100)	MD (20)	BC (100)
SS (20)	BC (75)	SS (20)	BC (50)	MD (50)	WS (20)		
BC (20)	WS (20)	BC (20)	WS (20)	MD (100)	SS (100)		
			Osaka				
RH=63%		*RH=65%*		*RH=90%*		*RH=65%*	
IS (100)	BC (100)	IS (20)	BC (100)	IS (20)	BC (100)	BC (20)	WS (20)
MD (20)	BC (100)	BC (20)	WS (20)	BC (20)	WS (20)		
SS (20)	BC (100)	BC (50)	IS (20)				
BC (50)	WS (20)						

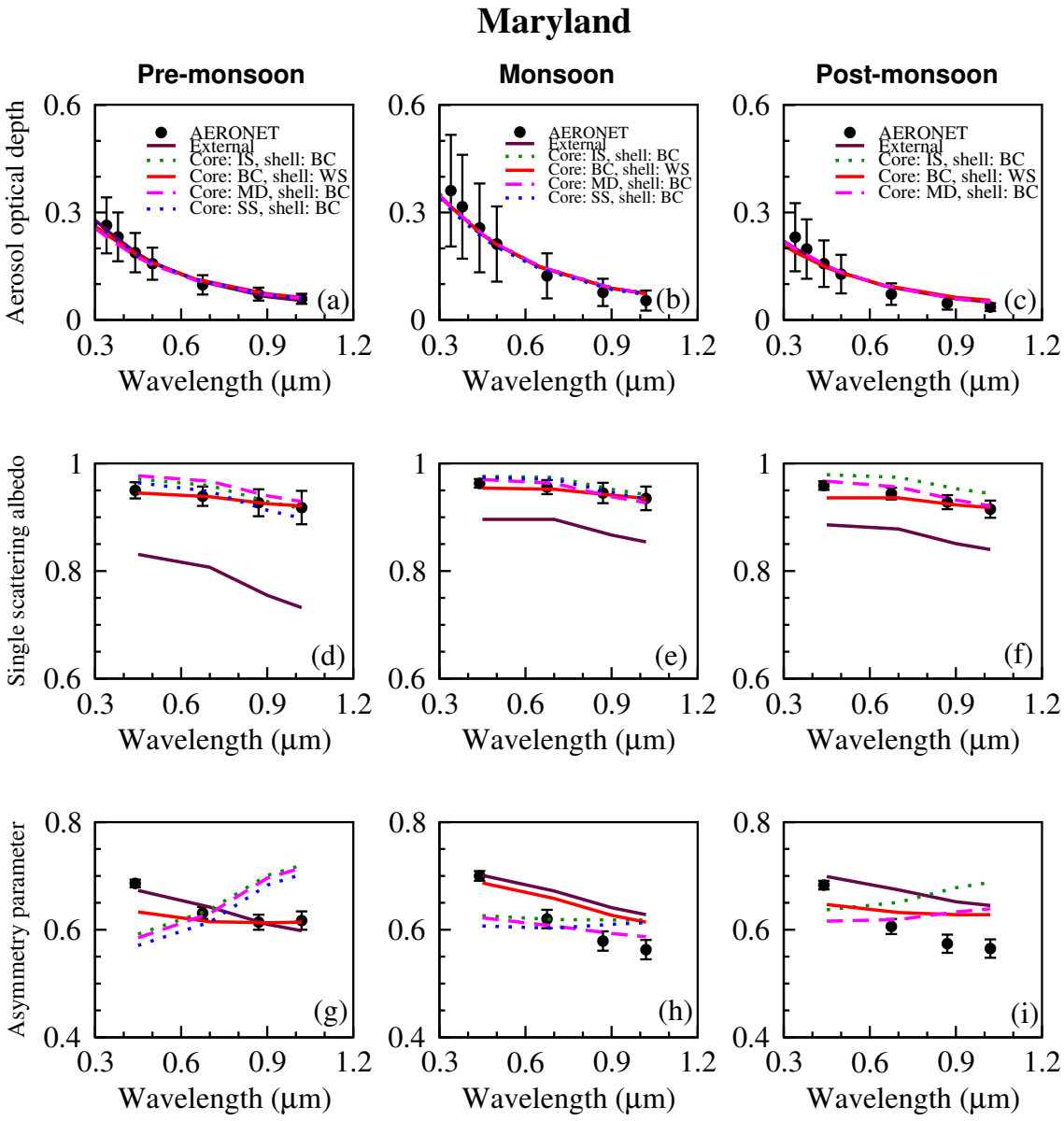

Figure 5.3: *Spectral aerosol parameters (a-c) aerosol optical depth, (d-f) single scattering albedo and (g-i) asymmetry parameter obtained from AERONET measurements in comparison with estimated aerosol properties for different mixing scenarios during pre-monsoon, monsoon and post-monsoon seasons over NASA GSFC, Maryland (USA). Vertical bars in AERONET data correspond to* $\pm 1\,\sigma$ *deviation from the mean.*

These features are consistent with the type of aerosols expected to be present over the locations; Mongu and Abu Dhabi are influenced by dust and biomass burning (*Magi*, 2009; *Reid et al.*, 2008), and Osaka is an urban city and influenced by dust transported from China (*Funasaka et al.*, 2003).

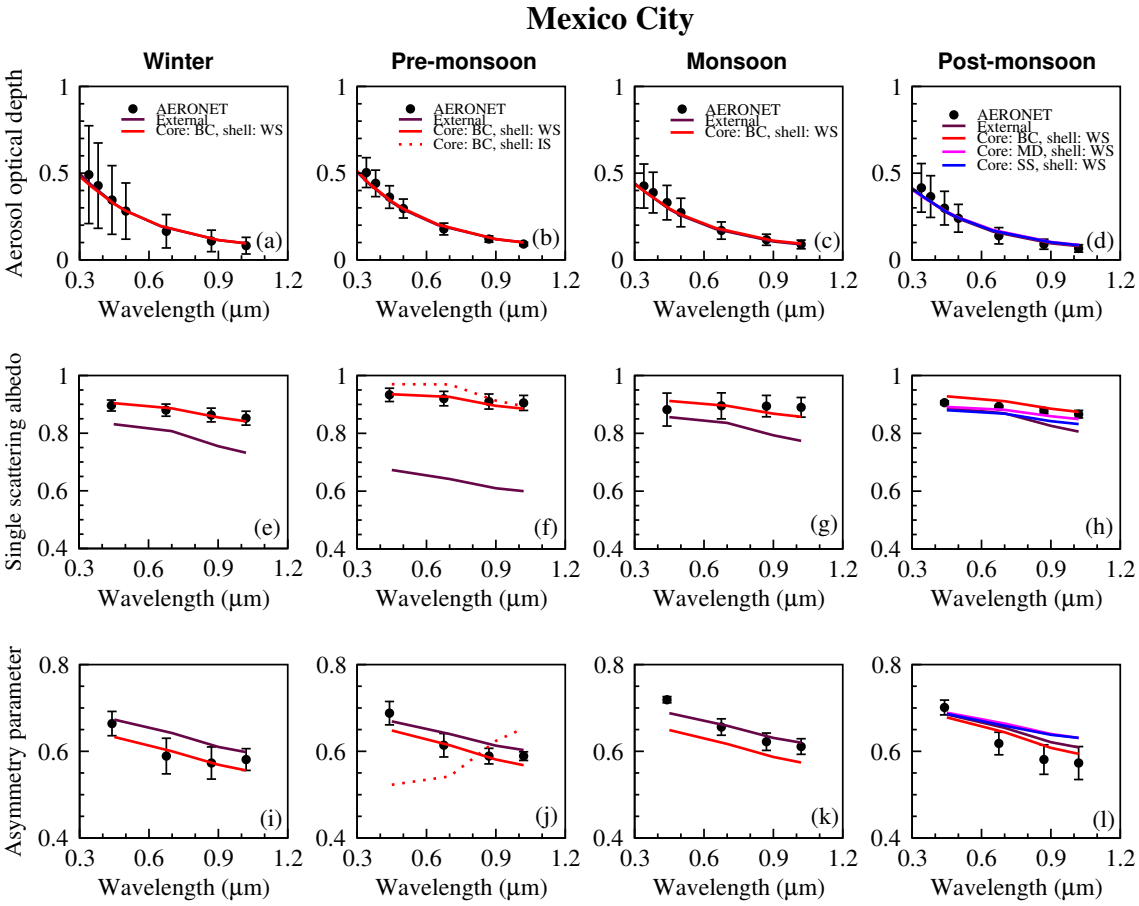

Figure 5.4: *Spectral aerosol parameters (a-d) aerosol optical depth, (e-h) single scattering albedo and (i-l) asymmetry parameter over Mexico City (Mexico). Vertical bars represent* $\pm 1\sigma$ *deviation from the mean. Aerosol optical properties for different mixing scenarios are also plotted.*

SSA, measure of scattering property of aerosols, shows significant variations though the AODs are similar. For example, in NASA GSFC SSA is >0.9 over the 0.4-1.0 μm wavelength range, while in Mexico city SSA is less than 0.9 (Figures 5.3, 5.4). SSA increases with wavelength over Tamanrasset and Djougou as both these locations are dust dominated, and dust SSA increases with wavelength. Djougou SSA is $\leq$0.9 and increases with wavelength, while in Mongu, a biomass burning aerosol dominant location, SSA is less than 0.8 at 0.4 μm and decreases sharply to 0.65 at 1 μm indicating the abundance of absorbing aerosols (Figure 5.7).

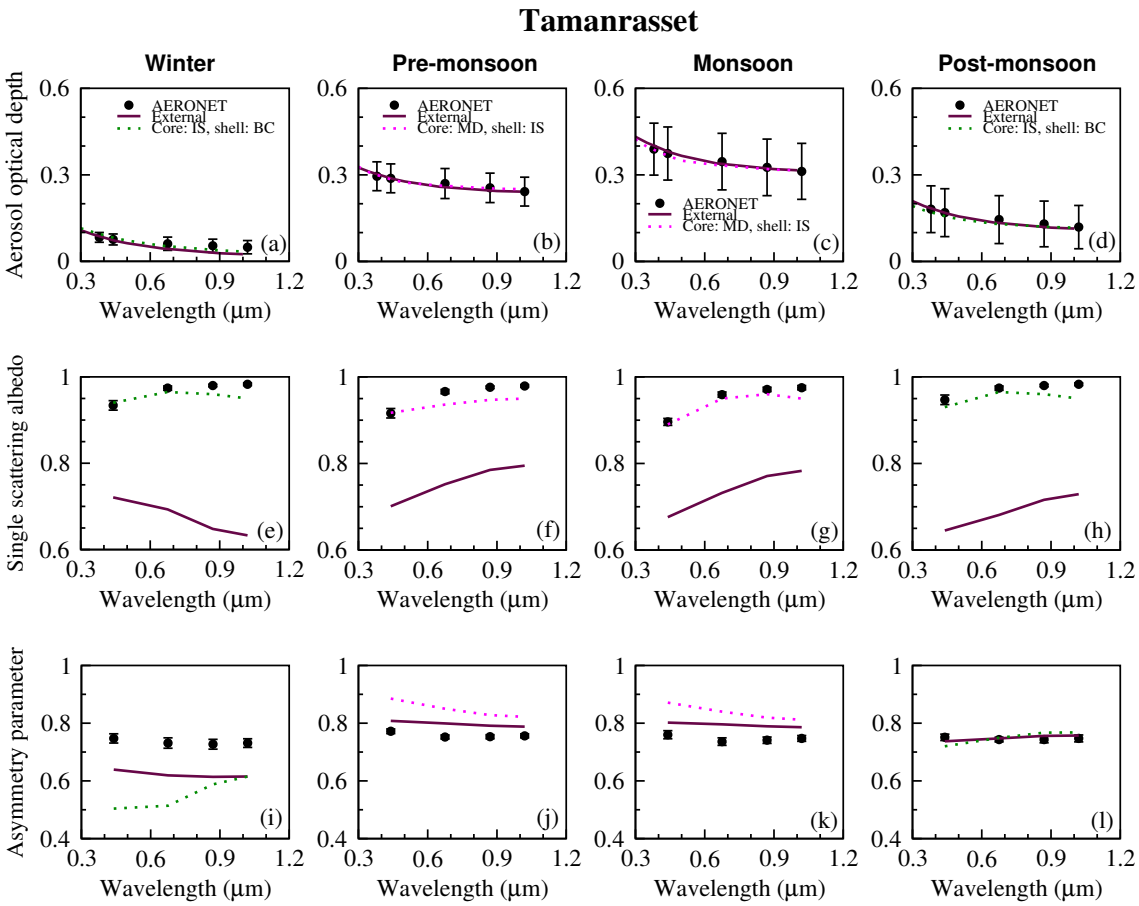

Figure 5.5: *Spectral aerosol parameters (a-d) aerosol optical depth, (e-h) single scattering albedo and (i-l) asymmetry parameter obtained from AERONET measurements in comparison with estimated aerosol properties for different mixing scenarios during winter, pre-monsoon, monsoon and post-monsoon seasons over Tamanrasset. Vertical bars in AERONET data correspond to* $\pm 1\,\sigma$ *deviation from the mean.*

Abu Dhabi spectral SSA features are similar to that of Djougou (Figure 5.8). SSA in Karachi is about 0.9 during pre-monsoon at 0.44 μm and increases to 0.95 at 1.02 μm due to the influence of dust (coarse mode). Singapore, Gwangju and Osaka SSA decrease as function of wavelength (Figures 5.10 - 5.12) consistent with type of mixed (urban emissions, biomass burning and dust) aerosols. In Abu Dhabi, another dust dominant location SSA increases with wavelength.

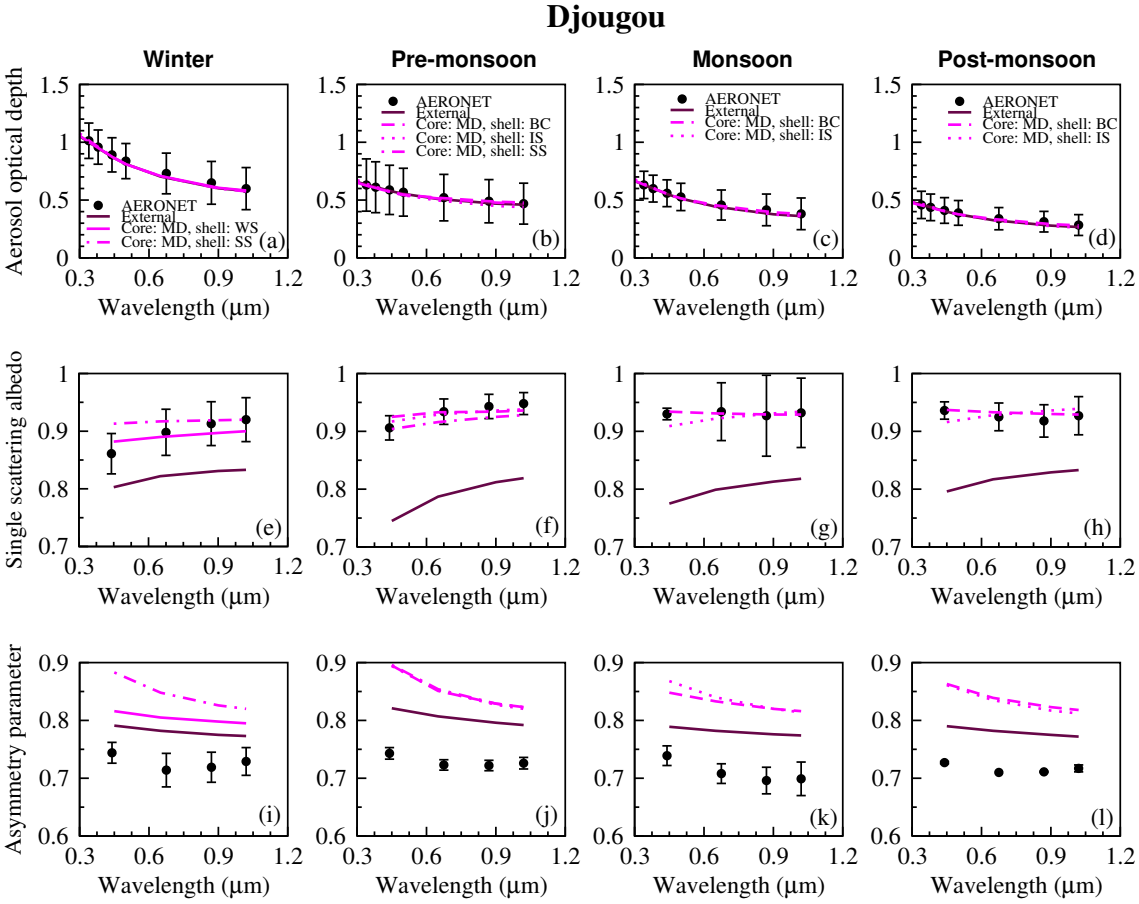

Figure 5.6: *Spectral AOD, SSA and g from AERONET measurements in comparison with estimates over Djougou during winter, pre-monsoon, monsoon and post-monsoon. Vertical bars indicate* $\pm 1\sigma$ *deviation from the mean.*

Asymmetry parameter depends on aerosol size distribution and chemical composition of aerosols, and relative humidity. g is higher for an aerosol size distribution comprising larger size particles. g decreases as wavelength increases over NASA GSFC and Mexico city owing to the dominance of fine mode aerosols (Figure 5.4). g remains more or less the same or shows a slight increase when dust and/or sea salt particles dominate (*e.g.*, Tamanrasset, Karachi, Djougou and Abu Dhabi). Spectral features of aerosols exhibit spatiotemporal variation and are quite consistent with the aerosols dominant over each location, both in terms of their type (black and organic carbon, water soluble, dust, sea salt etc.) and size (fine, coarse, or mixed).

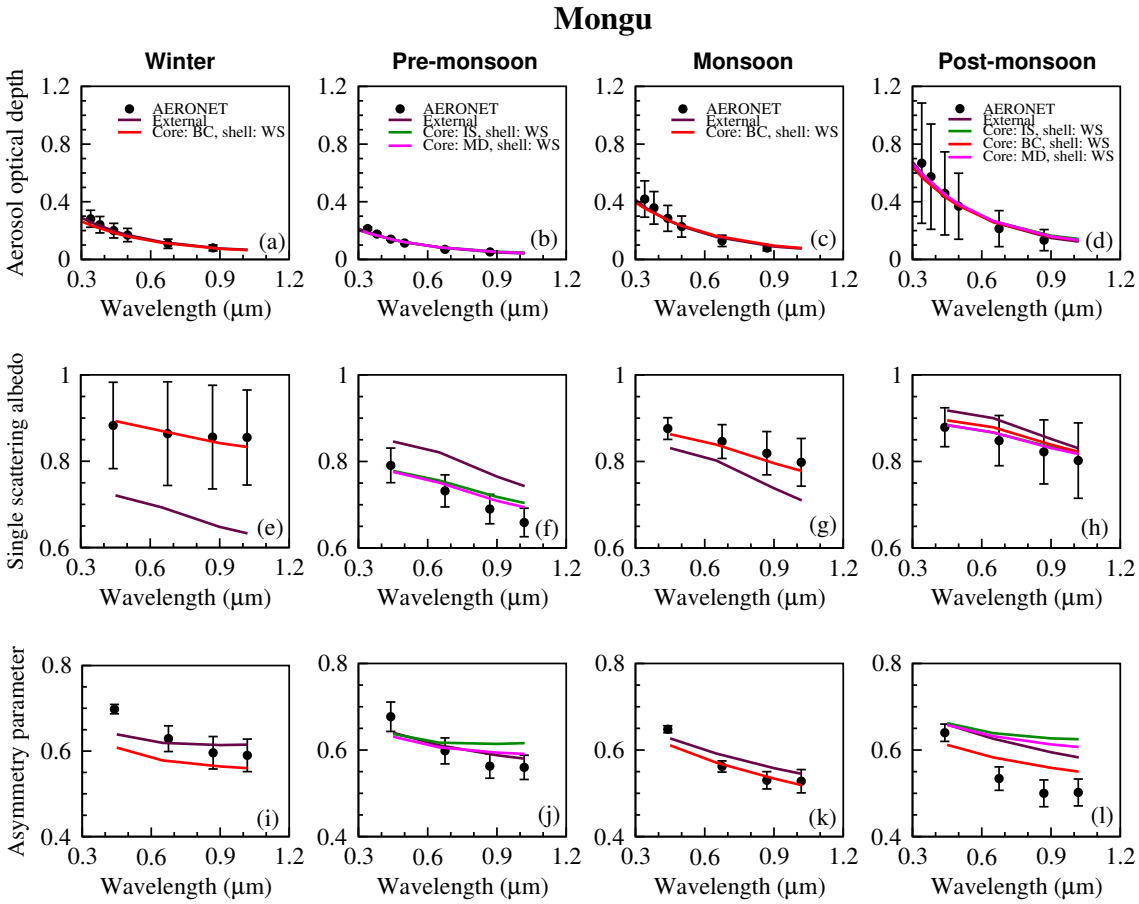

Figure 5.7: *Spectral aerosol parameters (a-d) aerosol optical depth, (e-h) single scattering albedo and (i-l) asymmetry parameter obtained from AERONET measurements in comparison with estimated aerosol properties for different mixing scenarios during winter, pre-monsoon, monsoon and post-monsoon seasons over Mongu. Vertical bars in AERONET data correspond to* $\pm 1\ \sigma$ *deviation from the mean.*

The aerosol mixing states exhibit spatial and temporal variations. One of the most preferred mixing states is BC (core) - MD (shell) among the study locations (Table 5.1). The percentage of core species coating the shell varies from 10% to 100%. In urban locations (Maryland and Mexico city), BC and water soluble aerosols are preferred as core (Table 5.1). In Maryland and Tamanrasset external mixing gives rise to lower SSA.

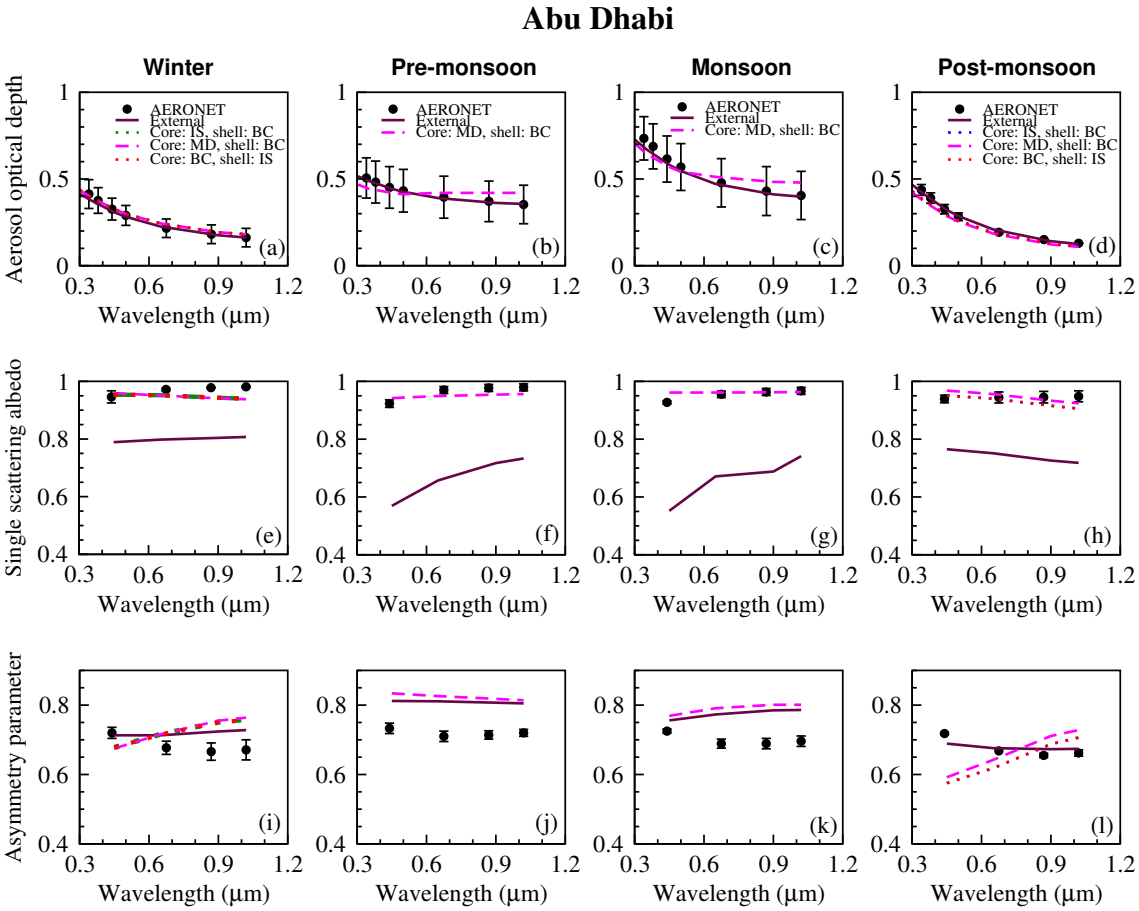

Figure 5.8: *Spectral aerosol parameters (a-d) aerosol optical depth, (e-h) single scattering albedo and (i-l) asymmetry parameter obtained from AERONET measurements in comparison with estimated aerosol properties for different mixing scenarios during winter, pre-monsoon, monsoon and post-monsoon seasons over Abu Dhabi. Vertical bars in AERONET data correspond to* $\pm 1\,\sigma$ *deviation from the mean.*

BC coating of dust is found to be the most probable mixing state over Abu Dhabi during pre-monsoon and monsoon (Table 5.1); during monsoon 5% of BC coats only 10% dust, while the remaining BC, MD and all the other aerosol species are externally mixed. However, during post-monsoon, other mixing states, namely, IS (core)-BC (shell), MD (core)-BC (shell) and BC (core)-IS (shell) also seem probable. The aerosol mixing states in Karachi, a dust dominant urban location, are the same as that of Abu Dhabi, however, the percentage of core-shell mixing of species differ (Table 5.1).

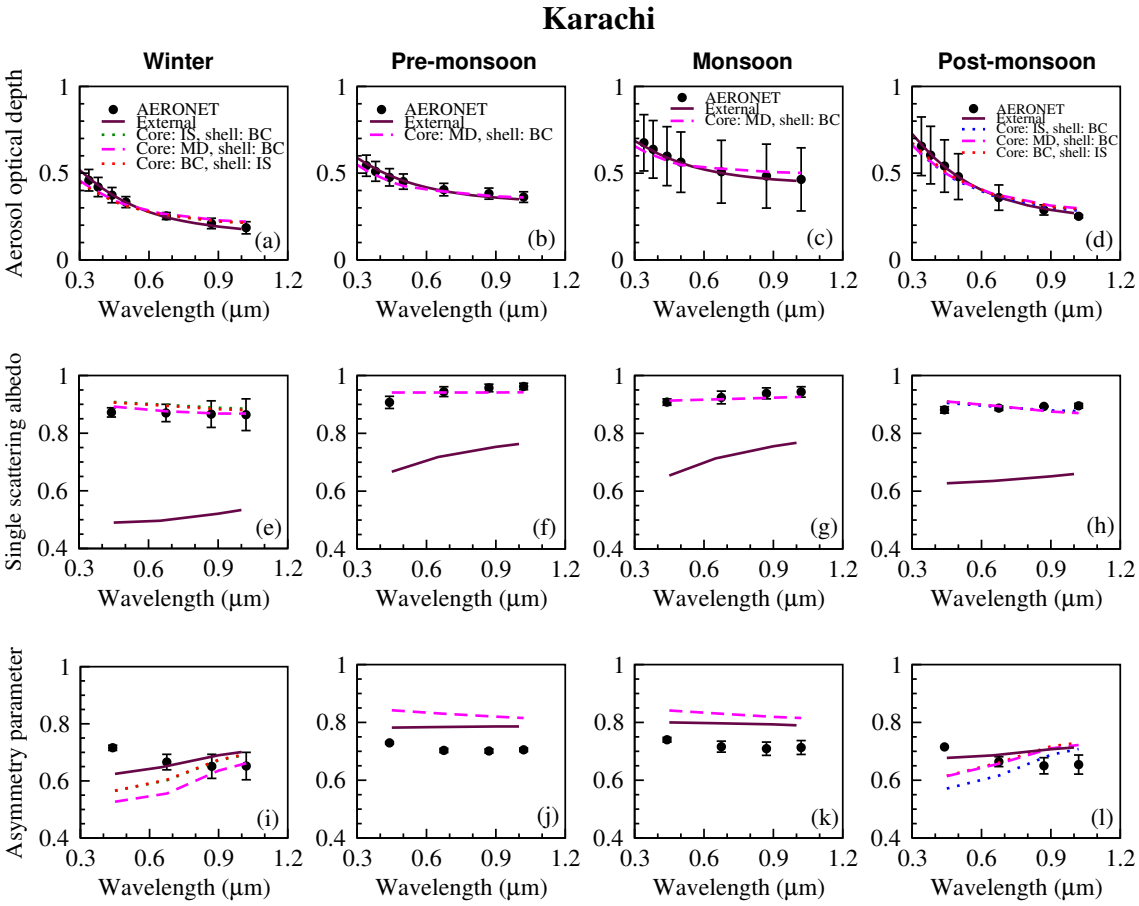

Figure 5.9: *Spectral aerosol parameters (a-d) aerosol optical depth, (e-h) single scattering albedo and (i-l) asymmetry parameter obtained from AERONET measurements in comparison with estimated aerosol properties for different mixing scenarios during winter, pre-monsoon, monsoon and post-monsoon seasons over Karachi. Vertical bars in AERONET data correspond to* $\pm 1\ \sigma$ *deviation from the mean.*

Singapore is dominated by water soluble-BC aerosol mixing in either core or shell throughout the year (Table 5.1). This mixing is consistent with the type of aerosols encountered over Singapore (biomass burning) consisting of water soluble organics and BC. Mineral dust in core coated with BC emerges as the most probable mixing state in Gwangju during all the seasons. Sea salt in core and BC in shell also emerges as one of the mixing states in pre-monsoon. This finding corroborates the aerosol chemical composition found over Gwangju during the year (*Lee et al.*, 2008), where the aerosol pathways included continental, local and marine, in addition to stagnant conditions.

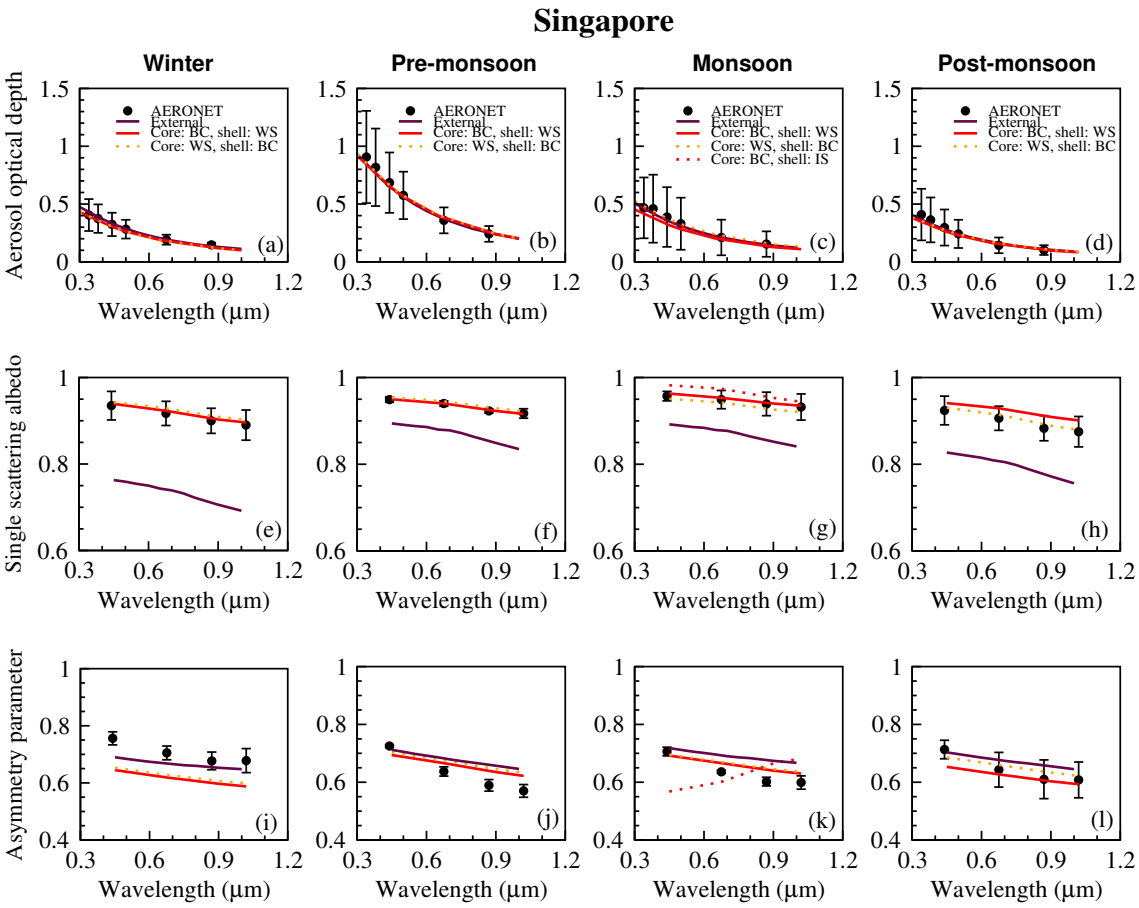

Figure 5.10: *Spectral aerosol parameters (a-d) aerosol optical depth, (e-h) single scattering albedo and (i-l) asymmetry parameter obtained from AERONET measurements in comparison with estimated aerosol properties for different mixing scenarios during winter, pre-monsoon, monsoon and post-monsoon seasons over Singapore. Vertical bars in AERONET data indicate* $\pm 1\,\sigma$ *deviation from the mean.*

MD (core)-SS (shell) mixing over Gwangju during monsoon is consistent with the reported observations (*Andreae et al.*, 1986). Osaka, an urban location, is dominated by mixing of aerosols found in the urban atmosphere such as water soluble, insoluble, and BC; MD (core)-BC (shell) and SS (core)-BC (shell) are also found to be the probable mixing states in winter (Table 5.1). Aerosol mixing states reported here corroborate the observations obtained on aerosol mixing during ACE-Asia (*Arimoto et al.*, 2006), over urban and nonurban sites in Japan (*Hasegawa and Ohta*, 2002), and over an urban region in Germany (*Vester et al.*, 2007). *Arimoto et al.* (2006) found that the mixing of BC with dust was common, as is also seen here (Table 5.1).

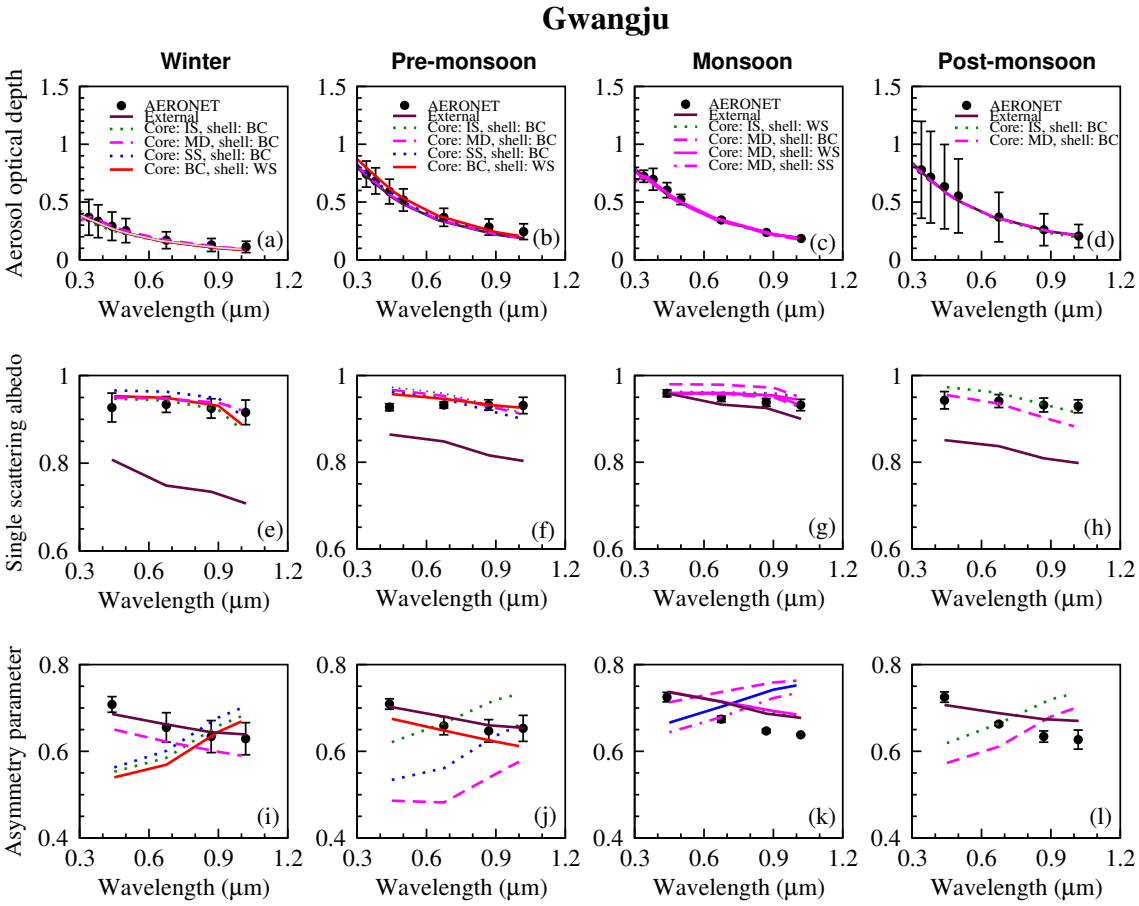

Figure 5.11: *Spectral aerosol parameters (a-d) aerosol optical depth, (e-h) single scattering albedo and (i-l) asymmetry parameter obtained from AERONET measurements in comparison with estimated aerosol properties for different mixing scenarios during winter, pre-monsoon, monsoon and post-monsoon seasons over Gwangju. Vertical bars in AERONET data correspond to* $\pm 1\ \sigma$ *deviation from the mean.*

Hasegawa and Ohta (2002) found that over urban and nonurban locations 19% to 72% of BC was covered with water soluble aerosol component, which is consistent with the aerosol mixing states determined over Osaka (Table 5.1), where 20% to 50% mass fraction of BC is covered by WS aerosols. *Vester et al.* (2007) found that fine particle fraction contained internal mixtures of water soluble organics, and that 20-40% of complex secondary aerosols contained soot inclusions, similar to the results obtained here (Table 5.1).

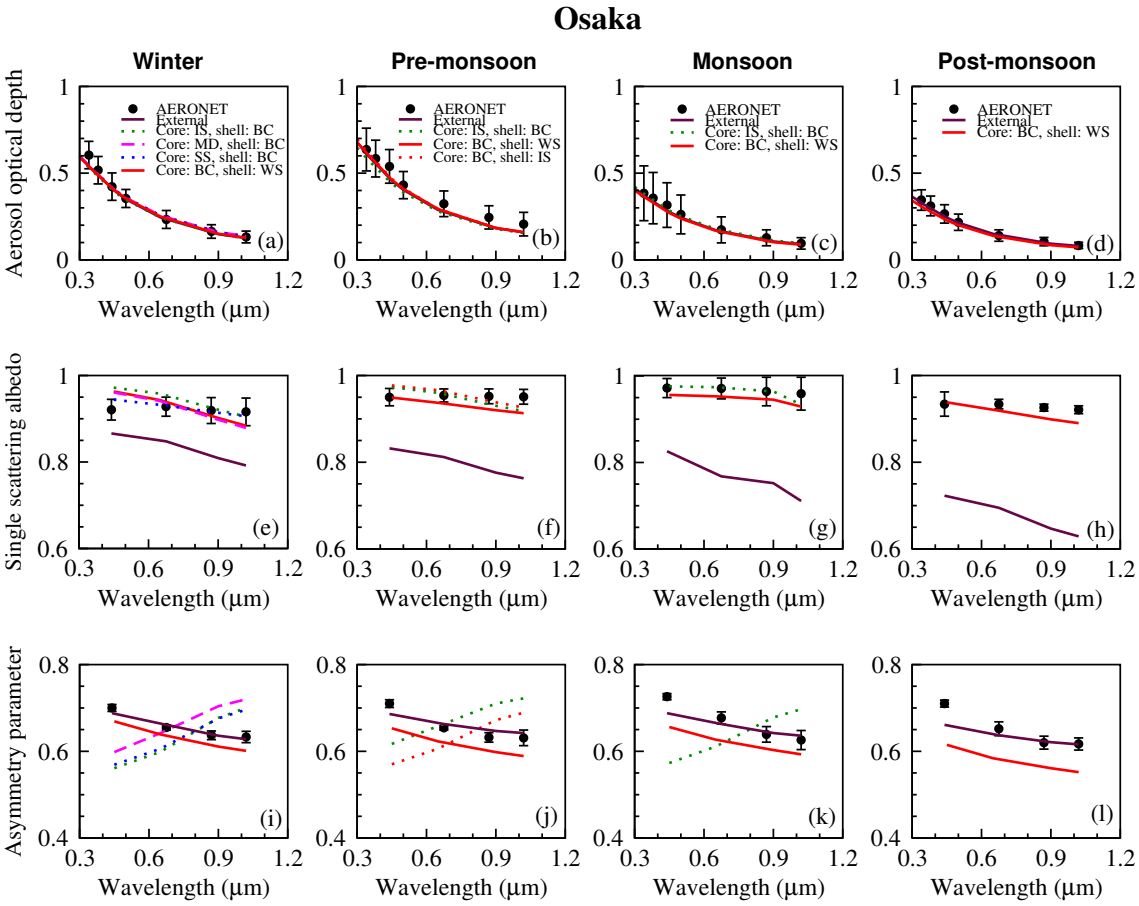

Figure 5.12: *Spectral aerosol parameters (a-d) aerosol optical depth, (e-h) single scattering albedo and (i-l) asymmetry parameter obtained from AERONET measurements in comparison with estimated aerosol properties for different mixing scenarios during winter, pre-monsoon, monsoon and post-monsoon seasons over Osaka. Vertical bars in AERONET data represent* $\pm 1\,\sigma$ *deviation from the mean.*

Regions influenced by biomass burning aerosols, BC (core)-WS (shell) emerges as one of the favorable mixing states, while over urban locations affected by dust, pollution aerosols (BC and WS) are found to coat dust. Thus, it is clear that aerosol mixing states and the degree of core-shell mixing can vary over different regions depending on the abundance and type of aerosols.

5.3.2 Radiative implications

Aerosol radiative forcing at the surface (SFC), in the atmosphere (ATM) and at the top of the atmosphere (TOA) over the study locations (Figures 5.13 - 5.16) exhibit large sea-

sonal and spatial variations consistent with the features seen in aerosol optical properties and mixing states. Surface forcing is nearly linearly related to AODs for the same SSA, and can change in a nonlinear fashion when SSA is different (Figure 5.14).

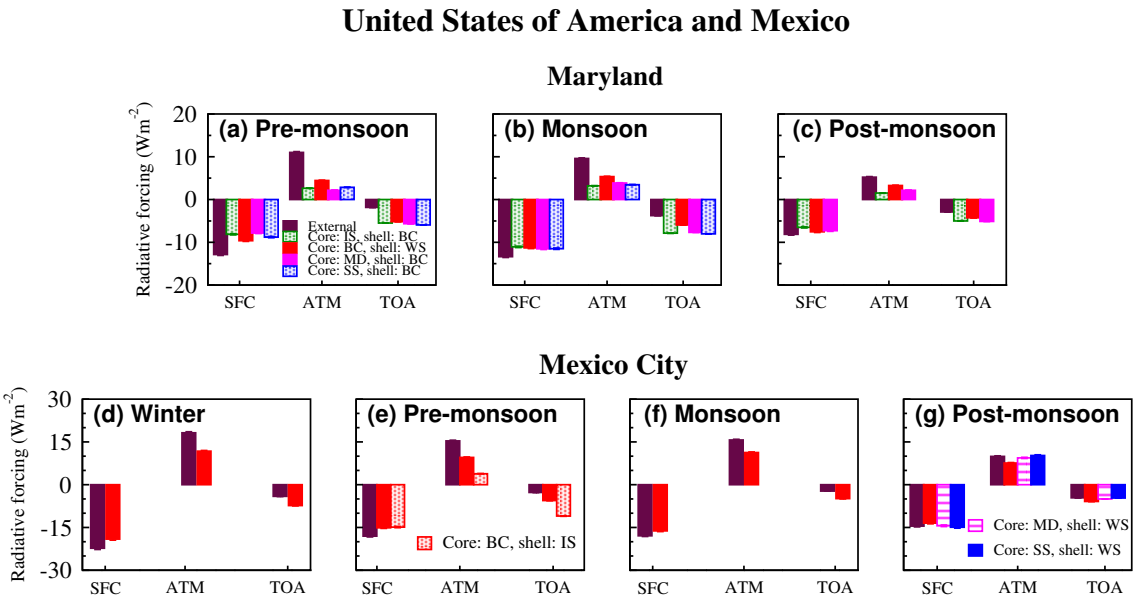

Figure 5.13: *Aerosol radiative forcing (Wm^{-2}) at the surface (SFC), in the atmosphere (ATM) and at the top of the atmosphere (TOA) over Maryland in United States of America and Mexico city, Mexico during pre-monsoon (a, e), monsoon (b, f), post-monsoon (c, g) and winter (d). Radiative forcing obtained for external and different scenarios of core-shell mixtures are drawn. Aerosol radiative forcing over Maryland during winter could not be estimated as aerosol optical properties were not available in winter during the study period.*

TOA forcing depends on SSA and surface albedo; for the same surface albedo TOA forcing is less (more) negative when SSA is lower (higher). TOA forcing can change sign and become positive when absorbing aerosols are abundant (low SSA) over high reflectance surfaces (*e.g.*, snow, desert) (*IPCC*, 2007). This suggests that variation will be seen in both TOA and SFC forcing for different mixing scenarios (Figure 5.14). TOA forcing is less negative for lower SSA and becomes more negative for higher SSA (Figure 5.13), and changes sign when SSA is lower (Figure 5.14 b).

In Abu Dhabi, the change in aerosol forcing is maximum during pre-monsoon and monsoon owing to significant differences in SSA between external mixture (low SSA) and core-shell (high SSA) (Figure 5.15).

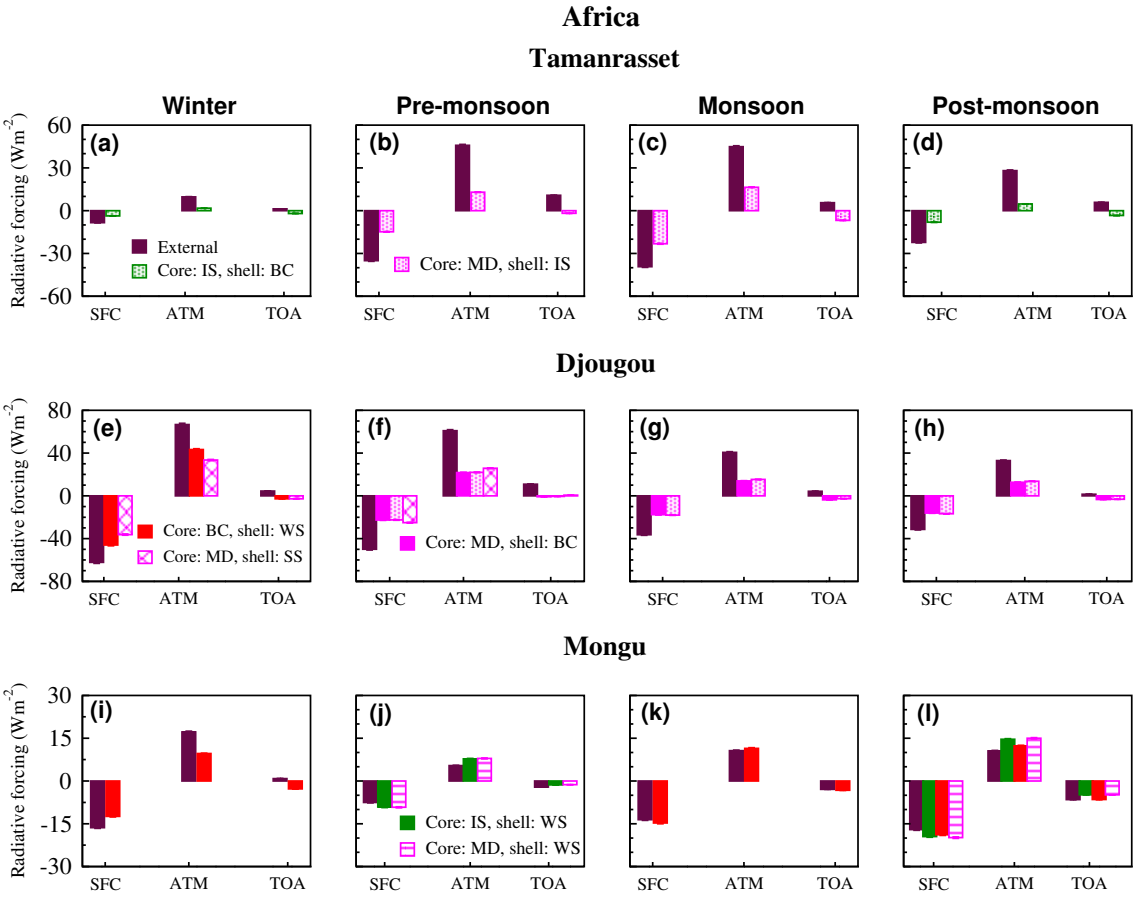

Figure 5.14: *Aerosol radiative forcing at SFC, ATM and TOA over the study locations in Africa for different aerosol mixing scenarios. Radiative forcing over Tamanrasset, Djougou and Mongu during winter (a, e, i), pre-monsoon (b, f, j), monsoon (c, g, k) and post-monsoon (d, h, l) respectively.*

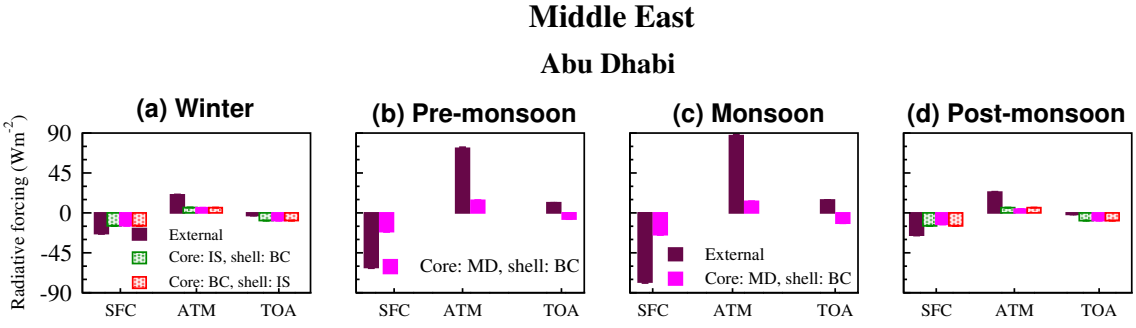

Figure 5.15: *Aerosol radiative forcing at the surface, in the atmosphere and at top of the atmosphere for external and different probable mixing states of different aerosol species viz., water insoluble (IS), black carbon (BC) and mineral dust (MD) over Abu Dhabi during (a) winter, (b) pre-monsoon, (c) monsoon and (d) post-monsoon.*

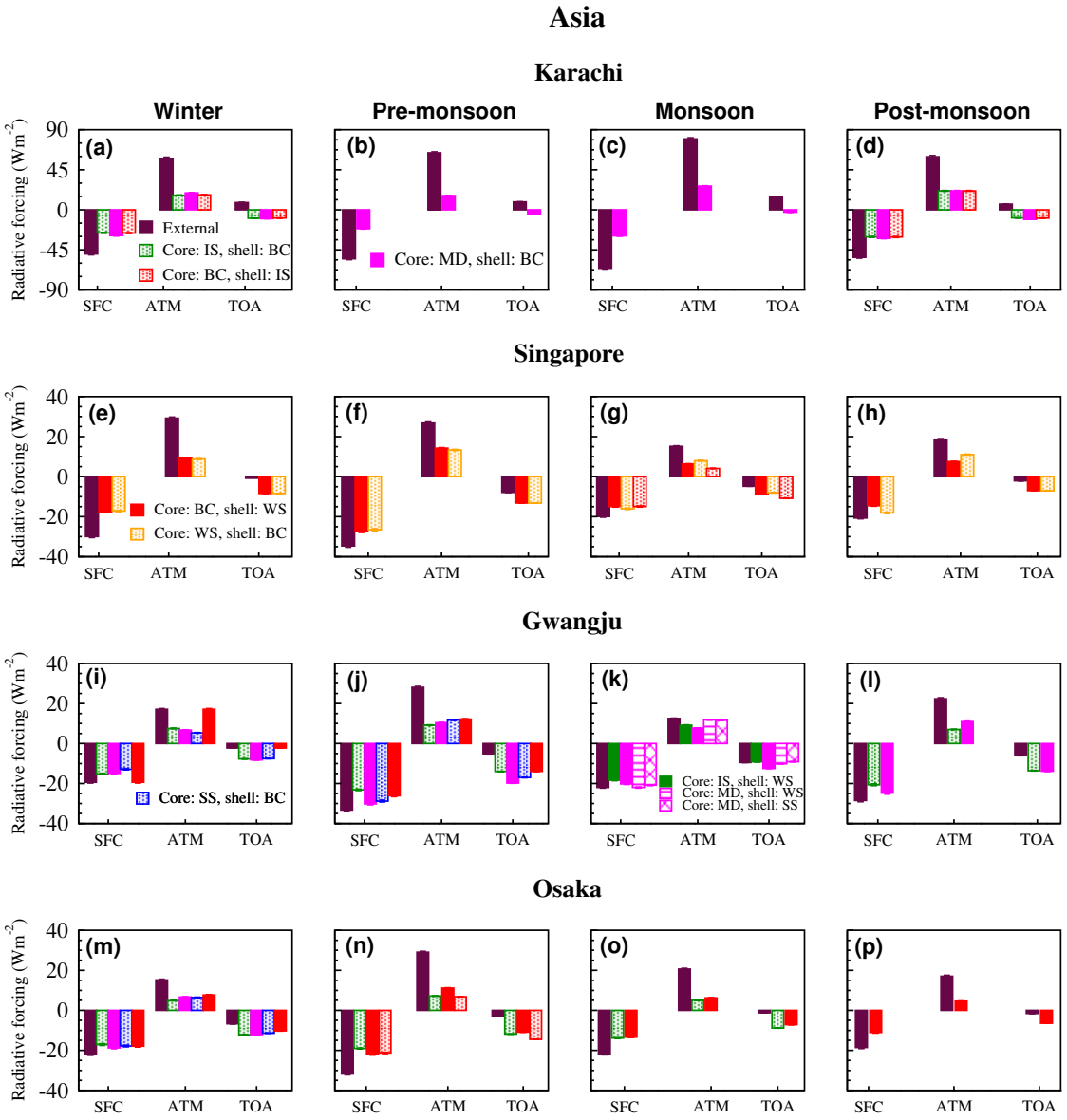

Figure 5.16: *Aerosol radiative forcing at the surface, in the atmosphere and at top of the atmosphere for external and different probable mixing states of different aerosol species viz., insoluble (IS), water soluble (WS), black carbon (BC), mineral dust (MD) and sea salt (SS) over (a-d) Karachi, (e-h) Singapore, (i-l) Gwangju and (m-p) Osaka during winter, pre-monsoon, monsoon and post-monsoon.*

ATM forcing is significantly higher because of positive TOA (low SSA) and surface forcing (Figure 5.15). Karachi, a dust dominated urban location, exhibits similar features as that of Abu Dhabi (Figure 5.16). In Singapore, Gwangju and Osaka aerosol forcing for external mixture is higher when compared to core-shell mixing. Radiative

forcing among the different core-shell mixtures is comparable (Figure 5.16). Asymmetry parameter (g) for external and core-shell mixtures exhibit differences when compared to observations, in terms of magnitude and shape (Figures 5.3 - 5.12); however, this effect is found to cause negligible difference in aerosol radiative forcing (Figure 5.16 f, 5.16 i); the differences in forcing over Gwangju among different mixing states arise due to the variations in TOA forcing which can be attributed mainly due to different SSA. These results confirm that variations in g do not contribute significantly to the differences in aerosol radiative forcing as also shown in *Mishchenko et al.* (1997). Aerosol mixing states and their radiative effects are found to exhibit large temporal and regional variations, this is in contrast to global climate model simulations where one mixing state is imposed and aerosol radiative forcing is estimated (e.g., *Jacobson*, 2001; *Chung and Seinfeld*, 2002). The seasonally varying aerosol mixing states obtained in this study will be useful to incorporate in global climate model simulation studies to determine the continental-global scale influence of aerosols and will be helpful to reduce the uncertainties in aerosol radiative impact.

Chapter 6

Summary and scope for future work

The important results obtained and described in the thesis are summarized in this chapter, in addition to scope for future work.

6.1 Summary of results

6.1.1 Aerosol radiative forcing from observations and model estimates

Aerosol radiative forcing and efficiency for different months of 2008 are estimated from the simultaneously measured downwelling global fluxes and aerosol optical depths (AODs) over an urban location Ahmedabad. Single scattering albedo (SSA) obtained from aethalometer and nephelometer measured absorption and scattering coefficients, Goddard Chemistry Aerosol Radiation and Transport (GOCART) model and Ozone Monitoring Instrument (OMI) are utilized. Semi model dependent and model independent approaches have been adopted to calculate aerosol forcing efficiency and radiative forcing, and are compared with model estimated aerosol radiative forcing In order to understand the differences between observed and model derived forcing mixing states of aerosols are determined and aerosol radiative forcing is estimated over Ahmedabad during 2008. The major findings from the observed and model estimated aerosol forcing, and mixing state calculations include :

- Aerosol optical depths show an increase from winter to monsoon. AOD increases significantly when relative humidity (RH) increases due to the hygroscopic growth of water soluble aerosols, and this increase in AOD overwhelms the changes in AOD due to the removal of BC aerosols and increase of sea salt aerosols over an urban environment.

- SSA exhibits a large seasonal variability; near surface SSA is the highest in monsoon (> 0.8) and lower in post-monsoon. Columnar SSA (GOCART and OMI) are higher than those measured at the surface using aethalometer and nephelometer.

- Surface forcing efficiency estimated by all the methods ((i) 24 hour average net flux, (ii) hybrid and (iii) differential) agree well. Surface aerosol forcing efficiency is found to be lower in monsoon as SSA is higher.

- Surface aerosol radiative forcing shows higher values in monsoon season. Surface forcing estimated by method 2, hybrid approach (involves observation and model), and method 3 differential approach (uses only measured fluxes) are more or less similar for all the seasons. The surface radiative forcing during post-monsoon is higher when compared to that of pre-monsoon, while AOD was found to be lower. The higher surface forcing is attributed to lower SSA during post-monsoon.

- Surface forcing derived using GOCART and OMI derived SSA agrees well with observations for all the seasons except monsoon, while forcing derived using near surface SSA is consistent with the observed forcing in monsoon but exhibits large differences during other seasons. During monsoon, GOCART SSA can be uncertain due to high RH and discrepancy in sea salt flux estimation, and OMI SSA could be higher due to the selection of a pre-defined weakly absorbing aerosol model.

- Black carbon in core and sulfate in shell enhances the absorption and reduces the single scattering albedo as compared to external mixing of BC/sulfate species. SSA is lower when BC is present in shell and invariant when BC mass is $\geq 50\%$ in core-shell mixing. A crossover occurs between external and BC core mixing when BC mass is half of the total mass. SSA in case of BC coating of dust is independent of the size of dust because the core radius is estimated using core-shell ratio which is independent of the modal properties of the core species, while external mixing between dust and BC results in lower SSA for coarse mode

dust.

- SSA spectra of core-shell mixing is mainly governed by the shell species and the spectra for different mixing scenarios merge when BC mass is $\geq$ 50% of the total mass. SSA spectra strongly depends on the mixing type and the mass fraction of BC involved in the mixing, and the changes are quite significant for smaller BC mass fraction.

- AOD is higher for external mixing and lower for BC coated by water soluble aerosols in an urban atmosphere. SSA is higher for water insoluble (shell) and BC (core) mixing. Surface and atmospheric forcing are about two times higher when aerosols are externally mixed.

- The probable mixing states determined corresponding to near surface SSA are different than those obtained for columnar SSA, thus emphasizing that probable mixing state of aerosols can vary for same location and same season depending on the value of SSA.

- Surface aerosol radiative forcing estimated for probable mixing states from Ozone Monitoring Instrument (OMI) derived SSA follows the forcing calculated from the observed flux during all the seasons except monsoon. Surface forcing in case of external mixing is higher when compared to forcing estimated for mixing states derived for OMI SSA. Aerosol forcing in the atmosphere corresponding to probable mixing states derived for in situ SSA is about 3 to 7 times higher than those estimated for OMI SSA.

- TOA forcing during pre-monsoon and monsoon is positive and changes its sign during winter and post-monsoon in case of external mixing, while it is always positive and negative for mixing states for near surface and columnar SSA respectively. Thus, these results clearly show that the state of aerosol mixing can play an important role in the Earth's radiative balance between the surface and the top of the atmosphere.

- This study shows that aerosol radiative forcing deduced from model agrees well with observations for columnar SSA during most seasons and emphasizes that

SSA should be more accurate as aerosol forcing is quite sensitive to SSA. In addition mixing state of aerosols significantly affect the optical properties of aerosols especially SSA and hence it is important in assessing the impact of aerosols on regional and global climate.

6.1.2 Mixing state of aerosols over Indo-Gangetic Plain

Using the measured and modeled aerosol optical properties the seasonal variation of mixing state of aerosol is determined over Kanpur and Gandhi College in Indo-Gangetic Plain (IGP). In addition, estimated aerosol radiative forcing and its seasonal variation is also discussed. The sensitivity of aerosol radiative forcing to non-sphericity of aerosol is also assessed.

The major findings are as follows:

- The probable mixing states of aerosols over Kanpur and Gandhi College in IGP are found to exhibit seasonal variations. Different fractions of black carbon (BC) - water soluble (WS) aerosols in core-shell mixing are found to be probable during winter, monsoon and post-monsoon, while mineral dust (MD) and BC core-shell mixing is found to be probable during pre-monsoon and monsoon. In addition, WS aerosols coated over MD can also be a probable mixing state during monsoon. External mixing is probable during monsoon and post-monsoon seasons.

- Over Gandhi College, a rural location the probable mixing states are found to be IS - sea salt (SS) core-shell mixture during winter, MD/IS - BC core-shell mixture in pre-monsoon and monsoon while in monsoon MD - WS, BC - WS and WS - SS core-shell mixtures are also probable in addition to MD - BC core-shell mixing. During post-monsoon, IS - BC, SS - BC, and MD - BC core-shell mixing are the most probable over Gandhi College. External mixing is found to be most probable during winter and monsoon.

- Aerosol radiative forcing over Kanpur and Gandhi College at the surface, in the atmosphere and at the top of the atmosphere (TOA) for various probable mixing

states agree well for a season. TOA forcing changes its sign from positive for external mixing to negative for probable mixing states during pre-monsoon over both the locations. Aerosol forcing is higher during post-monsoon over Kanpur and during winter over Gandhi College.

- Differences in modeled and measured asymmetry parameter (g) arise due the non-spherical shape of aerosols. Sensitivity results reconfirm that aerosol radiative forcing at TOA and surface is less sensitive to g, and the difference in g is found to produce only a small change in aerosol forcing over IGP due to higher surface albedo.

6.1.3 Mixing state of aerosols over different regions of the world

Spatial and seasonal differences in aerosol mixing state and their impact on optical properties and radiative effects are crucial to estimate the aerosol impact on climate accurately. Probable mixing states of aerosols have been determined over ten environmentally distinct locations spread across the globe using the measured spectral aerosol optical properties. The radiative implications due to different aerosol mixing states are examined and the following inferences are drawn.

- Aerosol optical properties (aerosol optical depth (AOD), single scattering albedo (SSA) and asymmetry parameter (g)) exhibit spectral, spatial and temporal variations. AOD, SSA and g decrease as function of wavelength over fine mode dominated locations (urban, biomass burning emissions) such as Maryland, Mexico city, Mongu, Singapore, Gwangju and Osaka. AODs are almost similar in the 0.34-1.02 μm with wavelength range, and SSA and g are either linear or increase wavelength over Abu Dhabi, Karachi, and Djougou, which are dominated by dust and sea salt.

- Aerosol mixing states exhibit large spatial and temporal variations consistent with the variation and the type of aerosols over each location. Mineral dust (MD) in core and black carbon (BC) in shell emerges as one of the most preferred aerosol mixing states. Locations dominated by fine mode aerosols (e.g.,

Maryland and Mexico city), BC (core)-water soluble (WS, shell) mixing is preferred over biomass burning aerosol dominant locations, while over urban regions influenced by dust manmade (BC and WS) coat the dust particle. Percentage of core species coating the shell in core-shell mixture varies from 10% to 100%. Aerosol mixing states in Karachi, a dust dominant urban location, are the same as that of Abu Dhabi, though the percentage of core-shell mixing of species is different. The core-shell mixing scenarios are consistent with the type of aerosols and support the observations. These results emphasize that aerosol mixing states and the degree of core-shell mixing can vary depending on the abundance and the type of aerosol species.

- Aerosol radiative forcing exhibits large seasonal and spatial variations consistent with the features seen in aerosol optical properties and mixing states. Top of the atmosphere (TOA) forcing is less negative for lower SSA and becomes more negative for higher SSA, and changes sign when SSA is lower. This occurs in locations dominated by urban, industrial emissions such as Maryland and Mexico city. In Abu Dhabi, the change in aerosol forcing is maximum during pre-monsoon and monsoon owing to significant differences in SSA between external (low SSA) and core-shell mixture (high SSA). Atmospheric forcing is significantly higher because of positive TOA (low SSA) and surface forcing. Karachi exhibits similar features in aerosol radiative forcing as that of Abu Dhabi. In Singapore, Gwangju and Osaka aerosol forcing for external mixture is higher when compared to core-shell mixing. The influence of asymmetry parameter (g) on aerosol radiative forcing is estimated to be not quite significant.

- Aerosol mixing states and their radiative effects exhibit large temporal and regional variations, thus, highlighting the need to include regionally and temporally varying mixing states in global climate models to ascertain more accurately the radiative effects of aerosols as opposed to prescribing one mixing state across the globe.

6.2 Scope for future work

Aerosol forcing deduced from direct measurements is more accurate as it is independent of model assumptions. Comparison between the forcing deduced from observations and estimated from radiative transfer model more often shows large differences (*Srivastava et al.*, 2011). As the aerosol characteristics are highly variable in space and time, collocated measurements of aerosol optical properties and solar radiation fluxes are necessary in order to estimate aerosol radiative forcing more accurately.

Lack of information on the vertical profile of aerosols also contributes significantly to the uncertainty in atmospheric forcing, as the distribution of aerosol radiative forcing and heating rate at different altitudes are governed by the vertical profile of aerosols. Spaceborne lidars *viz.,* Geoscience Laser Altimeter System (GLAS) and the Cloud-Aerosol Lidar and Infrared Pathfinder Satellite Observation (CALIPSO) provide aerosol backscatter and extinction vertical profiles, but do not have the global coverage due to their narrow footprint. Therefore, measurements of vertical profile of aerosols is important for an accurate estimate of aerosol radiative properties.

The determination of probable mixing state of aerosol needs *a priori* knowledge of mass concentration of different aerosol species and aerosol optical properties. Improving the understanding of species wise aerosol mass concentration will lead to less uncertainty in the derivation of mixing state of aerosols. Size segregated chemical composition measurements of aerosols at environmentally distinct sites will be useful to refine the derivation of probable mixing state. In contrast to general circulation models (e.g. *Chung and Seinfeld*, 2002; *Jacobson*, 2000) where only one mixing state is assumed over the globe, global climate model simulations can be performed by incorporating the spatio-temporal variation in aerosol mixing scenarios, and the radiative impact of aerosols can be assessed in order to reduce the uncertainty in climate change prediction due to aerosols.

References

Anderson, T., R. J. Charlson, S. E. Schwartz, R. Knutti, O. Boucher, H. Rodhe, and J. Heintzenberg (2003), Climate forcing by aerosols: A hazy picture, *Science*, *300*, 1103–1104.

Anderson, T. L., and J. A. Ogren (1998), Determining aerosol radiative properties using the TSI 3563 integrating nephelometer, *Aero. Sci. Technol.*, *29*, 57–69.

Anderson, T. L., et al. (1996), Performance characteristics of a high-sensitivity, three-wavelength total scatter/backscatter nephelometer, *J. Atmos. Oceanic Technol.*, *13*, 967–986.

Andreae, M. O., R. J. Charlson, F. Bruynseels, H. Storms, R. V. Grieken, and W. Maenhaut (1986), Internal mixture of sea salt, silicates, and excess sulfate in marine aerosols, *Science*, *232*, 1620–1623.

Andrews, E., et al. (2006), Comparison of methods for deriving aerosol asymmetry parameter, *J. Geophys. Res.*, *111*, doi:10.1029/2004JD005734.

Arimoto, R., et al. (2006), Characterization of Asian Dust during ACE-Asia, *Glob. Planet. Change*, *52*, 23–56.

Balasubramanian, R., W.-B. Qian, S. Decesari, M. C. Facchini, and S. Fuzzi (2003), Comprehensive characterization of $PM_{2.5}$ aerosols in Singapore, *J. Geophys. Res.*, *108*, doi:10.1029/2002JD002517.

Bauer, S. E., and D. Koch (2005), Impact of heterogeneous sulfate formation at mineral dust surfaces on aerosol loads and radiative forcing in the Goddard Institute for Space Studies general circulation model, *J. Geophys. Res.*, *110*, doi:10.1029/2005JD005870.

Bodhaine, B. A. (1995), Aerosol absorption measurements at Barrow, Mauna Loa and the south pole, *J. Geophys. Res.*, *100*, 8967–8975.

Bohren, C. F., and D. R. Huffman (1983), *Absorption and scattering of light by small Particles*, 483–489 pp., John Wiley & Sons, Inc.

Bond, T., and R. W. Bergstrom (2006), Light absorption by carbonaceous particles: An investigative review, *Aero. Sci. Technol.*, *40*, 27–67.

Chin, M., P. Ginoux, S. Kinne, O. Torres, B. N. Holben, B. N. Duncan, R. V. Martin, J. A. Logan, and A. Higurashi (2002), Tropospheric aerosol optical thickness from the GOCART model and comparisons with satellite and sunphotometer measurements, *J. Atmos Sci.*, *59*, 461–483.

Chin, M., T. Diehl, O. Dubovik, T. F. Eck, B. N. Holben, A. Sinyuk, and D. G. Streets (2009), Light absorption by pollution, dust, and biomass burning aerosols: A global model study and evaluation with AERONET measurements, *Ann. Geophys.*, *27*, 3439–3464.

Chinnam, N., S. Dey, S. N. Tripathi, and M. Sharma (2006), Dust events in Kanpur, Northern India: Chemical evidence for source and implications to radiative forcing, *Geophys. Res. Lett.*, *33*, doi:10.1029/2005GL025278.

Christopher, S. A., and J. Zhang (2004), Cloud-free shortwave aerosol radiative effect over oceans: Strategies for identifying anthropogenic forcing from Terra satellite measurements, *Geophys. Res. Lett.*, *31*, doi:10.1029/2004GL020510.

Chung, C. E., V. Ramanathan, D. Kim, and I. A. Podgorny (2005), Global anthropogenic aerosol direct forcing derived from satellite and ground-based observations, *J. Geophys. Res.*, *110*, doi:10.1029/2005JD006356.

Chung, S. H., and J. H. Seinfeld (2002), Global distribution and climate forcing of carbonaceous aerosols, *J. Geophys. Res.*, *107*, doi:10.1029/2001JD001397.

Clarke, A. D., et al. (2004), Size distributions and mixtures of dust and black carbon aerosol in asian outflow: Physiochemistry and optical properties, *J. Geophys. Res.*, *109*, doi:10.1029/2003JD004378.

Collaud Coen, M., et al. (2010), Minimizing light absorption measurement artifacts of the Aethalometer: Evaluation of five correction algorithms, *Atmos. Meas. Tech.*, *3*, 457–474.

Conant, C. (2000), An observational approach for determining aerosol surface radiative forcing: Results from the field phase of INDOEX, *J. Geophys. Res.*, *105*, 15,347–15,360.

d'Almeida, G. A., P. Koepke, and E. P. Shettle (1991), *Atmospheric Aerosols: Global Climatology and Radiative Characteristics*, 561 pp., A. Deepak, Hampton, Virginia, USA.

Dey, S., and S. N. Tripathi (2007), Estimation of aerosol optical properties and radiative effects in the Ganga basin, northern India, during the wintertime, *J. Geophys. Res.*, *112*, doi:10.1029/2006JD007267.

Dey, S., and S. N. Tripathi (2008), Aerosol direct radiative effects over Kanpur in the Indo-Gangetic basin, northern India: Long-term (2001-2005) observations and implications to regional climate, *J. Geophys. Res.*, *113*, doi:10.1029/2007JD009029.

Dey, S., S. N. Tripathi, and S. K. Mishra (2008), Probable mixing state of aerosols in the Indo-Gangetic Basin, northern India, *Geophys. Res. Lett.*, *35*, doi:10.1029/2007GL032622.

Di Girolamo, et al. (2004), Analysis of Multi-angle Imaging SpectroRadiometer (MISR) aerosol optical depths over greater india during winter 2001-2004, *Geophys. Res. Lett.*, *31*, doi:10.1029/2004GL021273.

Dubovik, O., and M. D. King (2000), A flexible inversion algorithm for retrieval of aerosol optical properties from sun and sky radiance measurements, *J. Geophys. Res.*, *105*, 20,673–20,696.

Dubovik, O., A. Smirnov, B. N. Holben, M. D. King, Y. J. Kaufman, T. F. Eck, and I. Slutsker (2000), Accuracy assessments of aerosol optical properties retrieved from Aerosol Robotic Network (AERONET) Sun and sky radiance measurements, *J. Geophys. Res.*, *105*, 9791–9806.

Dubovik, O., et al. (2006), Application of spheroid models to account for aerosol particle nonsphericity in remote sensing of desert dust, *J. Geophys. Res.*, *111*, doi: 10.1029/2005JD006619.

Dutkiewicz, V. A., S. Alvi, B. M. Ghauri, M. I. Choudhary, and L. Husain (2009), Black carbon aerosols in urban air in South Asia, *Atmos. Env.*, *43*, 1737–1744.

Eck, T. F., et al. (2005), Columnar aerosol optical properties at AERONET sites in central eastern Asia and aerosol transport to the tropical mid-Pacific, *J. Geophys. Res.*, *110*, doi:10.1029/2004JD005274.

Funasaka, K., M. Sakai, M. Shinya, T. Miyazaki, T. Kamiura, S. Kaneco, K. Ohta, and T. Fujit (2003), Size distributions and characteristics of atmospheric inorganic particles by regional comparative study in Urban Osaka, Japan, *Atmos. Env.*, *37*, 4597–4605.

Ganguly, D., and A. Jayaraman (2006), Physical and optical properties of aerosols over an urban location in western India: Implications for shortwave radiative forcing, *J. Geophys. Res.*, *111*, doi:10.1029/2006JD007393.

Guazzotti, S. A., K. R. Coffee, and K. A. Prather (2001), Continuous measurements of size-resolved particle chemistry during INDOEX-Intensive Field phase 99, *J. Geophys. Res.*, *106*, 28,607–28,628.

Guieu, C., R. Duce, and R. Arimoto (1994), Dissolved input of manganese to the ocean: Aerosol source, *J. Geophys. Res.*, *99*, 18,789–18,800.

Habib, G., C. Venkataraman, I. Chiapello, S. Ramachandran, O. Boucher, and M. S. Reddy (2006), Seasonal and interannual variability in absorbing aerosols over India derived from TOMS: Relationship to regional meteorology and emissions, *Atmos. Env.*, *40*, 1909–1921.

Hansen, A. D. A., H. Rosen, and T. Novakov (1984), The Aethalometer - an instrument for the real-time measurement of optical absorption by aerosol particles, *Sci. Total Environ.*, *36*, 191–196.

Hasegawa, S., and S. Ohta (2002), Some measurement of mixing state of soot containing particles at urban and nonurban sites, *Atmos. Env.*, *36*, 3899–3908.

Haywood, J., and O. Boucher (2000), Estimates of the direct and indirect radiative forcing due to tropospheric aerosols: A review, *Rev. Geophys.*, *38*, 513–543.

Hess, M., P. Koepke, and I. Schult (1998), Optical Properties of Aerosols and Clouds: The Software Package OPAC, *Bull. Am. Meteorol. Soc.*, *79*, 831–844.

Holben, B. N., et al. (2001), An emerging ground-based aerosol climatology: Aerosol optical depth from AERONET, *J. Geophys. Res.*, *106*, 12,067–12,097.

Intergovernmental Panel on Climate Change (IPCC) (2001), Climate Change 2001: The Scientific Basis. Contribution of Working Group I to the Third Assessment Report of the Intergovernmental Panel on Climate Change, edited by Houghton, J., Y. Ding, D. Griggs, M. Noguer, and P. J. van der Linden, 374 pp., Cambridge University Press, New York.

Intergovernmental Panel on Climate Change (IPCC) (2007), Summary for policymakers, in Climate Change 2007: The Physical Science Basis. Contribution of Working Group I to the Fourth Assessment Report of the Intergovernmental Panel on Climate Change, edited by Solomon, S., D. Qin, M. Manning, Z. Chen, M. Marquis, K. Averyt, M.Tignor, and H. Miller, 129–234 pp., Cambridge University Press, New York.

Jacobson, M. Z. (2000), A physically-basedt reatment of elemental carbon optics: Implications for global direct forcing of aerosols, *Geophys. Res. Lett.*, *27*, 217–220.

Jacobson, M. Z. (2001), Strong radiative heating due to the mixing state of black carbon, *Nature*, *409*, 695–697.

Jacobson, M. Z., D. B. Kittelson, and W. F. Watts (2005), Enhanced coagulation due to evaporation and its effect on nanoparticle evolution, *Env. Sci. Tech.*, *39*, 9486–9492.

Jaenicke, R. (1993), *Tropospheric aerosols in aerosol-cloud-climate interactions*, 1–31 pp., Academic, San Diego, California.

Jordan, C. E., J. E. Dibb, B. E. Anderson, and H. E. Fuelberg (2003), Uptake of nitrate and sulfate on dust aerosols during TRACE-P, *J. Geophys. Res.*, *108*, doi:10.1029/2002JD003101.

Kaufman, Y. J., D. Tanré, and O. Boucher (2002), A satellite view of aerosols in the climate system, *Nature, 419*, 215–223.

Kedia, S., and S. Ramachandran (2011), Seasonal variations in aerosol characteristics over an urban location and a remote site in western India, *Atmos. Env.*, *45*, 2120–2128.

Kedia, S., S. Ramachandran, A. Kumar, and M. M. Sarin (2010), Spatiotemporal gradients in aerosol radiative forcing and heating rate over Bay of Bengal and Arabian Sea derived on the basis of optical, physical, and chemical properties, *J. Geophys. Res.*, *115*, doi:10.1029/2009JD013136.

Kim, D. H., B. J. Sohn, T. Nakajima, and T. Takamura (2005), Aerosol radiative forcing over East Asia determined from ground-based radiation measurements, *J. Geophys. Res.*, *110*, doi:10.1029/2004JD004678.

Kopp, R. E., and D. L. Mauzerall (2010), Assessing the climatic benefits of black carbon mitigation, *Proc. Nat. Acad. Sci., USA*, *107*, 11,703–11,708.

Lacis, A. A., and M. I. Mishchenko (1995), Climate forcing, climate sensitivity, and climate response: A radiative and modeling perspective on atmospheric aerosols in *Aerosol Forcing of Climate*, 11–42 pp., John Wiley, Hoboken, N. J.

Lau, K.-M., M.-K. Kim, and K.-M. Kim (2006), Asian summer monsoon anomalies induced by aerosol direct forcing: The role of the Tibetan Plateau, *Clim. Dyn.*, *26*, 855–864.

Lee, H., S. S. Park, K. W. Kim, and Y. J. Kim (2008), Source identification of $PM_{2.5}$ particles measured in Gwangju, Korea, *Atmos. Env.*, *88*, 199–211.

Lesins, G., P. Chylek, and U. Lohmann (2002), A study of internal and external mixing scenarios and its effect on aerosol optical properties and direct radiative forcing, *J. Geophys. Res.*, *107*, doi:10.1029/2001JD000973.

Lohmann, U., J. Feichter, C. C. Chuang, and J. E. Penner (1999), Prediction of the number of cloud droplets in the ECHAM GCM, *J. Geophys. Res.*, *104*, 9169–9198.

Magi, B. I. (2009), Chemical apportionment of southern African aerosol mass and optical depth, *Atmos. Chem. Phys.*, *9*, 7643–7655.

Magi, B. I., P. V. Hobbs, B. Schmid, and J. Redemann (2003), Vertical profiles of light scattering, light absorption, and single scattering albedo during the dry, biomass burning season in southern Africa and comparisons of in situ and remote sensing measurements of aerosol optical depths, *J. Geophys. Res.*, *108*, doi:10.1029/2002JD002361.

Mallet, M., J. C. Roger, S. Despiau, J. P. Putaud, and O. Dubovik (2004), A study of the mixing state of black carbon in urban zone, *J. Geophys. Res.*, *109*, doi:10.1029/2003JD003940.

Mallet, M., et al. (2008), Aerosol direct radiative forcing over Djougou (northern Benin) during the African Monsoon Multidisciplinary Analysis dry season experiment (Special Observation Period-0), *J. Geophys. Res.*, *113*, doi:10.1029/2007JD009419.

McClatchey, R., R. Fenn, J. Salby, F. Volz, and J. Garing (1972), *Optical Properties of the Atmosphere*, *Environ. Res. Pap.*, *411*, 3rd ed., 108 pp., AFCRL, Cambridge, Mass.

McComiskey, A., S. E. Schwartz, B. Schmid, H. Guan, E. R. Lewis, P. Ricchiazzi, and J. A. Ogren (2008), Direct aerosol forcing: Calculation from observables and sensitivities to inputs, *J. Geophys. Res.*, doi:10.1029/2007JD009170.

Menon, S., J. Hansen, L. Nazarenko, and Y. Luo (2002), Climate effects of black carbon aerosols in China and India, *Science*, *297*, 2250–2253.

Michalsky, J. J., G. P. Anderson, J. Barnard, J. Delamere, C. Gueymard, S. Kato, P. Kiedron, A. McComiskey, and P. Ricchiazzi (2006), Shortwave radiative closure studies for clear skies during the Atmospheric Radiation Measurement 2003 Aerosol Intensive Observation Period, *Geophys. Res. Lett.*, *111*, doi:10.1029/2005JD006341.

Mishchenko, M. I., L. D. Travis, R. A. Kahn, and R. A. West (1997), Modeling phase functions for dustlike tropospheric aerosols using a shape mixture of randomly oriented polydisperse spheroids, *J. Geophys. Res.*, *102*, 16,831–16,847.

Morys, M. F., M. M. III, S. Hagerup, S. E. Anderson, A. Baker, J. Kia, and T. Walkup (2001), Design calibration, and performance of MICROTOPS II handheld ozone monitor and sun photometer, *J. Geophys. Res.*, *106*, 14,573–14,582.

Mukai, S., I. Sano, M. Satoh, and B. N. Holben (2006), Aerosol properties and air pollutants over an urban area, *Atmos. Res.*, *82*, 643–651.

Murphy, D. M., et al. (2006), Single-particle mass spectrometry of tropospheric aerosol particles, *J. Geophys. Res.*, *111*, doi:10.1029/2006JD007340.

Murphy, D. M., S. Solomon, R. W. Portmann, K. H. Rosenlof, P. M. Forster, and T. Wong (2009), An observationally based energy balance for the Earth since 1950, *J. Geophys. Res.*, *114*, doi:10.1029/2009JD012105.

Pandithurai, G., R. T. Pinker, T. Takamura, and P. C. S. Devara (2004), Aerosol radiative forcing over a tropical urban site in India, *Geophys. Res. Lett.*, doi:10.1029/2004GL019702.

Parekh, P., B. Ghauri, Z. R. Siddiqi, and L. Husain (1987), The use of chemical and statistical methods to identify sources of selected elements in ambient air aerosols in Karachi, Pakistan, *Atmos. Env.*, *21*, 1267–1274.

Patadia, F., P. Gupta, and S. A. Christopher (2008), First observational estimates of global clear sky shortwave aerosol direct radiative effect over land, *Geophys. Res. Lett.*, *25*, doi:10.1029/2007GL032314.

Penndorf, R. (1957), Tables of the refractive index for standard air and the Rayleigh scattering coefficient for the spectral region between 0.2 and 20 μm and their application to atmospheric optics, *J. Opt. Soc. Am.*, *47*, 176–182.

Pilinis, C., S. N. Pandis, and J. H. Seinfeld (1995), Sensitivity of direct climate forcing by atmospheric aerosols to aerosol size and composition, *J. Geophys. Res.*, *100*, 18,739–18,754.

Ramachandran, S., and S. Kedia (2010), Black carbon aerosols over an urban region: Radiative forcing and climate impact, *J. Geophys. Res.*, *115*, doi:10.1029/2009JD013560.

Ramachandran, S., R. Rengarajan, A. Jayaraman, M. M. Sarin, and S. K. Das (2006), Aerosol radiative forcing during clear, hazy, and foggy conditions over a continental polluted location in north India, *J. Geophys. Res.*, *111*, doi:10.1029/2006JD007142.

Ramachandran, S., S. Kedia, and R. Srivastava (2011), Aerosol optical depth trends over different regions of India, *Atmos. Env.*, *(Under Review)*.

Raman, R. S., and S. Ramachandran (2011), Source apportionment of the ionic components in precipitation over an urban region in Western India, *Environ. Sci. Pollut. Res.*, *18*, 212–225.

Ramana, M. V., V. Ramanathan, I. A. Podgorny, B. B. Pradhan, and B. Shrestha (2004), The direct observations of large aerosol radiative forcing in Himalaya region, *Geophys. Res. Lett.*, *31*, doi:10.1029/2003GL018824.

Ramanathan, V., and G. Carmichael (2008), Global and regional climate changes due to black carbon, *Nat. Geosci.*, *1*, 221–227.

Ramanathan, V., P. J. Crutzen, J. T. Kiehl, and D. Rosenfeld (2001a), Atmosphere: Aerosols, climate, and the hydrological cycle, *Science*, *294*, 2119–2124.

Ramanathan, V., et al. (2001b), Indian Ocean Experiment: An integrated analysis of the climate forcing and effects of the great Indo-Asian haze, *J. Geophys. Res.*, *106*, 28,371–28,398.

Ramanathan, V., et al. (2005), Atmospheric brown clouds: Impacts on South Asian climate and hydrological cycle, *Proc. Nat. Acad. Sci., USA*, *102*, 5326–5333.

Reid, J. S., E. A. Reid, A. Walker, S. Piketh, S. Cliff, A. A. Mandoos, S. Tsay, and T. F. Eck (2008), Dynamics of southwest Asian dust particle size characteristics with implications for global dust research, *J. Geophys. Res.*, *113*, doi:10.1029/2007JD009752.

Remer, L. A., et al. (2008), Global aerosol climatology from the MODIS satellite sensors, *J. Geophys. Res.*, *113*, doi:10.1029/2007JD009661.

Ricchiazzi, P., S. Yang, C. Gautier, and D. Sowle (1998), SBDART: A Research and Teaching Software Tool for Plane-Parallel Radiative Transfer in the Earth's Atmosphere, *Bull. Am. Meteorol. Soc.*, *79*, 2101–2114.

Schwarz, J. P., et al. (2008), Coatings and their enhancement of black carbon light absorption in the tropical atmosphere, *J. Geophys. Res.*, *113*, doi:10.1029/2007JD009042.

Seinfeld, J., and S. Pandis (1998), *Atmospheric Chemistry and Physics: From Air Pollution to Climate Change*, 1362 pp., John Wiley, Hoboken, N. J.

Singh, R. P., S. Dey, S. N. Tripathi, V. Tare, and B. Holben (2004), Variability of aerosol parameters over Kanpur, northern India, *J. Geophys. Res.*, *109*, doi:10.1029/2004JD004966.

Smirnov, A., B. N. Holben, T. F. Eck, O. Dubovik, and I. Slutsker (2000), Cloud-screening and quality control algorithms for the AERONET database, *Rem. Sen. Env.*, *73*, 337–349.

Spencer, M. T., J. C. Holecek, C. E. Corrigan, V. Ramanathan, and K. A. Prather (2008), Size-resolved chemical composition of aerosol particles during a monsoonal transition period over the Indian Ocean, *J. Geophys. Res.*, *113*, doi:10.1029/2007JD008657.

Srivastava, R., S. Ramachandran, T. A. Rajesh, and S. Kedia (2011), Aerosol radiative forcing deduced from observations and model estimates over an urban location and sensitivity to single scattering albedo, *Atmos. Env.*, *45*, 6163–6171.

Stamnes, K., S. C. Tsay, W. Wiscombe, and K. Jayaweera (1988), Numerically stable algorithm for discrete-ordinate-method radiative transfer in multiple scattering and emitting layered media, *Appl. Opt.*, *27*, 2502–2509.

Takemura, T., T. . Nakajima, O. Dubovik, B. N. Holben, and S. Kinne (2002), Single-Scattering Albedo and Radiative Forcing of Various Aerosol Species with a Global Three-Dimensional Model, *J. Climate*, *15*, 333–352.

Tare, V., et al. (2006), Measurements of atmospheric parameters during Indian Space Research Organization Geosphere Biosphere Program Land Campaign II at a typical location in the Ganga Basin: 2. Chemical properties, *J. Geophys. Res.*, *111*, doi:10.1029/2006JD007279.

Torres, O., A. Tanskanen, B. Veihelmann, C. Ahn, R. Braak, P. K. Bhartia, P. Veefkind, and P. Levelt (2007), Aerosols and surface UV products from Ozone Monitoring Instrument observations: An overview, *J. Geophys. Res.*, *112*, doi:10.1029/2007JD008809.

Twomey, S. (1977), *Atmospheric Aerosols*, 302 pp., Elsevier Scientific Publishing Co., New York, USA.

Uno, I., et al. (2009), Asian dust transported one full circuit around the globe, *Nat. Geosci.*, *2* 557–560.

Vega, E., et al. (2010), Particulate air pollution in Mexico City: A detailed view, *Aeros. Air Qual. Res.*, *10*, 193–211.

Venkataraman, C., G. Habib, A. Eiguren-Fernandez, A. H. Miguel, and S. K. Friedlander (2005), Residential biofuels in South Asia: Carbonaceous aerosol emissions and climate impacts, *Science*, *307*, 1454–1456.

Vester, B. P., M. Ebert, E. B. Barnert, J. Schneider, K. Kandler, L. Schutz, and S. Weinbruch (2007), Composition and mixing state of the urban background aerosol in the Rhein-Main area (Germany), *Atmos. Env.*, *41*, 6102–6115.

Wang, Y., G. Zhuang, Y. Sun, and Z. An (2005), Water-soluble part of the aerosol in the dust storm season – evidence of the mixing between mineral and pollution aerosols, *Atmos. Env.*, *39*, 7020–7029.

Weingartner, E., H. Saathoff, M. Schnaiter, N. Streit, B. Bitnar, and U. Baltensperger (2003), Absorption of light by soot particles: Determination of the absorption coefficient by means of aethalometers, *J. Aero. Sci.*, *34*, 1445–1463.

Zhang, D., J. Zang, G. Shi, Y. Iwasaka, A. Matsuki, and D. Trochkine (2003), Mixing states of individual Asian particles at a coastal site of Qingdao, China, *Atmos. Env.*, *37*, 3895–3901.

List of Publications

1. *Aerosol Radiative Forcing over an urban location: Observations and Model estimates*

   Rohit Srivastava and S. Ramachandran

   Indian Aerosol Science and Technology Association Bulletin, 19, (1–2), ISSN: 0971-4570, 387–389, 2010.

2. *Aerosol radiative forcing deduced from observations and models over an urban location and sensitivity to Single Scattering Albedo*

   Rohit Srivastava, S. Ramachandran, T. A. Rajesh and Sumita Kedia

   Atmospheric Environment, 45, 6163–6171, 2011.

3. *Influence of aerosol mixing state on aerosol optical properties and radiative forcing*

   Rohit Srivastava and S. Ramachandran

   Environmental Science and Pollution Research (Under review) 2011.

4. *Probable mixing state of aerosols over Indo-Gangetic plain and its impact on radiative forcing*

   Rohit Srivastava and S. Ramachandran

   Quaternary Journal of Royal Meteorological Society (Under review), 2011.

5. *Variability in aerosol optical properties due to external and core-shell mixing: Influence of relative humidity*

   S. Ramachandran and **Rohit Srivastava**

   Quaternary Journal of Royal Meteorological Society (Under review), 2011.

6. *Mixing state of aerosols over different regions of the globe derived using measured aerosol properties and its impact on radiative effects*

   S. Ramachandran and **Rohit Srivastava**

   Atmospheric Environment (Under review), 2011.

7. *Aerosol characteristic and radiative impacts during normal monsoon and drought years over India*

   S. Ramachandran, **Rohit Srivastava** and Sumita Kedia

   Atmospheric Environment (Under review), 2011.

8. *Contribution of natural and manmade aerosols to optical properties and radiative effects over an urban location deduced from observations*

   S. Ramachandran, **Rohit Srivastava**, Sumita Kedia and T.A. Rajesh

   Quaternary Journal of Royal Meteorological Society (Under review), 2011.

9. *Aerosol optical depth trends over different regions of India*

   S. Ramachandran, Sumita Kedia and **Rohit Srivastava**

   Atmospheric Environment (Under review), 2011.

Atmospheric Environment 45 (2011) 6163–6171

Contents lists available at SciVerse ScienceDirect

Atmospheric Environment

journal homepage: www.elsevier.com/locate/atmosenv

Aerosol radiative forcing deduced from observations and models over an urban location and sensitivity to single scattering albedo

Rohit Srivastava*, S. Ramachandran, T.A. Rajesh, Sumita Kedia

Space and Atmospheric Sciences Division, Physical Research Laboratory, Ahmedabad 380 009, India

ARTICLE INFO

Article history:
Received 12 April 2011
Received in revised form
17 June 2011
Accepted 7 August 2011

Keywords:
Observations
Model estimates
Aerosol radiative forcing
Single scattering albedo
Urban region

ABSTRACT

Aerosol radiative forcing at the Earth's surface is estimated by simultaneous measurements of broad-band global fluxes and aerosol optical depths (AODs) over an urban location in western India during 2008. AODs at 0.5 μm show large seasonal variability with higher values (0.52) during monsoon. Higher AOD during monsoon is mainly due to increase in relative humidity which overwhelms the effects of wet removal of aerosols and addition of sea salt. Forcing efficiency for monsoon season is found to be lower as compared to other seasons. Surface aerosol radiative forcing has the highest value of −44 Wm^{-2} during monsoon. The forcing values are similar for model independent and semi model dependent methods. Single scattering albedo (SSA) is higher in monsoon followed by pre-monsoon, winter and lowest in post-monsoon. SSA derived from ground-based measurements (aethalometer and nephelometer) is lower than columnar SSA estimated from Goddard Chemistry Aerosol Radiation and Transport (GOCART) model and derived from Ozone Monitoring Instrument (OMI). Lower radiative forcing at the surface is attributed to higher SSA during pre-monsoon. Model estimated surface forcing using ground-based SSA is about two times higher than observed forcing for different seasons except for monsoon. However, model estimated forcing using columnar SSA agrees well with observations except in monsoon. The differences during monsoon are probably caused by overestimation of SSA from GOCART and OMI. The study reveals that a small change in SSA can lead to significant change in aerosol forcing.

1. Introduction

Aerosols affect the climate directly by scattering and absorbing the incoming solar and outgoing terrestrial radiation, and indirectly by increasing the lifetime and albedo of clouds and modifying the precipitation. The role of aerosols in the Earth's radiation budget is one of the largest sources of uncertainty in validating the model prediction of climate change (Solomon et al., 2007). In majority of investigations, aerosol optical properties are measured and used in radiative transfer models to estimate aerosol radiative forcing. Assumptions associated with aerosol optical properties and their vertical structure can cause uncertainties in the estimation of aerosol radiative forcing using radiative transfer models (Solomon et al., 2007). However, aerosol radiative forcing estimated from direct flux measurements which are highly sensitive and accurate can have less uncertainty than that estimated using models.

South Asia is densely populated and therefore is a potential source region of aerosols which produces various anthropogenic aerosols such as sulfate, nitrates and black carbon etc. The influence of radiative effects of aerosols on Earth's radiation budget over this region on regional scale and its global impact are important as it is a hot spot. Surface aerosol radiative forcing was estimated based on direct measurements of surface fluxes and aerosol optical properties over south Asia during winter (Conant, 2000; Ramanathan et al., 2001; Ramana et al., 2004). Flux measurements over continental India are rare except for a few e.g., Pandithurai et al. (2004). Aerosol radiative forcing at the surface derived using measured aerosol optical properties and a radiative transfer model over Ahmedabad was found to vary from −41 (monsoon) to −63 Wm^{-2} (winter) (Ganguly and Jayaraman, 2006), while annual mean aerosol radiative forcing over Kanpur and Delhi, in Indo-Gangetic plain were −32 Wm^{-2} and −67 Wm^{-2} respectively (Dey and Tripathi, 2008; Singh et al., 2010). Aerosol forcing at Pune was measured to be −26 Wm^{-2} during dry season (Pandithurai et al., 2004), while it was found to vary from −25 Wm^{-2} (summer monsoon) to −53 Wm^{-2} (winter monsoon) over Trivandrum (Babu et al., 2007).

For the first time, in this study, aerosol radiative forcing on a seasonal mean basis is obtained using the measured fluxes and aerosol optical properties over Ahmedabad, an urban location, in western India, and compared and contrasted with the model

* Corresponding author. Tel.: +91 7926314661; fax: +91 7926314659.
E-mail address: rohits@prl.res.in (R. Srivastava).

1352-2310/$ – see front matter © 2011 Elsevier Ltd. All rights reserved.
doi:10.1016/j.atmosenv.2011.08.015

results, and inferences are drawn. In this study we derive the seasonal variation of surface aerosol forcing from the observed flux which is rare and so far not available, to the best of our knowledge over India. We apply various methodologies to estimate aerosol radiative forcing from the measured flux. Single scattering albedo derived from ground-based measurements of aerosol absorption and scattering coefficients, Goddard Chemistry Aerosol Radiation and Transport (GOCART) model and satellite borne-sensor Ozone Monitoring Instrument (OMI) are used in the radiative transfer model to simulate aerosol radiative forcing, and the influence of different SSA values on aerosol forcing is determined.

2. Observations and data analysis

2.1. Measurement location

Ahmedabad (23.03°N, 72.55°E, 55 m AMSL) is an urban, industrial and densely populated city, and has a variety of large and small scale industries, and large number of vehicles (Fig. 1). Thar desert and the Arabian Sea are situated in the northwest and southwest of Ahmedabad respectively (Fig. 1), which serve as the major sources of mineral dust and sea salt during pre-monsoon (March–May) and monsoon (June–September) respectively. The meteorological conditions over Ahmedabad exhibit large seasonal variations. The low level winds are calm and north westerly or north easterly during winter (December–February) which transport aerosols of continental origin and land derived dust particles. During monsoon season of June–September the winds are south westerly, stronger and carry moist air from the Arabian sea to the study location (Ramachandran and Kedia, 2010). During pre-monsoon season (March–May), winds are north westerly or south westerly which transport mineral dust from Thar desert and the surrounding arid regions. During post-monsoon season (October–November) the winds are calm and undergo a change in their direction from south west to north east.

2.2. Aerosol optical depths

Simultaneous measurements of aerosol optical depths (AODs) at five wavelengths (0.38, 0.44, 0.50, 0.675 and 0.87 μm) using Microtops II (*Solar Light Co. U.S.A.*) sunphotometer are conducted at 1-h resolution between 0900 and 1700 IST (Indian Standard Time, GMT + 5.5 h) over Ahmedabad in 2008. Microtops sunphotometer has a field of view 2.5° and bandwidth of each wavelength channel is 0.01 μm. Sunphotometer was periodically calibrated at a high altitude remote site Gurushikhar (24.65°N, 72.78°E, 1.7 km AMSL) (Fig. 1) during 2008. The overall uncertainty in the AOD is estimated to be 2–5% at all the wavelengths (Kedia and Ramachandran, 2011).

2.3. Flux observation

Ground reaching broad-band global, direct and diffuse fluxes in the wavelength range of 0.31–2.8 μm are measured using a set of pyranometers (*Kipp and Zonen Model CM21*) over Ahmedabad. The sources of uncertainty in the flux measurements and their values are given in Table S1. The maximum error in pyranometer measured fluxes taking into account all the sources is about 2%. Downwelling fluxes measured at each second during cloudy and clear sky days of year 2008 and averaged for 5 min are used in the study. The flux data are available for a total of 274 days including cloudy and clear sky days of 2008. The clear sky days correspond to the cloud free days when diurnal profile of global flux is continuous

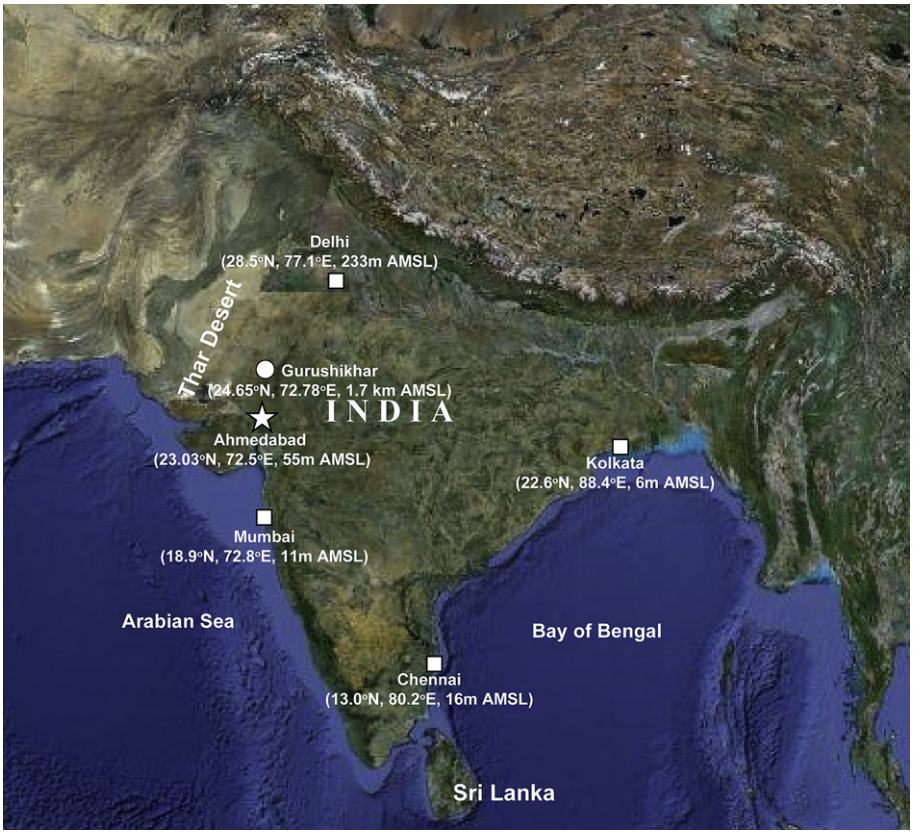

Fig. 1. Measurement location Ahmedabad (Google Earth image). The metro cities (Delhi, Kolkata, Mumbai and Chennai) and Gurushikhar in Mount Abu, where the Microtops instrument is periodically calibrated are also shown.

and free from any sudden changes due to clouds. Simultaneous measurements of clear sky flux and AOD are necessary for the present study, which brought down the number of days to 91 spread over different seasons during the year.

2.4. Aerosol absorption and scattering coefficients

Aerosol absorption coefficients are measured using a seven wavelength aethalometer (*AE-47, Magee Scientific, USA)*. This instrument measures the attenuation of light beam at 0.37, 0.47, 0.52, 0.59, 0.66, 0.88 and 0.95 μm transmitted through the sample collected on a quartz fiber filter. Absorption coefficients of aerosols as a function of wavelength are calculated following Weingartner et al. (2003). From the absorption coefficients black carbon (BC) mass concentrations can be determined, the details of which are given in Ramachandran and Kedia (2010). Aethalometer is operated at a flow rate of 3 l min^{-1} for 24 h d^{-1} at a time resolution of 5 min. The most notable uncertainties in absorption coefficient and BC mass concentration estimates using aethalometer measurements arise due to the changes in filter scattering due to aerosol loading, underestimation of the measured aethalometer signals (or BC mass concentrations) with increasing filter loads, and empirical conversion from optical absorption to BC mass (Bodhaine, 1995; Weingartner et al., 2003). Two correction factors are important for the estimation of absorption coefficient and BC mass : (i) correction factor (C) applied to account for any change in the absorption occurring due to multiple light scattering effects on the filter, and (ii) empirical correction factor (R) which describes the change in the aethalometer response with increased particle loading on the filter. In the present study, wavelength dependent values for C following Bodhaine (1995) are used. The values of C and R are found to vary depending upon the measurement location. Collaud Coen et al. (2010) obtained a range of C and R values at 0.66 μm varying from a minimum of 2.88 and 1.01 over a free tropospheric location (Jungfraujoch), to a maximum of 4.26 and 1.09 over a polluted city (Thessaloniki). The absorption coefficient, estimated using the range of new Collaud Coen correction coefficients covering the maximum and minimum values of C and R, is found to differ from the absorption coefficient used in the study by 8–21%. The instrumental artifacts, *viz.,* flow rate, filter spot area, and detector response are estimated to contribute an error of ~3%. The overall uncertainty in the absorption coefficients and BC mass concentrations is found to lie in the range of 10–20% including all instrument artifacts and uncertainty in correction factors.

A three-wavelength integrating nephelometer (*model 3563, TSI Inc., USA)* which measures total aerosol scattering (β_{sca}) coefficients at 0.45, 0.55 and 0.70 μm is used in the study. The measurement is done in continuous mode with data averaging time of 5 min. The scattering coefficient measured by the nephelometer is highly sensitive to relative humidity (RH). As SSA is calculated using the aethalometer and nephelometer measurements, the scattering coefficients are corrected for the truncation error but not for RH. The uncertainties in nephelometer measurements arise due to noise in the filtered air scattering coefficient, calibration drift, calibration of the instrument for Rayleigh scattering of dry air and CO_2, and truncation of near scattered forward light. The overall uncertainty in β_{sca} in the current study taking into account the above sources is estimated to be about 15%.

Single scattering albedo (SSA) is calculated using the aerosol scattering coefficient (β_{sca}) and the absorption coefficient (β_{abs}). Absorption coefficient (β_{abs}) at 0.55 μm over Ahmedabad is calculated following the wavelength dependence of β_{abs} ($\beta_{abs} = K\lambda^{-\alpha}$, where K and α are the absorption Ångström coefficients, and α (Ångström exponent) is a measure of spectral dependence of aerosol absorption). The overall uncertainty in scattering and absorption coefficients which includes all the sources of instrumental error in addition to the error associated with the correction factors in absorption coefficient estimation are used in error propagation method to calculate the uncertainty in SSA. The maximum relative standard error in SSA using the uncertainties in aethalometer derived absorption coefficients and nephelometer derived scattering coefficients is found to be <10%.

2.5. GOCART model derived single scattering albedo

Monthly mean single scattering albedo at 0.55 μm over Ahmedabad is calculated from the monthly mean GOCART model simulated AODs of different species during 2001–2007 as GOCART data beyond 2007 were not available. The GOCART model simulates separately sulfate, sea salt, black carbon, dust and organic carbon (OC) AODs. GOCART computes aerosol optical depths of different species by adopting the published emission inventories and assimilated meteorological fields as inputs to chemical transport model (Chin et al., 2009).

The GOCART model produces a global gridded output at a lat–lon resolution of 2.0° × 2.5°. AODs of individual species are obtained at the above resolution centered around the study location corresponding to the lat–lon of 22°N, 72.5°E. In the present study, SSA is estimated by weighting the individual SSA of BC, sulfate, OC, dust and sea salt with their corresponding AODs following Chung et al. (2005). Sulfate, OC and sea salt aerosols (conservative scatterer) have an SSA of 1 at 0.55 μm, while SSA of BC is 0.2 (Hess et al., 1998). SSA of dust was found to vary e.g., the midvisible SSA of aerosol sampled by aircraft during dust dominated events were in the range of 0.95–0.97 (Anderson et al., 2003). Chung et al. (2005) parameterized the dust SSA based on the Aerosol Robotic Network (AERONET) results reported in Eck et al. (2005) and several field studies reported in Clarke et al. (2004) and Kim et al. (2005). Following Chung et al. (2005), SSA of dust was allowed to vary from 0.98 to 0.90. The ratio of BC AOD to the sum of dust and BC AODs was chosen as the criteria to determine the dust SSA; when this ratio was less than 0.1, the dust SSA was 0.98 and when this ratio was greater than 0.5 then the dust was assigned an SSA value of 0.90. Dust SSA linearly increased from 0.90 to 0.98 when the value of the ratio decreased from 0.5 to 0.1. GOCART SSA was found to agree well with AERONET derived SSA in both seasonal variation and magnitude with little bias over Kanpur (26.51°N, 80.23°E) in India (Chin et al., 2009). In GOCART, the threshold velocity of dust erosion, biomass burning emission factors, wind dependent sea salt flux function and biogenic OC emission are reported to be highly uncertain. The other parameters e.g., hygroscopic properties, refractive indices and mixing state, used in the calculation of mass extinction efficiency can also contribute to uncertainties in AODs derived from GOCART (Chin et al., 2009). A comparison of GOCART derived SSA with AERONET measurements revealed that improvements in aerosol size distribution, refractive indices of dust and black carbon aerosols are necessary in order to better quantify the aerosol absorption in the atmosphere (Chin et al., 2009).

2.6. Satellite derived SSA

Monthly mean SSA at 0.50 μm is obtained from Ozone Monitoring Instrument (OMI). OMI is a high resolution spectrograph which measures the top of the atmosphere upwelling radiance in ultraviolet and visible regions (0.27–0.50 μm) of solar spectrum. OMI Level 3 data at a lat–lon resolution of 1° × 1° centered around Ahmedabad are used in the study. OMI AOD and SSA were validated with AERONET sunphotometer over several locations in Asia, Africa and South America (Torres et al., 2007). SSA obtained from

AERONET and OMI for carbonaceous aerosols was found to agree well yielding a root mean square (RMS) difference of 0.03, while for desert dust aerosols the comparison yielded an RMS difference of 0.02 (Torres et al., 2007). SSA obtained at 0.388 μm is used to obtain SSA at 0.354 and 0.50 μm based on OMAERUV algorithm (Torres et al., 2007). However, this can increase the dependence of the algorithm on the assumed aerosol model which can lead to an uncertainty in the SSA at 0.50 μm. In addition, cloud contamination, for example, during monsoon in OMI pixels can also affect the estimation of AOD and SSA (Torres et al., 2007).

2.7. Other atmospheric parameters and surface reflectance

For aerosol radiative transfer calculations, atmospheric profiles of temperature, pressure, ozone and water vapor are required in addition to aerosol properties. The standard tropical atmospheric profiles of temperature and pressure are used (McClatchey et al., 1972). Monthly mean columnar ozone and water vapor over Ahmedabad are obtained from the daily mean data of OMI on-board Aura, and National Center for Environmental Prediction (NCEP) reanalysis respectively. Surface reflectance measured by MODerate resolution Imaging Spectroradiometer (MODIS) on-board Terra and Aqua satellites (8 Day, Level 3 Global 500m ISIN Grid product, MOD09A1 (Terra) and MYD09A1 (Aqua)) at seven wavelength bands in the 0.469–2.13 μm wavelength range (Table 1) are utilized in the study. The surface reflectance over Ahmedabad is higher during monsoon and pre-monsoon seasons (Table 1). Columnar ozone is high during summer (pre-monsoon and monsoon) when compared to winter and post-monsoon, which is consistent with the seasonal variations over the tropics (Table 2). Columnar water vapor and relative humidity are highest during monsoon season (June to September) due to transport of moisture from the Arabian sea (Table 2). Columnar ozone, water vapor and RH are low during winter when compared to other seasons.

3. Estimation of aerosol radiative forcing and forcing efficiency

Three different methods have been adopted to derive aerosol forcing efficiency and aerosol radiative forcing using the measured fluxes and AODs over Ahmedabad which are described below.

3.1. Method 1 (24-h average net flux)

In this method, 24-h average global flux for each clear sky day is calculated from the measured 5 min interval global (direct and diffuse) fluxes. 24-h average net surface fluxes (down minus up) are calculated from the above 24-h average global fluxes using MODIS derived broad-band surface albedo. 24-h average net fluxes for each month are plotted against the corresponding mean aerosol optical depths at 0.5 μm. The slope of the best fit line between the average net flux versus corresponding mean AOD yields surface forcing efficiency (Ramana et al., 2004).

Table 1
MODIS derived seasonal mean surface reflectance over Ahmedabad during 2008.

Wavelength (μm)	Winter	Pre-monsoon	Monsoon	Post-monsoon
0.469	0.132 ± 0.014	0.151 ± 0.005	0.241 ± 0.019	0.127 ± 0.004
0.555	0.220 ± 0.003	0.247 ± 0.016	0.346 ± 0.025	0.232 ± 0.000
0.645	0.068 ± 0.008	0.078 ± 0.003	0.206 ± 0.017	0.065 ± 0.001
0.859	0.111 ± 0.009	0.126 ± 0.005	0.236 ± 0.018	0.110 ± 0.002
1.24	0.234 ± 0.002	0.260 ± 0.011	0.332 ± 0.016	0.243 ± 0.005
1.64	0.228 ± 0.009	0.252 ± 0.006	0.304 ± 0.019	0.227 ± 0.012
2.13	0.188 ± 0.021	0.211 ± 0.004	0.219 ± 0.012	0.180 ± 0.008

Table 2
Seasonal mean and standard deviation of columnar ozone (Dobson Unit, DU), water vapor (cm) and relative humidity (%) over Ahmedabad during 2008. Accumulated rainfall (mm) over Ahmedabad as a function of season is also given.

Atmospheric parameters	Winter	Pre-monsoon	Monsoon	Post-monsoon
Columnar ozone (DU)	249 ± 5	272 ± 6	275 ± 4	257 ± 13
Columnar water vapor (cm)	1.4 ± 0.6	2.0 ± 0.4	4.7 ± 0.6	2.3 ± 0.5
Relative humidity (%)	30 ± 6	37 ± 12	84 ± 8	43 ± 6
Rainfall (mm)	6.1	7.1	601.7	0.3

3.2. Method 2 (hybrid approach)

This approach is dependent on model partially as radiative transfer model is used to estimate flux for aerosol free clear sky fluxes. Clear sky, aerosol free net surface fluxes for all months of 2008 are estimated using the measured columnar ozone and water vapor concentration in the Santa Barbara DISORT Atmospheric radiative transfer (SBDART) model (Ricchiazzi et al., 1998). SBDART solves plane parallel radiative transfer in clear sky conditions within the Earth's atmosphere. The fluxes calculated by SBDART model were found to lie within 2% of direct and diffuse irradiance measurements (Michalsky et al., 2006). Surface reflectance at seven wavelengths is used to reproduce the surface reflectance in required wavelength range (0.31–2.8 μm) using a combination of vegetation, sand and water albedos given in SBDART. Radiative transfer calculation is performed for 8 radiation streams and downwelling, upwelling and direct fluxes in the wavelength range of pyranometer (i.e. 0.31–2.8 μm) at 1-h interval are estimated. Modeled aerosol free 24 h average net flux is then subtracted from the observed 24 h average net surface flux, and surface aerosol radiative forcing is calculated for each clear sky day of 2008. The advantage of this method is that it can be used to estimate aerosol radiative forcing for all aerosols including the background aerosols (Conant, 2000). The uncertainty in radiative forcing in hybrid approach is estimated to be ~10% including the uncertainties in measured and model estimated fluxes.

3.3. Method 3 (differential approach)

This approach is completely based on the observations of global surface flux and aerosol optical depth. Reference day among the clear sky days for each month of 2008 is chosen based on the lowest mean aerosol optical depth at 0.5 μm. 24 h average net surface flux for the reference day (lowest AOD day) is then subtracted from average net fluxes for the rest of the days in a month and surface aerosol radiative forcing is estimated. The reference days, diurnal mean AOD and standard deviation corresponding to each month are shown in Table 3. During the reference day the diurnal variation in AOD was the lowest among the other days. The advantage of this approach is that it is independent of model uncertainty and since observed clear sky fluxes are subtracted in this approach, forcing is also not sensitive to calibration error (Conant, 2000). The aerosol forcing efficiency is calculated from the slope of the best fit line between daily mean surface aerosol radiative forcing and corresponding mean aerosol optical depth. In this approach as measured fluxes only are used, the uncertainty in radiative forcing estimates is less and is ~7%.

3.4. Aerosol radiative forcing from model based approach

In the present study, SBDART model is used for radiative transfer calculation in the wavelength range of 0.31–2.80 μm.

Table 3
Aerosol optical depth (AOD) (0.5 μm) along with $\pm 1\sigma$ for clear sky day of each month/season over Ahmedabad during 2008 which is used as reference day.

Month	Jan	Feb	Mar	Apr	May	Jun–Sep	Oct	Nov	Dec
Date of Reference Day	16	17	5	22	17	4 Jun	9	27	2
Mean AOD	0.265	0.236	0.228	0.316	0.333	0.416	0.286	0.167	0.276
$\pm 1\sigma$	0.008	0.002	0.048	0.008	0.013	0.030	0.002	0.021	0.023

Radiative transfer calculations are done for clear sky conditions with and without aerosols in the atmosphere. Model estimation of flux for without aerosol case is already described in Method 2 (Hybrid approach), while flux with aerosols is estimated using measured aerosol optical properties in SBDART model. Measured aerosol optical parameters (AOD and SSA) are used to constrain the output of OPAC (Optical Properties of Aerosols and Clouds) model (Hess et al., 1998). Among the ten aerosol components in OPAC, the most suitable aerosol components based on aerosol source regions and transport over Ahmedabad are found to be water insoluble, water soluble, black carbon, mineral dust and sea salt (Ganguly and Jayaraman, 2006; Ramachandran and Kedia, 2010). The number concentration of these aerosols is altered to match the monthly mean measured AOD spectra and SSA at ambient relative humidity for each month (Table 2). The number concentration of each component is altered iteratively until the following conditions are satisfied: (1) The root mean square (rms) difference between the measured AOD and model AOD spectra is <0.03, thus constraining the rms differences to within 0.1 AOD. (2) Ångström wavelength exponent α obtained from the measured AODs in the 0.38–0.87 μm wavelength region is consistent with model derived α values. (3) BC mass concentration in OPAC should be the same as that of the aethalometer measured BC mass. (4) OPAC single scattering albedo should match with aethalometer and nephelometer, GOCART and OMI derived SSAs as the case may be. The aerosol optical properties so obtained are then employed in SBDART to estimate flux at the Earth's surface from which aerosol radiative forcing is calculated. The absolute total uncertainty in the modeled aerosol radiative forcing was found to vary in the range of 0.2–3.1 Wm^{-2} by considering different aerosol optical properties, and single scattering albedo was found to be the largest contributor to the above uncertainty, and relative total uncertainties in aerosol radiative forcing were higher when fluxes were lower (McComiskey et al., 2008). The relative standard error in aerosol radiative forcing is found to be <15% by taking into account the uncertainties in aerosol input parameters, additional inputs and flux estimates.

4. Results and discussion

4.1. Variations in aerosol optical depths

Daily and seasonal mean aerosol optical depths at 0.5 μm for year 2008 are shown in Fig. 2. AOD shows an increasing trend from winter to monsoon and then decreases (Fig. 2b). The transport of dust by the strong north westerly wind can give rise to higher AOD during pre-monsoon. The boundary layer height is also higher during pre-monsoon and monsoon because of higher temperature and stronger convection, which provide longer atmospheric column to accommodate more natural and anthropogenic aerosols (Kedia and Ramachandran, 2011). Although Ahmedabad gets all of its annual rainfall during monsoon season (Table 2), no visible decrease is seen in AODs due to wet removal of aerosols because the rainfall is not uniformly distributed over the entire season, but occurs in discreet events. However, wet removal is found to be more efficient in reducing the near surface aerosols; for example, it has been observed that BC mass decreased from 3.9 μg m^{-3} (pre-monsoon) to 2.1 μg m^{-3} (monsoon) over Ahmedabad (Ramachandran and Kedia, 2010). Over Ahmedabad sea salt concentration is found to increase from 5 μg m^{-3} during pre-monsoon to 10 μg m^{-3} during monsoon (e.g., Raman and Ramachandran, 2011; and references cited therein).

The effects of wet removal, hygroscopic growth of aerosols and addition of sea salt on AOD is estimated using OPAC urban model at 37% and 84% RH which were the corresponding RH values during pre-monsoon and monsoon respectively (Table 2). Urban aerosol model comprises three dominant aerosol species *viz.*, water soluble, insoluble and BC (Hess et al., 1998). AODs estimated for different scenarios taking into account the variation in the mass concentration of aerosol species and RH during pre-monsoon and monsoon are given in Table 4. Case 1 represents aerosol properties of urban model corresponding to an RH of 37%. A reduction of BC mass by half and an addition of sea salt leads to a decrease of 12% in AOD (case 2) at the same RH indicating that the reduction of BC mass predominantly affects the AOD. Further, when the sea salt mass concentration is doubled with respect to its value in case 2,

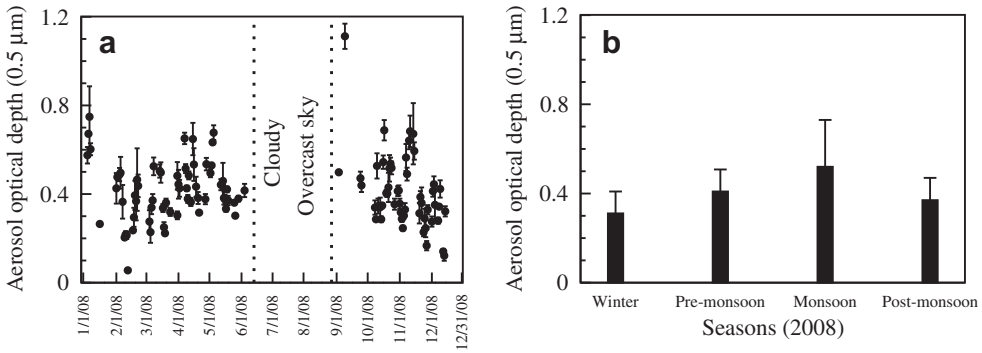

Fig. 2. Day to day and seasonal variation of aerosol optical depth (0.5 μm) over Ahmedabad. Vertical bars represent $\pm 1\sigma$ deviation from the mean.

Table 4
Mass concentrations of water insoluble (IS), water soluble (WS), black carbon (BC) and sea salt (SS) for urban environment and for different temporal conditions. Aerosol optical depth (AOD) and single scattering albedo (SSA) at 0.5 μm for different scenarios (relative humidity, RH) are given.

Cases	Environment/ Condition	Mass concentration ($\mu g\ m^{-3}$)				Aerosol optical depth	Single scattering albedo
		IS	WS	BC	SS		
1 (RH = 37%)	Urban	35.6	51.2	7.8	0.0	0.51	0.74
2 (RH = 37%)	Pre-monsoon	35.6	51.2	3.9	5.0	0.45	0.83
3 (RH = 37%)	Pre-monsoon	35.6	51.2	3.9	10.0	0.46	0.84
4 (RH = 84%)	Monsoon	35.6	94.3	2.1	10.0	0.76	0.94

AOD increases only by 2% (case 3), confirming that an increase in sea salt mass concentration does not contribute significantly to midvisible AOD. In case 4, a decrease in BC and addition of sea salt accompanied with an increase in RH from 37 to 84% that lead to an increase in the water soluble aerosol mass concentrations, and decrease in the BC mass results in a 49% increase in AOD with respect to case 1 (urban environment). This feature of an increase in the water soluble aerosols and sea salt aerosol mass concentrations, and decrease in the BC mass from pre-monsoon to monsoon is consistent with mass concentration measurements reported earlier over Ahmedabad (Raman and Ramachandran, 2011 and references cited therein; Ramanchandran and Kedia, 2010). The simulation clearly shows that AOD increases significantly when RH increases mainly due to the hygroscopic growth of water soluble aerosols, and that this increase overwhelms the removal of BC and increase of sea salt aerosols over an urban regime.

4.2. Single scattering albedo

Seasonal mean variation of single scattering albedo (SSA) at 0.55 μm during 2008 over Ahmedabad is shown in Fig. 3. SSA at 0.55 μm is estimated from the ground-based absorption and scattering coefficients measured using aethalometer and nephelometer respectively. GOCART model and OMI (Aura) satellite derived SSA at 0.55 and 0.50 μm respectively are also shown in Fig. 3. Aethalometer and nephelometer derived SSA correspond to near surface, while GOCART and OMI (Aura) SSA correspond to column. Aethalometer and nephelometer derived SSA is higher during monsoon (0.82) as compared to other seasons because black carbon mass concentration is lowest during monsoon (2.1 μg m^{-3}) (Ramachandran and Kedia, 2010). SSA during post-monsoon and winter are lower due to the dominance of absorbing aerosols. It is clear from Table 4 that 50% decrease in BC mass and addition of sea salt in urban environment can lead to a 12% increase in SSA with respect to case 1. The effect of doubling of sea salt can increase midvisible SSA only by 1% (cases 2 and 3), where as a decrease in BC and increase in RH from 37 to 84% results in a 27% increase in SSA (case 4), suggesting that the amount of absorbing aerosols in an urban regime primarily determines the SSA. SSA derived using aethalometer and nephelometer measurements are lower than GOCART and OMI derived SSA as Ahmedabad is an urban location and absorbing aerosols are more dominant near surface. SSA derived using aethalometer and nephelometer measurements was found to vary from 0.72 (dry season) to 0.81 (monsoon) over Ahmedabad during 2002–2005 (Ganguly and Jayaraman, 2006) consistent with the present values. Similar differences in SSA were seen over Delhi, a mega-city, where surface SSA was found to be ~0.74 while the columnar SSA varied from 0.89 to 0.93 during winter (Soni et al., 2010). Columnar SSA derived from AERONET over Kanpur was found to be in the range of 0.80–0.95 during 2002–2006 (Eck et al., 2010). Such differences in SSA as a function of altitude have been seen earlier depending upon the types of aerosols and layers present at higher altitudes (Clarke et al., 2004).

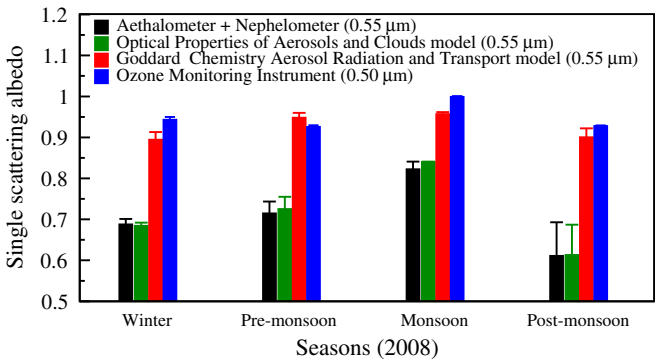

Fig. 3. Seasonal variation in single scattering albedo (SSA) value derived using aethalometer and nephelometer, and obtained from GOCART and OMI (Aura) over Ahmedabad. SSA estimated using OPAC is also shown. Vertical bars represent $\pm 1\sigma$ deviation from the mean.

4.3. Aerosol forcing efficiency

Diurnal mean (24 h) global net (down minus up) fluxes are linearly fitted with aerosol optical depth at 0.5 μm in Fig. 4a. Surface aerosol radiative forcing calculated using hybrid approach (method 2) and differential approach (method 3) are linearly

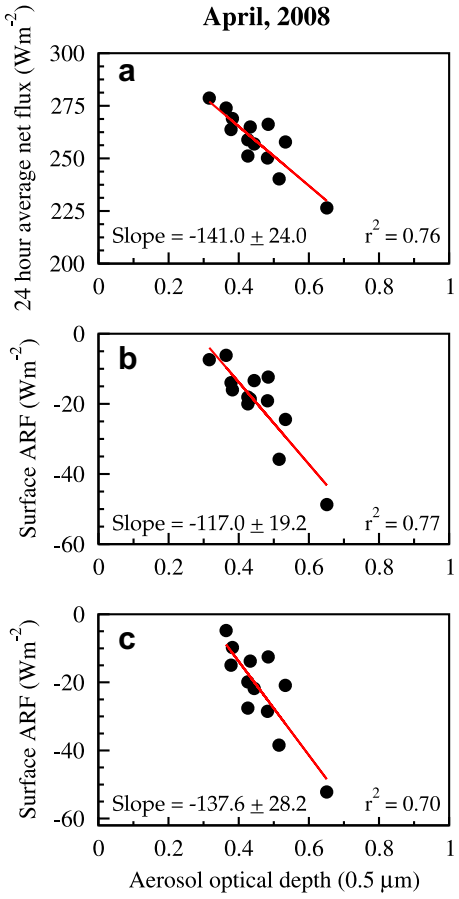

Fig. 4. (a) 24 hour average net surface flux, and surface aerosol radiative forcing deduced, (b) using method 2 and (c) method 3 as a function of aerosol optical depths (0.5 μm) for April 2008. The straight lines are the least square fits.

correlated with corresponding mean AOD (Fig. 4). All the three methods show the same slope within the standard error and have similar regression coefficients. Aerosol surface radiative forcing efficiency which is obtained from the slope of the least square fits is shown in Fig. 5. Forcing efficiency could not be estimated in monsoon season for method 3 because the sky is mostly cloudy during the season. The magnitude of forcing efficiency estimated using methods 1 and 2 is found to be the lowest in monsoon (<-50 Wm^{-2}).

Aerosol forcing efficiency obtained by all the methods are in the range of -67 to -89 Wm^{-2}/AOD during winter while it was found to be -73 Wm^{-2}/AOD over Kathmandu (27.67°N, 85.31°E) in the Himalayas. During the Indian Ocean Experiment (INDOEX) conducted from January to March 1999, forcing efficiency was found to be -75 Wm^{-2}/AOD (Ramanathan et al., 2001), which also lies in the range of forcing efficiency values observed over Ahmedabad during winter. Over another urban, tropical location, Pune, India forcing efficiency was found to be -88 Wm^{-2}/AOD during dry seasons (November–April) of 2001 and 2002 (Pandithurai et al., 2004). Forcing efficiency over Ahmedabad during November to April (post-monsoon, winter and pre-monsoon) ranges from -65 to -71 Wm^{-2}/AOD. The lower forcing efficiency obtained over Ahmedabad could be due to higher values of columnar SSA as compared to Pune (0.81).

4.4. Surface aerosol radiative forcing

Seasonal mean surface aerosol radiative forcing estimated using method 2 (hybrid approach) and method 3 (differential approach) are plotted in Fig. 6. Seasonal mean AODs at 0.5 μm are also mentioned in the figure. It is clear from the figure that higher AOD results in higher surface forcing thereby suggesting that AOD and forcing exhibit a linear relationship. Forcing values obtained by two approaches, hybrid (semi model dependent) and differential (model independent) are consistent within $\pm1\sigma$ for all the seasons. The magnitude of radiative forcing follows the same trend as AOD and is higher during monsoon. Forcing in both methods 2 and 3 during pre-monsoon is lower despite higher AOD (0.41). Lower radiative forcing during pre-monsoon arises due to higher SSA when compared to post-monsoon (Fig. 3). The lower surface forcing at higher SSA is consistent with earlier results including Ahmedabad and Delhi (Ramachandran and Kedia, 2010; Singh et al., 2010). Thus, the seasonal mean radiative forcing follows a linear behavior with corresponding AOD except for pre-monsoon over Ahmedabad.

4.5. Surface aerosol radiative forcing: observation and model estimates

Surface forcing during different seasons of 2008, estimated by method 3, is compared with model estimated surface forcing over

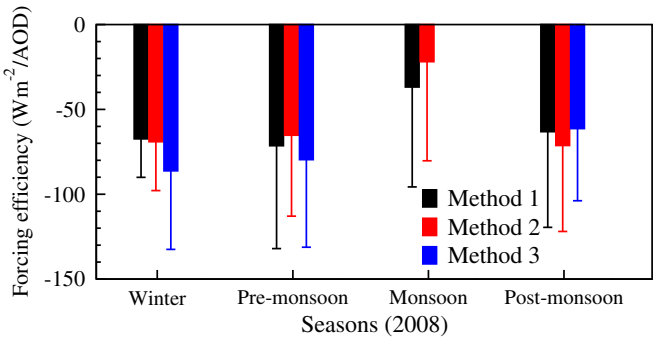

Fig. 5. Seasonal variation of aerosol forcing efficiency estimated by methods 1, 2 and 3. Vertical bars represent $\pm1\sigma$ deviation from the mean.

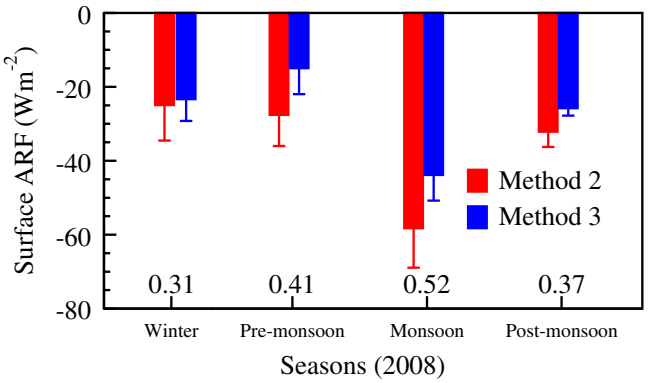

Fig. 6. Aerosol radiative forcing (ARF) at the surface calculated using methods 2 (hybrid approach) and 3 (differential approach). Seasonal mean aerosol optical depths are mentioned in the figure. Vertical bars represent $\pm1\sigma$ deviation from the mean.

Ahmedabad for three different cases (Fig. 7). Forcing obtained in method 3 is chosen for comparison because it is completely based on the observations. In the first case, aethalometer and nephelometer derived SSA are used, while in the second and third cases GOCART model derived and OMI derived columnar SSA respectively are used in radiative transfer model (Fig. 7). Aerosol optical depth, columnar ozone, water vapor and surface albedo are maintained the same for all the cases, and only the SSA spectra is changed. The measured AOD spectra and SSA for three different cases are reconstructed by altering the number concentrations of water insoluble, water soluble, black carbon, mineral dust and sea salt aerosols in OPAC model following the conditions 1, 2 and 4 described earlier in section 3.4. Condition 3 in which measured BC mass is used (in OPAC) cannot reproduce the SSA derived from GOCART and OMI. The observed surface forcing shows large differences when compared to the model estimated forcing when SSA is lower (case 1). However, for cases 2 and 3, model estimated forcing is in accordance with the observations during winter, pre- and post-monsoon, while it shows large deviation during monsoon season. During monsoon model estimated forcing in case 1 deviates less (15% of observed forcing) from observation while forcing in cases 2 and 3 is about a factor of two higher (less negative) when compared to the observed forcing.

During monsoon forcing estimated using the near surface SSA is closer to the observed forcing, while during other seasons forcing estimated with GOCART and OMI SSA agree well (Fig. 7).

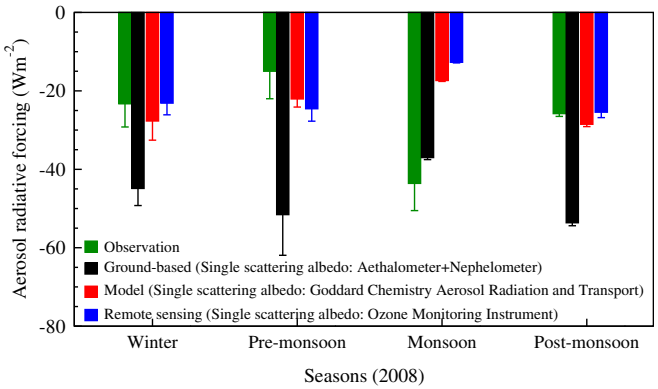

Fig. 7. Seasonal aerosol radiative forcing at surface from observation and model in which aethalometer and nephelometer (case 1), GOCART (case 2), and OMI (Aura) (case 3) single scattering albedo are used. Vertical bars represent $\pm1\sigma$ deviation from the mean.

The wet removal of near surface aerosols, presence of abundant sea salt particles which is transported from the Arabian Sea, and hygroscopic growth of water soluble aerosols could have given rise to higher SSA during monsoon over Ahmedabad (Fig. 3, Table 4). GOCART and OMI derived SSAs during monsoon are even higher than the in situ measurements. SSA estimated using GOCART AODs during monsoon can be affected by the uncertainties listed in section 2.5. OMI derived SSA during monsoon is $\geq$0.99 which could occur due to the assumption that all the aerosols present in the atmosphere are scatterers. Such a high SSA obtained from GOCART and OMI can lead to lower forcing than that estimated using measured flux. Thus, it is clear that SSA is a sensitive parameter in the determination of aerosol radiative forcing and a little change in SSA can lead to a significant change in aerosol radiative forcing.

5. Summary and conclusions

Aerosol radiative forcing and efficiency for different months of 2008 are estimated from the simultaneously measured downwelling global fluxes and aerosol optical depths (AODs). Single scattering albedo (SSA) obtained from aethalometer and nephelometer measured absorption and scattering coefficients, Goddard Chemistry Aerosol Radiation and Transport (GOCART) and zone Monitoring Instrument (OMI) are utilized. Semi model dependent and model independent approaches have been adopted to calculate aerosol forcing efficiency and radiative forcing, and are compared with model estimated aerosol radiative forcing.

The major findings from this study are:

1. Aerosol optical depths show an increase from winter to monsoon. AOD increases significantly when relative humidity (RH) increases due to the hygroscopic growth of water soluble aerosols, and this increase in AOD overwhelms the changes in AOD due to the removal of BC aerosols and increase of sea salt aerosol over an urban environment.
2. Single scattering albedo exhibits a large seasonal variability; near surface SSA is the highest in monsoon ($>$0.8) and lower in post-monsoon. Columnar SSA (GOCART and OMI) are higher than those measured at the surface using aethalometer and nephelometer.
3. Surface forcing efficiency estimated by all the methods agree well. Surface aerosol forcing efficiency is found to be lower in monsoon as SSA is higher.
4. Surface aerosol radiative forcing shows higher values in monsoon season. Surface forcing estimated by method 2, hybrid approach (involves observation and model), and method 3 differential approach (uses only measured fluxes) are more or less similar for all the seasons. The surface radiative forcing during post-monsoon is higher when compared to that in pre-monsoon while AOD was found to be lower. The higher surface forcing is attributed to lower SSA during post-monsoon.
5. Surface forcing derived using GOCART and OMI derived SSA agrees well with observations for all the seasons except monsoon, while forcing derived using near surface SSA is consistent with the observed forcing in monsoon but exhibits large differences during other seasons. During monsoon, GOCART SSA can be uncertain due to high RH and discrepancy in sea salt flux estimation, and OMI SSA could be higher due to the selection of a pre-defined weakly absorbing aerosol model.

This study shows that aerosol radiative forcing deduced from model agrees well with observations for columnar SSA during most seasons and emphasizes that SSA should be more accurate as aerosol forcing is quite sensitive to SSA.

Acknowledgments

We thank ISRO-GBP, ISRO Headquarters, Bengaluru, for funding support. Columnar ozone from OMI and GOCART model derived AODs are downloaded from GES-DISC, NASA. Relative humidity and columnar water vapor data obtained from NCEP reanalysis, and rainfall data obtained from NOAA, NESDIS National data center, USA are used in the study.

Appendix. Supplementary data

Supplementary data associated with this article can be found, in the online version, at doi:10.1016/j.atmosenv.2011.08.015.

References

Anderson, T., Charlson, R.J., Schwartz, S.E., Knutti, R., Boucher, O., Rodhe, H., Heintzenberg, J., 2003. Climate forcing by aerosols: a hazy picture. Science 300, 1103–1104.

Babu, S.S., Moorthy, K.K., Satheesh, S.K., 2007. Temporal heterogeneity in aerosol characteristics and the resulting radiative impacts at a tropical coastal station – part 2: direct short wave radiative forcing. Annales Geophysicae 25, 2309–2320.

Bodhaine, B.A., 1995. Aerosol absorption measurements at Barrow, Mauna Loa and the south Pole. Journal of Geophysical Research 100, 8967–8975.

Chin, M., Diehl, T., Dubovik, O., Eck, T.F., Holben, B.N., Sinyuk, A., Streets, D.G., 2009. Light absorption by pollution, dust, and biomass burning aerosols: a global model study and evaluation with AERONET measurements. Annales Geophysicae 27, 3439–3464.

Chung, C.E., Ramanathan, V., Kim, D., Podgorny, I.A., 2005. Global anthropogenic aerosol direct forcing derived from satellite and ground-based observations. Journal of Geophysical Research 110, 1–17.

Clarke, A.D., et al., 2004. Size distributions and mixtures of dust and black carbon aerosol in Asian outflow: physiochemistry and optical properties. Journal of Geophysical Research 109 (D15S09), 1–20.

Collaud Coen, M., et al., 2010. Minimizing light absorption measurement artifacts of the aethalometer: evaluation of five correction algorithms. Atmospheric Measurement Techniques 3, 457–474.

Conant, C., 2000. An observational approach for determining aerosol surface radiative forcing: results from the field phase of INDOEX. Journal of Geophysical Research 105, 15347–15360.

Dey, S., Tripathi, S.N., 2008. Aerosol direct radiative effects over Kanpur in the Indo-Gangetic basin, northern India: long-term (2001–2005) observations and implications to regional climate. Journal of Geophysical Research 113. doi:10.1029/2007JD009029.

Eck, T.F., et al., 2005. Columnar aerosol optical properties at AERONET sites in central eastern Asia and aerosol transport to the tropical mid-Pacific. Journal of Geophysical Research 110. doi:10.1029/2004JD005274.

Eck, T.F., et al., 2010. Climatological aspects of the optical properties of fine/coarse mode aerosol mixtures. Journal of Geophysical Research 115. doi:10.1029/2010JD014002.

Ganguly, D., Jayaraman, A., 2006. Physical and optical properties of aerosols over an urban location in western India: implications for shortwave radiative forcing. Journal of Geophysical Research 111. doi:10.1029/5132006JD007393.

Hess, M., Koepke, P., Schult, I., 1998. Optical properties of aerosols and clouds: the software package OPAC. Bulletin of the American Meteorological Society 79, 831–844.

Kedia, S., Ramachandran, S., 2011. Seasonal variations in aerosol characteristics over an urban location and a remote site in western India. Atmospheric Environment 45, 2120–2128.

Kim, D.H., Sohn, B.J., Nakajima, T., Takamura, T., 2005. Aerosol radiative forcing over East Asia determined from ground-based radiation measurements. Journal of Geophysical Research 110. doi:10.1029/2004JD004678.

McClatchey, R., Fenn, R., Salby, J., Volz, F., Garing, J., 1972. Optical properties of the atmosphere. In: Environ. Res. Pap., third ed., vol. 411. AFCRL, Cambridge, Mass, 108 pp.

McComiskey, A., Schwartz, S.E., Schmid, B., Guan, H., Lewis, E.R., Ricchiazzi, P., Ogren, J.A., 2008. Direct aerosol forcing: calculation from observables and sensitivities to inputs. Journal of Geophysical Research 113. doi:10.1029/2007JD009170.

Michalsky, J.J., et al., 2006. Shortwave radiative closure studies for clear skies during the atmospheric radiation measurement 2003 aerosol Intensive observation Period. Journal of Geophysical Research 111. doi:10.1029/2005JD006341.

Pandithurai, G., Pinker, R.T., Takamura, T., Devara, P.C.S., 2004. Aerosol radiative forcing over a tropical urban site in India. Geophysical Research Letters. doi:10.1029/2004GL019702.

Ramachandran, S., Kedia, S., 2010. Black carbon aerosols over an urban region: radiative forcing and climate impact. Journal of Geophysical Research 115. doi:10.1029/2009JD013560.

Raman, R.S., Ramachandran, S., 2011. Source apportionment of the ionic components in precipitation over an urban region in Western India. Environmental Science and Pollution Research 18, 212–225.

Raman, R.S., Ramachandran, S., 2010. Annual and seasonal variability of ambient aerosols over an urban region in western India. Atmospheric Environment. doi:10.1016/j.atmosenv.2009.12.008.

Ramana, M.V., Ramanathan, V., Podgorny, I.A., Pradhan, B.B., Shrestha, B., 2004. The direct observations of large aerosol radiative forcing in Himalaya region. Geophysical Research Letters 31. doi:10.1029/2003GL018824.

Ramanathan, V., et al., 2001. Indian Ocean experiment: an integrated analysis of the climate forcing and effects of the great Indo-Asian haze. Journal of Geophysical Research 106, 28371–28398.

Ricchiazzi, P., Yang, S., Gautier, C., Sowle, D., 1998. SBDART: a research and teaching software tool for plane-parallel radiative transfer in the Earth's atmosphere. Bulletin of the American Meteorological Society 79, 2101–2114.

Singh, S., Soni, K., Bano, T., Tanwar, R.S., Nath, S., Arya, B.C., 2010. Clear-sky direct aerosol radiative forcing variations over mega-city Delhi. Annales Geophysicae 28, 1157–1166.

Solomon, S., Qin, D., Manning, M., Chen, Z., Marquis, M., Averyt, K., Tignor, M., Miller, H (Eds.), 2007. Intergovernmental Panel on Climate Change (IPCC). Cambridge University Press, New York

Soni, K., Singh, S., Bano, T., Tanwar, R., Nath, S., Arya, B., 2010. Variations in single scattering albedo and Angstrom absorption exponent during different seasons at Delhi, India. Atmospheric Environment 44, 4355–4363.

Torres, O., Tanskanen, A., Veihelmann, B., Ahn, C., Braak, R., Bhartia, P.K., Veefkind, P., Levelt, P., 2007. Aerosols and surface UV products from ozone monitoring instrument observations: an overview. Journal of Geophysical Research 112. doi:10.1029/2007JD008809.

Weingartner, E., Saathoff, H., Schnaiter, M., Streit, N., Bitnar, B., Baltensperger, U., 2003. Absorption of light by soot particles: determination of the absorption coefficient by means of aethalometers. Journal of Aerosol Science 34, 1445–1463.

Indian Aerosol Science and Technology Association (IASTA) Bulletin, 2010

Volume: 19 (1-2), pages: 387-389, ISSN: 0917-4570.

Aerosol Radiative Forcing over an Urban Location:

Observations and Model Estimates

Rohit Srivastava* and S. Ramachandran

Physical Research Laboratory,Ahmedabad, India

* rohits@prl.res.in

Introduction

Atmospheric aerosols play an important role in earth – atmosphere radiation balance. They scatter and absorb the incoming solar radiation, and outgoing terrestrial radiation. The role of aerosols in the radiation budget is one of the largest source of uncertainty in validating the model prediction of climate change [*IPCC*, 2007]. Generally the aerosol radiative forcing estimated by the modeled fluxes with external mixing of aerosols provide the lower bound of the forcing i.e., more cooling than the homogeneous internal mixture, with core - shell result in between [*Lesins et al.*, 2002]. According to the simulation for elemental carbon forcing, the core - shell mixing state shows 50% higher forcing than external and 40% lower forcing than well internally mixed aerosols [*Jacobson*, 2000]. The uncertainly in the observed flux is lesser than the fluxed estimated by models based on several assumptions. The down – welling fluxes and aerosol optical parameters are simultaneously measured and aerosol radiative forcing will be estimated using these aerosol parameters in radiative transfer model and differences between them will be studied.

Measurements and Methodology

Ground reaching broad-band global and diffuse fluxes in wavelength range 0.31 to 2.8 µm are measured over an urban location Ahmedabad (23.03^{o}N, 72.55^{o}E) during 2008 using set of pyranometers (*Kipp and Zonen Model CM21*). Down – welling fluxes are measured at every five minute resolution during each clear sky day of year 2008. The absolute accuracy in pyranometer measured fluxes is 5%, however the uncertainty due to the directional response can be ±10 Wm^{-2}. Simultaneous measurements of aerosol optical depth (AOD) at five wavelengths (0.38, 0.44, 0.5, 0.675, 0.88 µm) using Microtops II sunphotometer are also conducted. Column ozone and water vapour are also observed using Microtops II ozonometer. The absolute uncertainty in the AOD values are less than 0.03 at all wavelengths.

Measurement Location and Meteorology

All the measurements are performed at the campus of the Physical Research Laboratory (23.03^{o}N, 72.55^{o}E, 55 m amsl), located in the west of the Ahmedabad an urban city with large and small scale industries and variety of vehicles. Thar desert and the Arabian Sea are present in the northwest and southwest of the Ahmedabad respectively, which are the major sources of the mineral dust and sea salt. The location is affected with both anthropologically produced sub-micron aerosols along with the naturally produced coarser mineral dust and sea salt aerosols.

During winter (December – February), winds over Ahmedabad are either north easterly or north westerly, which transport aerosols of continental origin and land derived dust particles, while during pre- monsoon (March – May) and monsoon season (June – September), the winds are north-westerly or south-westerly which transport aerosols of marine origin. During post-monsoon (October – November) season the winds are calm and from the random direction.

Results and Discussion

The diurnal variations of total and diffuse fluxes along with the aerosol optical depths on 06, 16 January and 14 May 2008 are shown in figure 1. Higher AOD and lower diffuse flux are observed on 16 Jan when compared to 06 Jan and 14 May. The enhancement in diffuse flux on 06 Jan is observed due to large scattering of the solar flux by the aerosols. On 06 Jan total flux is lower than that on 16 Jan, because the direct flux is reduced due the large aerosol extinction (absorption and scattering) of the direct flux and hence total flux is also reduced. The total flux is higher in May, because of the higher solar insolation in May. The diffuse flux on May 14 is high in comparison to that on 06 Jan while the AOD is low. The more scattering of solar flux occur due to the dominance of scattering aerosols (e.g. Sea salt) over the location during May which are transported by the south- westerly winds. Thus aerosols significantly modify the direct and diffuse fluxes.

Aerosol optical properties are also be used to simulate total, direct and diffuse fluxes. The measured AOD, SSA, and black carbon mass concentration are used to constrain the output of OPAC model [*Hess et al.*, 1998] considering external mixture of the aerosols, and hence aerosol optical depth, single scattering albedo along with asymmetry parameter are estimated for the entire shortwave region. The aerosol optical parameters such as AOD, SSA and asymmetry parameter are then used as inputs in the radiative transfer model (SBDART) [*Ricchiazzi et al.*, 1998] to estimate fluxes at earth's surface, atmosphere and top of the atmosphere.

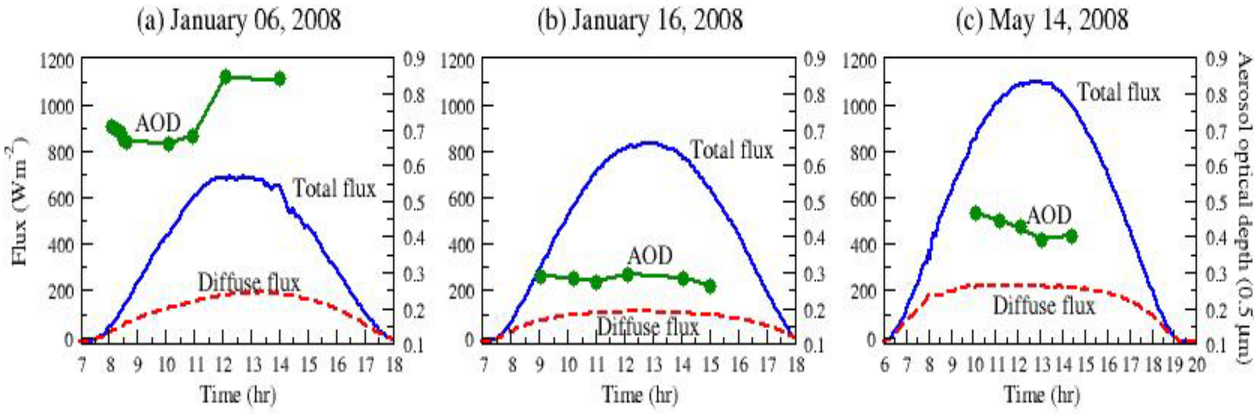

Figure 1. Diurnal variations of ground reaching broad-band total, diffuse fluxes and aerosol optical depths at 0.5 ìm over an urban location Ahmedabad (23.03oN, 72.55oE) on (a) January 06, (b) January 16, and (c) May 14, 2008

Fluxes will also be estimated by models using the measured optical parameters of aerosols and aerosol radiative forcing will be calculated. It is anticipated that the comparison between the observed and model estimated fluxes will provide the better understanding of the aerosol's impact on the radiation balance regarding the states of compositional mixing of the aerosols.

Summary

The observed and model estimated fluxes and the radiative effects of aerosols during different seasons are studied. The comparison between them will lead to information of state of compositional mixing of the aerosols. Down - welling total and diffuse fluxes simultaneously with the AOD are measured over and urban location Ahmedabad. Higher AOD shows the enhancement in the diffuse fluxes and reduction in total fluxes. However, the dominance of particular type aerosols, e.g. scattering aerosols can also increase the diffuse flux. The fluxes, using measured aerosols optical parameters into the radiative transfer model, will be simulated and aerosol radiative forcing will be calculated and compared with observed one. Detailed results obtained on the observed and model estimated fluxes and aerosol radiative forcing and their seasonal variability will be presented and discussed.

References

Intergovernmental Panel on Climate Change (IPCC) (2007), S. Solomon, D. Qin, M. Manning, Z. Chen, M. Marquis, K. Averyt, M. Tignor, H. Miller, Cambridge University Press, New York.

Jacobson, M.,Z. (2001), Strong radiative heating due to the mixing state of black carbon in atmospheric aerosols, *Nature, 409*, 695-697.

Hess, M., P., Koepke., and I., Schult (1998), Optical properties of aerosols and clouds: the software package OPAC, *Bull. Amer. Meteor. Soc., 79*, 831— 844.

Lesins, G., P. Chylek, U. Lohmann, (2002), A study of internal and external mixing scenarios and its effect on aerosol optical properties and direct radiative forcing, *J. Geophys. Res., 107*, doi:10.1029/201JD000973.

Ricchiazzi, P., S. Yang, C. Gautier, and D. Sowle (1998), SBDART: A research and teaching tool for plane- parellel radiative transfer in the Earth's atmosphere, *Bull. Am. Meteorol. Soc., 79*, 2101 — 2114.